

---

Theses and Dissertations

---

Fall 2012

# Developing an improved, shock-capturing watershed model for simulating spatially variable runoff and soil erosion processes at the hillslope scale

Dimitrios Charalampos Dermisis  
*University of Iowa*

Copyright © 2012 Dimitrios Charalampos Dermisis

This dissertation is available at Iowa Research Online: <https://ir.uiowa.edu/etd/5930>

---

## Recommended Citation

Dermisis, Dimitrios Charalampos. "Developing an improved, shock-capturing watershed model for simulating spatially variable runoff and soil erosion processes at the hillslope scale." PhD (Doctor of Philosophy) thesis, University of Iowa, 2012.  
<https://ir.uiowa.edu/etd/5930>. <https://doi.org/10.17077/etd.e84e7wcv>

---

Follow this and additional works at: <https://ir.uiowa.edu/etd>



Part of the [Civil and Environmental Engineering Commons](#)

DEVELOPING AN IMPROVED, SHOCK-CAPTURING WATERSHED MODEL FOR  
SIMULATING SPATIALLY VARIABLE RUNOFF AND SOIL EROSION  
PROCESSES AT THE HILLSLOPE SCALE

by  
Dimitrios Charalampos Dermisis

An Abstract

Of a thesis submitted in partial fulfillment  
of the requirements for the Doctor of  
Philosophy degree in Civil and Environmental Engineering  
in the Graduate College of  
The University of Iowa

December 2012

Thesis Supervisor: Professor Athanasios N. Papanicolaou

## ABSTRACT

The overarching objective of this study was the development, validation and testing of an improved watershed modeling framework that accounts for the effects of spatial heterogeneity on overland flow and erosion processes and it is computationally sound for shallow, overland flows with shock waves. Most of the existing soil erosion models determine fluxes of water and sediment with the assumption of a homogeneous hill. In these models the physical and biogeochemical properties of the heterogeneous hill are spatially averaged, without considering roughness and longitudinal curvature effects as well as differences in the land use/land cover -LU/LC- and soil properties along the hill. This issue was addressed by improving the Water Erosion Prediction Project (WEPP-Original version 2010.1) soil erosion model at the hillslope scale to account for the physics in terms of spatial heterogeneity in flow using a well-established shock-capturing numerical scheme.

The improved WEPP model, referred to as “WEPP-Improved” model was (i) validated via detailed field experiments within an experimental plot and (ii) tested via generic simulations at the hillslope scale covering a variety of scenarios in terms of topography, LU/LC and soil type. Results showed that the WEPP-Improved model could effectively simulate the unsteadiness of the flow as well as the required time (lag) for the flow rate to reach equilibrium conditions. However, the model provided only a steady-state sediment transport rate and could capture only the equilibrium conditions. Further, the WEPP-Improved model reflected the effects of curvature, LU/LC and soil type on flow, as the model did not treat the hillslope as a homogeneous unit. Based on the generic simulations, landscape variability resulted to differences in the predicted peak runoff rate,  $Q_{\text{peak}}$ , between the WEPP-Improved vs. WEPP-Original models ranging ~ 3 – 62 % (avg. 19 %) due to curvature effects only, ~ 17 – 170 % (avg. ~ 66 %) due to added effects of LU/LC variability and ~ 5 % – 200 % (avg. ~ 52 %) due to added effects of soil

type variability. The highest reported differences on the predicted  $Q_{\text{peak}}$  between the two models were attributed to the formation of the shock waves; these differences were dominant for the low in magnitude storm event and attenuated for the high event.

It is believed that if the physical processes are represented accurately at the hillslope scale using the suggested modeling framework, then by utilizing an appropriate routing scheme of the flow and sediment within the stream network, it will be possible to scale-up the flow/sediment routing from the hillslope to the watershed scale without losing the degree of heterogeneity encapsulated from different hillslopes within the drainage network.

Abstract Approved: \_\_\_\_\_  
Thesis Supervisor  
\_\_\_\_\_  
Title and Department  
\_\_\_\_\_  
Date

DEVELOPING AN IMPROVED, SHOCK-CAPTURING WATERSHED MODEL FOR  
SIMULATING SPATIALLY VARIABLE RUNOFF AND SOIL EROSION  
PROCESSES AT THE HILLSLOPE SCALE

by

Dimitrios Charalampos Dermisis

A thesis submitted in partial fulfillment  
of the requirements for the Doctor of  
Philosophy degree in Civil and Environmental Engineering  
in the Graduate College of  
The University of Iowa

December 2012

Thesis Supervisor: Professor Athanasios N. Papanicolaou

Copyright by  
DIMITRIOS CHARALAMPOS DERMISIS  
2012  
All Rights Reserved

Graduate College  
The University of Iowa  
Iowa City, Iowa

CERTIFICATE OF APPROVAL

---

PH.D. THESIS

---

This is to certify that the Ph.D. thesis of

Dimitrios Charalampos Dermisis

has been approved by the Examining Committee  
for the thesis requirement for the Doctor of Philosophy  
degree in Civil and Environmental Engineering at the December 2012  
graduation.

Thesis Committee: \_\_\_\_\_  
Athanasios N. Papanicolaou, Thesis Supervisor

\_\_\_\_\_  
Jerald Schnoor

\_\_\_\_\_  
Christopher Wilson

\_\_\_\_\_  
David Bennett

\_\_\_\_\_  
Jerry Anthony

To my beloved late uncle Professor Vasileios Dermisis who always inspired me...



When you set out on your journey to Ithaca, pray that the road is long, full of adventure,  
full of knowledge.

Konstantinos P. Kavafis, Ithaca (1911)

## ACKNOWLEDGMENTS

This dissertation has been the culmination of the research work performed for several years in the Department of Civil and Environmental Engineering, University of Iowa, U.S.A., under the supervision of Professor Thanos Papanicolaou.

No great feat is ever accomplished independent of help from others. I indulge myself now to acknowledge those individuals who have helped to make this part of my life's journey a joyous success.

Many people contributed in various degrees towards the completion of this dissertation. To begin with, I would like to express my gratitude to my advisor, Dr. Thanos Papanicolaou. His intellectual influence and professional guidance have permanently shaped my scientific character and personality. He has never ceased to amaze me with his ingenuity and enthusiasm for research. His passion, work ethic and intellectual rigorousness made and will continue to make a remarkable impact on my professional life. His demand on excellence made me better prepared for challenges that I will be soon encounter as an educator, researcher, and independent thinker. His absolute devotion to deliver high quality of research made him a tough person to work with, but it all paid off in the end. I feel I need to express my eternal appreciation to him for training me these years and for his patience, flexibility, genuine caring, concern, unconditional support and faith in me.

I would like to express my appreciation to the committee members, Dr. Jerald Schnoor, Dr. Christopher Wilson, Dr. David Bennett and Dr. Jerry Anthony for their time to read my dissertation, their valuable discussions and accessibility, their helpful comments and critiques, and the "outside of the box" perspective that they provided to my research work.

I would like also to thank Dr. Ozan Abaci who mentored and guided me over the nitty-gritty of the WEPP model and Ben Abban for helping me endless nights with the

numerical coding of WEPP as well as my colleagues Ken Wacha, Danny Moustakides, Tommy Sutarto, Achilleas Tsakiris, and Will Ettema for all their psychological support, endless brainstorming, assistance in performing these unforgettable field experiments and overall helping me to complete this dissertation. I am indebted to my colleagues for providing a stimulating and fun environment in which I learned and grew as a personality. I consider myself extremely lucky to meet these intellectual and caring people, who have helped me unconditionally during the difficult moments. Further, I would like to thank the staff in Model Annex, Tim Houser and Brandon Barquist for providing me solutions pertaining the performance of the field experiments, as well as the local farmers in the South Amana area who provided us access to their fields in order to perform the experiments.

I should not forget to thank Dr. Dennis Flanagan and Mr. Jim Frankenberger from the USDA-ARS National Soil Erosion Research Laboratory in West Lafayette, Indiana, who provided me guidance and their technical assistance concerning the WEPP numerical code as well as all the other people whose names I did not include here, but they provided me with the necessary help and made it possible for me to write this dissertation.

At this moment, I would like also to gratefully acknowledge the generous scholarship provided to me from the Alexander S. Onassis Public Benefit Foundation in Greece, at a critical moment during this journey, and allowed me to complete my research work.

A Ph.D. dissertation is not successfully completed by only having excellent professors and colleagues who are willing to help. I would like to give special thanks to my family for all the support that they provided me throughout this journey. Thank you everybody.

## ABSTRACT

The overarching objective of this study was the development, validation and testing of an improved watershed modeling framework that accounts for the effects of spatial heterogeneity on overland flow and erosion processes and it is computationally sound for shallow, overland flows with shock waves. Most of the existing soil erosion models determine fluxes of water and sediment with the assumption of a homogeneous hill. In these models the physical and biogeochemical properties of the heterogeneous hill are spatially averaged, without considering roughness and longitudinal curvature effects as well as differences in the land use/land cover -LU/LC- and soil properties along the hill. This issue was addressed by improving the Water Erosion Prediction Project (WEPP-Original version 2010.1) soil erosion model at the hillslope scale to account for the physics in terms of spatial heterogeneity in flow using a well-established shock-capturing numerical scheme.

The improved WEPP model, referred to as “WEPP-Improved” model was (i) validated via detailed field experiments within an experimental plot and (ii) tested via generic simulations at the hillslope scale covering a variety of scenarios in terms of topography, LU/LC and soil type. Results showed that the WEPP-Improved model could effectively simulate the unsteadiness of the flow as well as the required time (lag) for the flow rate to reach equilibrium conditions. However, the model provided only a steady-state sediment transport rate and could capture only the equilibrium conditions. Further, the WEPP-Improved model reflected the effects of curvature, LU/LC and soil type on flow, as the model did not treat the hillslope as a homogeneous unit. Based on the generic simulations, landscape variability resulted to differences in the predicted peak runoff rate,  $Q_{\text{peak}}$ , between the WEPP-Improved vs. WEPP-Original models ranging ~ 3 – 62 % (avg. 19 %) due to curvature effects only, ~ 17 – 170 % (avg. ~ 66 %) due to added effects of LU/LC variability and ~ 5 % – 200 % (avg. ~ 52 %) due to added effects of soil

type variability. The highest reported differences on the predicted  $Q_{\text{peak}}$  between the two models were attributed to the formation of the shock waves; these differences were dominant for the low in magnitude storm event and attenuated for the high event.

It is believed that if the physical processes are represented accurately at the hillslope scale using the suggested modeling framework, then by utilizing an appropriate routing scheme of the flow and sediment within the stream network, it will be possible to scale-up the flow/sediment routing from the hillslope to the watershed scale without losing the degree of heterogeneity encapsulated from different hillslopes within the drainage network.

## TABLE OF CONTENTS

LIST OF TABLES .....	x
LIST OF FIGURES .....	xi
LIST OF ABBREVIATIONS.....	xv
CHAPTER	
1. INTRODUCTION .....	1
1.1 Problem Statement.....	1
1.2 The role of key physical and biogeochemical parameters on runoff and soil erosion .....	3
1.3 Effects of spatio-temporal hillslope heterogeneity on spatial and time lags.....	7
1.4 Limitations of current models to reflect the effects of spatio- temporal hillslope heterogeneity.....	7
2. OBJECTIVE AND HYPOTHESIS .....	14
3. MODEL SELECTION AND LIMITATIONS .....	15
3.1 Model availability and selection criteria.....	15
3.2 WEPP model limitations.....	20
4. WEPP MODEL IMPROVEMENTS AND IMPLEMENTATION .....	25
4.1 Overland flow routing and shock formation criteria .....	25
4.2 Shock capturing schemes.....	26
4.2.1 Method of characteristics: Borah et al. (1980) .....	27
4.2.2 Finite difference: TVD MacCormack scheme .....	28
4.3 WEPP-Improved model implementation.....	31
5. FIELD EXPERIMENTS IN THE SOUTH AMANA SUB- WATERSHED.....	38
5.1 Reasoning for experimental study .....	38
5.2 Experimental set-up and instrumentation .....	39
5.2.1 Rainfall simulators.....	39
5.2.2 Soil moisture probes .....	40
5.2.3 Mapping of micro-topography .....	41
5.2.4 Measurement of flow and sediment transport rate .....	42
5.2.5 Measurement of flow depth.....	43
5.2.6 Tracers and other recordings .....	43
5.3 Experimental procedure.....	44
5.4 Results.....	46
5.4.1 Time series for flow rates, sediment discharges, and soil moisture .....	46
5.4.2 Measured vs. predicted flow rates, sediment transport rates, and flow depths.....	48

5.4.3	Tracer experiments and other recordings .....	50
6.	GENERIC SIMULATIONS TO TEST THE PERFORMANCE OF THE WEPP-IMPROVED MODEL .....	71
6.1	Selection of the input parameters .....	71
6.2	First set of scenarios: spatial heterogeneity of curvature and LU/LC .....	73
6.2.1	Homogeneous baseline conditions .....	74
6.2.2	Spatially heterogeneous hillslope conditions .....	75
6.2.3	Effects of climatic conditions .....	78
6.3	Second set of scenarios: spatial heterogeneity of curvature and soil type .....	79
6.4	Shock formation and propagation .....	80
7.	CONCLUSIONS .....	116
	REFERENCES .....	120

## LIST OF TABLES

### Table

3.1	Summary of existing soil erosion models.....	22
5.1	Flow depth measurements within the plot.....	53
5.2	Results from the tracer tests (Exp-1).....	53
5.3	Results from the tracer tests (Exp-2).....	54
6.1	Input data for the 2 LU/LC.....	84
6.2	Compositions of TAMA and DOWNS soil types.....	85
6.3	The first set of simulations to address the effects of LU/LC heterogeneity.....	85
6.4	Water balance for first set of scenarios.....	86
6.5	Summary table for the first set of scenarios (low rainfall intensity).....	88
6.6	The second set of scenarios to address the effects of soil type heterogeneity.....	89
6.7	Water balance for second set of scenarios.....	90
6.8	Summary table for the second set of scenarios (LU/LC = NTC-FTB).....	92
6.9	Summary table for the second set of scenarios (LU/LC = Bromegrass).....	93



## LIST OF FIGURES

### Figure

1.1	Maps of (a) Locations exceeding soil tolerance rate in the U.S.; (b) Average soil erosion in the state of Iowa; (c) Monitoring stations within the Clear Creek Watershed, IA.....	10
1.2	Definition sketch of surface micro-roughness types.....	11
1.3	Soil aggregates.....	11
1.4	Rill and interrill areas during erosion experiments at the hillslope scale. ....	12
1.5	Curvature variability in the South Amana Sub-Watershed (SASW), IA .....	12
1.6	Qualitative sketches of curvature effects on the erosion/deposition patterns along the downslope distance of a hill.....	13
3.1	Schematic representation of WEPP-Original components .....	23
3.2	WEPP-Original results from hypothetical, single storm, hillslope-scale simulations highlighting model's limitations for accounting curvature effects .....	24
4.1	Qualitative sketch of the outflow hydrograph and water surface profile (WSP) of a hill showing (a) formation of a shock due to the concave hillslope profile and (b) non-formation of shocks due to uniform hillslope .....	34
4.2	Example of shock formation.....	35
4.3	(a) Shock wave interaction in the space-time domain using the MOC and (b) instabilities in the simulated hydrograph at the outlet of the uniform hillslope profile shown in Figure 4.1b having different management practices .....	36
4.4	WEPP-Improved model implementation: routing of the overland flow .....	37
5.1	The experimental station within the South Amana Sub-Watershed located in the Clear Creek watershed, IA.....	55
5.2	The time series of the tipping bucket data located nearby the Experimental Station within the South Amana Sub-Watershed located in the Clear Creek watershed, IA.....	55
5.3	The 3 rainfall simulators placed in series located in the Experimental Station.....	56
5.4	Water tanks used to store the excess water from the return pipe in the rainfall simulator .....	56
5.5	Checking the pressure in the pipes during the experiment using binoculars.....	57
5.6	Water content reflectometer.....	57

5.7	The two laser diodes (due to the camera area of view only one is shown in the picture) generating a single beam on the surface (see red dashed line).....	58
5.8	(a) The camera used in the laser system; (b) the connectors in the back of the camera.....	58
5.9	The R3-CL frame grabber board .....	58
5.10	The laser carriage.....	59
5.11	(a) Calibration fixture with the LED light-bar; (b) camera view of the LED's in the light-bar; (c) laser beam projected on the soil surface.....	59
5.12	The weir at the plot outlet with the measured tapes to record the flow depth. Figure at the top right corner illustrates the flow depth at the weir during the experiment .....	60
5.13	The board side walls along the perimeter of the plot.....	60
5.14	A thin strip of the entrance covered with sprinkles of Portland concrete cement.....	61
5.15	Flow depth measurements during the experiment.....	61
5.16	The spray painted areas (red, white, blue) and the cross-sections (orange rope) indicating the locations for the flow depth measurements (looking downslope) .....	62
5.17	The rhodamine pills used as tracers.....	62
5.18	Video recording of the experiments via a video-camera placed at the plot outlet .....	63
5.19	Still images taken during the experiments.....	63
5.20	The Honda 1.5 Hp tiller used to till the soil.....	63
5.21	The plot set-up before the beginning of the experiment.....	64
5.22	The experimental plot covered with a tarp .....	64
5.23	Time series results for (a) flow rate, (b) soil moisture and (c) sediment flux for Exp-1 (low rainfall intensity).....	65
5.24	Time series results for (a) flow rate, (b) soil moisture and (c) sediment flux for Exp-2 (high rainfall intensity).....	66
5.25	Splash erosion.....	67
5.26	Comparison of the flow rates between measured vs. WEPP-Improved model for Exp-1 (low rainfall intensity).....	67
5.27	Comparison of the flow rates between measured vs. WEPP-Improved model for Exp-2 (high rainfall intensity).....	68

5.28	Comparison of the sediment fluxes between measured vs. WEPP-Improved model for Exp-1 (low rainfall intensity) .....	68
5.29	Comparison of the sediment fluxes between measured vs. WEPP-Improved model for Exp-2 (high rainfall intensity) .....	69
5.30	Rhodamine pills used during the experiment .....	69
5.31	Milk dye tracer applied during the progression of the experiment .....	70
5.32	Illustration of spray-painted areas during Exp-1 (red-summit, white-backslope, blue-toeslope) .....	70
6.1	The low (top) and high (bottom) single storm events used in the generic simulation .....	94
6.2	The examined hillslope profiles: (a) uniform; (b) concave; (c) convex. The colors at location B, C match the colors of the hydrographs in figures 6.3-6.18 .....	95
6.3	Runoff hydrographs for Sc-1 (OFE <sub>1</sub> : NTC-FTB, OFE <sub>2</sub> : NTC-FTB) for the low rainfall event and for the convex, uniform, and concave hillslopes .....	96
6.4	Runoff hydrographs for Sc-2 (OFE <sub>1</sub> : Bromegrass, OFE <sub>2</sub> : Bromegrass) for the low rainfall event and for the convex, uniform, and concave hillslopes .....	97
6.5	Runoff hydrographs for Sc-3 (OFE <sub>1</sub> : NTC-FTB, OFE <sub>2</sub> : Bromegrass) for the low rainfall event and for the convex, uniform, and concave hillslopes .....	98
6.6	Runoff hydrographs for Sc-4 (OFE <sub>1</sub> : Bromegrass, OFE <sub>2</sub> : NTC-FTB) for the low rainfall event and for the convex, uniform, and concave hillslopes .....	99
6.7	Runoff hydrographs for Sc-1 (OFE <sub>1</sub> : NTC-FTB, OFE <sub>2</sub> : NTC-FTB) for the high rainfall event and for the convex, uniform, and concave hillslopes .....	100
6.8	Runoff hydrographs for Sc-2 (OFE <sub>1</sub> : Bromegrass, OFE <sub>2</sub> : Bromegrass) for the high rainfall event and for the convex, uniform, and concave hillslopes .....	101
6.9	Runoff hydrographs for Sc-3 (OFE <sub>1</sub> : NTC-FTB, OFE <sub>2</sub> : Bromegrass) for the high rainfall event and for the convex, uniform, and concave hillslopes .....	102
6.10	Runoff hydrographs for Sc-4 (OFE <sub>1</sub> : Bromegrass, OFE <sub>2</sub> : NTC-FTB) for the high rainfall event and for the convex, uniform, and concave hillslopes .....	103
6.11	Runoff hydrographs for Sc-5 (OFE <sub>1</sub> : TAMA, OFE <sub>2</sub> : TAMA) and for the convex, uniform, concave hillslopes. LU/LC is NTC-FTB in both OFEs .....	104
6.12	Runoff hydrographs for Sc-6 (OFE <sub>1</sub> : DOWNS, OFE <sub>2</sub> : DOWNS) and for the convex, uniform, concave hillslopes. LU/LC is NTC-FTB in both OFEs .....	105
6.13	Runoff hydrographs for Sc-7 (OFE <sub>1</sub> : TAMA, OFE <sub>2</sub> : DOWNS) and for the convex, uniform, concave hillslopes. LU/LC is NTC-FTB in both OFEs .....	106
6.14	Runoff hydrographs for Sc-8 (OFE <sub>1</sub> : DOWNS, OFE <sub>2</sub> : TAMA) and for the convex, uniform, concave hillslopes. LU/LC is NTC-FTB in both OFEs .....	107

6.15	Runoff hydrographs for Sc-5 (OFE <sub>1</sub> : TAMA, OFE <sub>2</sub> : TAMA) and for the convex, uniform, concave hillslopes. LU/LC is Bromegrass in both OFEs.....	108
6.16	Runoff hydrographs for Sc-6 (OFE <sub>1</sub> : DOWNS, OFE <sub>2</sub> : DOWNS) and for the convex, uniform, concave hillslopes. LU/LC is Bromegrass in both OFEs.....	109
6.17	Runoff hydrographs for Sc-7 (OFE <sub>1</sub> : TAMA, OFE <sub>2</sub> : DOWNS) and for the convex, uniform, concave hillslopes. LU/LC is Bromegrass in both OFEs.....	110
6.18	Runoff hydrographs for Sc-8 (OFE <sub>1</sub> : DOWNS, OFE <sub>2</sub> : TAMA) and for the convex, uniform, concave hillslopes. LU/LC is Bromegrass in both OFEs.....	111
6.19	Water surface profile for Sc-2 (low magnitude event, concave profile, Bromegrass and TAMA soil for both OFEs).....	112
6.20	Water surface profile for the equivalent, uniform slope profile (low magnitude event, Bromegrass and TAMA soil for both OFEs) .....	112
6.21	Water surface profile for Sc-2 (low magnitude event, convex profile, Bromegrass and TAMA soil for both OFEs).....	113
6.22	Water surface profile for Sc-3 (low magnitude event, uniform profile, NTC-FTB/Bromegrass and TAMA soil for both OFEs) .....	113
6.23	Water surface profile for Sc-4 (low magnitude event, uniform profile, Bromegrass/NTC-FTB and TAMA soil for both OFEs).....	114
6.24	Water surface profile for Sc-7 (low magnitude event, uniform profile, TAMA/DOWNS and Bromegrass soil for both OFEs).....	114
6.25	Water surface profile for Sc-8 (low magnitude event, uniform profile, DOWNS/TAMA and Bromegrass soil for both OFEs).....	115

## LIST OF ABBREVIATIONS

$A$  = cross-sectional area ( $\text{m}^2$ )

$ah$  = denotes flow conditions ahead of the shock

$A_r$  = fraction of the total area in rills (-)

$b$  = coefficient based on the soil organic matter and clay contents (-)

$bh$  = denotes flow conditions behind the shock

$C$  = Chezy coefficient ( $\text{m}^{0.5}/\text{s}$ )

$c$  = corrector step for TVD MacCormack scheme

$C(Cr_i)$  = parameter for TVD MacCormack scheme

$C_{br}$  = adjustment factor for buried residue (-)

$c_i$  = celerity ( $\text{m}/\text{s}$ )

$C_L$  = spatial-lag coefficient (m)

$Cr_i$  = Courant number (-)

$D_i$  = interrill erosion independent of  $x$  ( $\text{kg}/\text{s}/\text{m}^2$ )

$F$  = cumulative infiltration depth (m)

$f$  = infiltration rate ( $\text{m}/\text{s}$ )

$f_{eq}$  = equivalent friction factor (-)

$f_i$  = interrill friction factor (-)

$f_r$  = rill friction factor (-)

$g$  = acceleration due to gravity ( $\text{m}/\text{s}^2$ )

$G$  = sediment load ( $\text{kg}/\text{s}/\text{m}$ )

$G(r_i)$  = parameter for TVD MacCormack scheme

$G_r$  = sediment load in rills ( $\text{kg}/\text{s}/\text{m}$ )

$h$  = overland flow depth (m)

$H_w$  = flow depth at the weir (m)

$i$  = subscript that denotes space in the kinematic wave equation

$j$  = subscript that denotes time in the kinematic wave equation

$K_e$  = effective hydraulic conductivity (m/s)

$k_r$  = rill erodibility (s/m)

$K_{sat}$  = saturated hydraulic conductivity (m/s)

$OR$  = oriented roughness (m)

$p$  = predictor step for TVD MacCormack scheme

$Q$  = overland flow discharge ( $m^3/s$ )

$Q$  = overland flow discharge ( $m^3/s$ )

$q$  = overland flow unit discharge ( $m^2/s$ )

$q_l$  = lateral flow rate (m/s)

$Q_{peak, WEPP-Improved}$  = predicted peak runoff rate from WEPP-Improved model ( $m^3/s$ )

$Q_{peak, WEPP-Original}$  = predicted peak runoff rate from WEPP-Original model ( $m^3/s$ )

$r$  = rainfall rate (m/s)

$R_c$  = cumulative rainfall since last tillage (m)

$r_i$  = ratio of successive gradients (-)

$RR$  = random roughness (m)

$RR_i$  = random roughness immediately after tillage (m)

$RR_t$  = random roughness at time  $t$  (m)

$S_d$  = depression storage (m)

$S_o$  = average OFE slope (m/m)

$t$  = denotes time (s)

$t_c$  = corrected time for ponding (s)

$T_c$  = transport capacity (kg/s/m<sup>2</sup>)

$T_{c,r}$  = transport capacity of the rill (kg/s/m<sup>2</sup>)

$TVD$  = dissipative term (m<sup>2</sup>)

$u$  = wave speed (m/s)

$v$  = rainfall excess rate (m/s)

$x$  = longitudinal direction

$\alpha$  = depth-discharge coefficient (-)

$\Delta t$  = time step (s)

$\Delta x$  = space interval (m)

$\theta$  = OFE slope angle (deg)

$\theta_w$  = angle of weir opening (deg)

$\mathfrak{D}_d$  = soil moisture deficit (m/m)

$\rho$  = water density (kg/m<sup>3</sup>)

$\tau_{c,r}$  = critical shear stress in the rill (Pa)

$\tau_{crk}$  = critical shear stress in the rill (Pa)

$\tau_r$  = applied flow shear stress in the rill (Pa)

$\tau_r$  = applied flow shear stress in the rill (Pa)

$\varphi(r_i)$  = flux limiter parameter for TVD MacCormack scheme (-)

$\Psi$  = average capillary potential (m)

## CHAPTER 1

### INTRODUCTION

#### 1.1 Problem statement

Soil erosion is a major soil degradation process as it affects the “skin” of earth with direct effects on soil quality and productivity by the breakdown of the soil structure and the reduction of nutrients, organic matter, and soil biota (e.g., Pimentel et al., 1995; de Vente et al., 2008). Human activity has greatly accelerated the rate of soil erosion. The increased demand for land-based resources has led to rapid changes of land use and land cover (LU/LC) through intense cultivation, urbanization, and infrastructural development (VanOost et al., 2009; Verheijen et al., 2009). It is estimated that 90% of U.S. cropland is losing soil above the tolerance rate, i.e., the maximum rate of annual soil erosion that will permit high crop productivity for an indefinite period of time (Pimentel et al., 1995; USDA, 2009) (Figure 1.1a). In a recent report by Cox et al. (2011), soil loss from certain croplands in Iowa was found to be up to 12 times higher than the estimated tolerance rate (Figure 1.1b). Moreover, the annual cost of erosion related problems in the U.S. is estimated to be between \$60 and \$100 billion (Cox et al., 2011). In addition to the loss of arable lands, soil erosion drastically lowers water quality as overland flow and erosion enhance the transport of dissolved chemicals and sediment-borne pollutants from the upland areas into the stream network (e.g., Lal and Stewart, 1994; Loperfido et al., 2010).

Several researchers (e.g., Merz and Bardossy, 1998; Papanicolaou et al., 2008) have reported significant spatial and temporal heterogeneity of key physical and biogeochemical parameters (e.g., topography, LU/LC, soil type, soil organic matter or SOM) at both the hillslope (< 10 ha) and watershed (> 8,000 ha; Zielinski, 2002) scales, which affects soil erosion discussed in section 1.2. Monitoring of flow and sediment transport across different spatial scales can be both costly and time-intensive by requiring



multiple sampling locations (Figure 1.1c) and frequent sampling periods (WATERS Network, 2008). In order to analyze the underlying flow and soil erosion processes and their interactions in hillslopes and watersheds, mechanistic soil erosion simulation models have become a necessary tool. In this study the emphasis is on the erosion models applicable up to the hillslope scale (1-10 ha; Zielinski, 2002), which is considered a representative scale unit for understanding better runoff and soil erosion processes (e.g., Woods et al., 1995). Hillslope (and watershed) scale erosion models are classified in terms of the:

(1) Time scale, for which are divided into *event* based, if they are used to simulate a single-storm event, and *continuous*, if they are used for a consecutive number of events occurring during a long period of time;

(2) Spatial variability of the input parameters, for which are divided into *lumped* models, which use single values of input parameters with no spatial variability, and *distributed*, which use spatially distributed parameters;

(3) Parameterization, for which are divided into *empirical*, which are developed mainly from parametric analysis of hydrologic/erosion data; *conceptual*, which represent a watershed as a system of storage units; and *physical*, which employ fundamental, physical equations.

However, most of the aforementioned models determine fluxes of water and sediment (i.e., runoff and sediment yield) with the assumption of a homogeneous hill. In these models the physical and biogeochemical properties of the heterogeneous hill are spatially averaged, without considering roughness and longitudinal curvature effects, as well as differences in the soil properties along the slope profile i.e., summit, shoulder, backslope, and toeslope (e.g., Wood et al., 1988; Stone et al., 1995; Merz and Bardossy, 1998). Under this assumption, an error may be introduced in the calculation of the overland flow depth, soil erosion/deposition along the hill and sediment yield at the hill outlet that exceeds 100% (e.g., Rieke-Zapp and Nearing, 2005; Jomaa et al., 2012). In

addition, some of these models do not account for sediment deposition within a hillslope but only for gross erosion and do not differentiate flow between rill and interrill areas (Hairsine and Rose, 1992a, b).

Due to the reported spatial heterogeneity in the key physical and biogeochemical parameters along a hillslope, there is a critical need for the development of physically based, distributed erosion models (e.g., Foster and Meyer, 1975; Moore and Burch, 1986; Nearing et al., 1990; Tucker et al., 2001; Coulthard et al., 2007). Such models are needed to: (1) simulate spatially variable hydrologic and soil erosion processes governed by different terrain attributes; (2) identify critical areas that contribute significantly to soil erosion (i.e., “hotspot” areas); and (3) assess optimal locations and number of Best Management Practices (BMPs) for controlling runoff and tillage-induced soil erosion (e.g., Fiener and Auerswald, 2006; Dermisis et al., 2010).

## 1.2 The role of key physical and biogeochemical parameters on runoff and soil erosion

Spatial heterogeneity along a hillslope can be attributed to variability of: (1) landscape topographic features (e.g., soil surface micro-roughness and macro-roughness); (2) LU/LC (e.g., bromegrass, corn, bean, conventional vs. conservation tillage); and (3) soil types (e.g., different soil texture at different hillslope position- summit vs. toeslope) (e.g., Foster and Meyer, 1975; Moore and Burch, 1986; and Nearing et al., 1990). The role of each of parameter as it affects runoff and soil erosion is discussed in detail.

Soil surface micro-roughness describes the variations in the soil surface elevation and is categorized as: (1) *Clod or Random Roughness (RR)* related to surface variations from cloddiness (Taconet et al., 2010; Rodriguez et al., 2011) (0-100 mm); and (2) *Tillage or Oriented Roughness (OR)* related to systematic differences in elevations from tillage implements (0-300 mm) (e.g., Papanicolaou and Dermisis, 2011) (Figure 1.2). Along a hillslope transect, *RR* mostly forms randomly over both interrill and rill areas by

the interaction of rainfall and soil aggregates (i.e., many fine particles held together in a single mass or cluster) (Figure 1.3) and has variable elevation. For clarity, interrill areas are places where erosion causes particle detachment due to raindrop impact (splash erosion) and transport by shallow overland flow (sheetwash), whereas rill areas are the places where the erosion is triggered by concentrated overland flow within small channels called rills (Figure 1.4). The *OR* denotes the roughness in-between the neighboring interrill areas and has relatively constant, average amplitude and wavelength, as it is mainly affected by the tillage practices (e.g., Romkens and Wang, 1986). Numerous field and laboratory studies have provided evidence that soil surface micro-roughness affects both overland flow hydraulics and soil erosion processes. Thompson et al. (2010) showed that micro-topography affects the partitioning in rainfall-runoff, since micro-topography increased markedly the proportion of rainfall infiltrating within the soil column. Finkner (1988) and Gilley and Finkner (1991) performed field experiments and produced empirical formulas that relate soil surface micro-roughness with hydraulic roughness (or flow resistance) expressed via the flow friction factor,  $f_f$ , or the Chezy's coefficient,  $C$ . Due to the shallow, overland flow conditions, surface micro-roughness may be comparable to and often larger than the overland flow depth (i.e., partial submergence), which is associated with high values of flow resistance (e.g., Lawrence, 1997; Lawrence, 2000; Smith et al., 2011).

Further, recent studies have shown that micro-roughness plays an important role on sediment yield and rill network development (e.g., Helming et al., 1998; Romkens et al., 2002; Gomez et al., 2003; Gomez and Nearing, 2005), as well as on the time to initiate runoff, since additional time is required to fill the depressions in the case of a rough vs. a smooth surface (Onstad, 1984; Chu et al., 2012). Effects of surface micro-roughness on soil erosion may be amplified or de-amplified based on the magnitude and duration of the storm event (Romkens et al., 2002; Thomson et al., 2010) and the overall gradient of the soil surface (Gomez and Nearing, 2005).

Macro-roughness, such as profile curvature (Figure 1.5), has significant effects on runoff along the longitudinal direction of the hill. Profile curvature determines the routing of surface runoff and delivery of soil. Limited but nonetheless valuable field (e.g., Young and Mutchler, 1969; Huang et al., 2002) and laboratory (e.g., Rieke-Zapp and Nearing, 2005; Hancock et al., 2006) studies have provided quantitative measurements highlighting the importance of the role of landscape profile curvature on runoff and soil delivery. These studies have shown that concave hillslopes produced the least runoff volume and sediment yield at the hill outlet compared to the uniform or convex hillslopes. It is believed that as the slope of the convex hill increases downhill, the runoff velocity tends to increase, allowing less infiltration and thus increasing the amount of runoff and soil loss (Young and Mutchler, 1969). However, concave hillslopes may result on the formation of shock waves due to their topographical shape, i.e., longitudinal slope changes from steep to mild (e.g., Kibler and Woolhiser, 1972; Borah et al., 1980). Shock waves are characterized by the formation of vertical, sharp wave fronts, resulting in localized, abrupt changes of the water surface profile (flow discontinuities), flow depth and flow shear stress (e.g., Borah et al., 1980; Nikora et al., 2007). Further, profile curvature may have a significant impact on the erosion/deposition patterns along the hill (Moore and Burch, 1986; Schmidt, 1992) (Figure 1.6) and on the spatial distribution of rills and partitioning of the flow (e.g., Rieke-Zapp and Nearing, 2005).

In the case of agricultural hillslopes, land use and associated management practices have profound influence on residue quantity/quality, decomposition rates of SOM, soil surface micro-roughness and ultimately the magnitude of soil erosion rates (e.g., Chenu et al., 2000; Gilley et al., 2002; Moorman et al., 2004; Lal, 2005; Abaci and Papanicolaou, 2009). For example, tillage brings subsurface soil to the surface, exposing it to weathering, thereby increasing the susceptibility of aggregates to detachment and thus increasing soil erosion (Beare et al., 1994; Paustian et al., 1997, 2000). Prolonged

application of conventional tillage reduces net primary productivity (and ultimately SOM) by increasing mineralization rates (e.g., Moorman et al., 2004). Conversely, conservation tillage enhances SOM by increasing residue cover and water holding capacity, and therefore improves soil quality (e.g., Lal, 2005). Along the same lines, residue cover has been found to reduce the initial dislodgement of grains due to raindrop impact in interrill areas and reduce the erodibility factor, i.e., an index that defines the rate at which erosion occurs (e.g., Gilley et al., 2002). Finally, recent studies (e.g., Dermisis et al., 2010) have shown that introduction of grassed waterways (GWWs) at the bottom of the hill may affect significantly the runoff volume and associated peak runoff rates depending on the hydrologic conditions and the topography of the contributing hills.

The variability in the soil types along the hill is associated with differences in the (1) soil texture, SOM, bulk density (i.e., intrinsic soil properties) and (2) erodibility and critical erosion strength (reflecting the ability of the soil to resist erosion) along the hill. The intrinsic soil properties in conjunction with the effects of the LU/LC and precipitation (i.e., extrinsic factors) (e.g., Tietje and Richter, 1992; Papanicolaou et al., 2008; West et al., 2008) affect the saturated hydraulic conductivity of the soil,  $K_{sat}$ .  $K_{sat}$  is a key variable in hydrogeologic studies and is used as a dynamic index for assessing the amount of runoff and eroded surface soil that are delivered to local waterways, thereby affecting both in-field soil quality and in-stream water quality (e.g., Potter, 1990; Nearing et al., 1996; Schoeneberger and Wysocki, 2005). Finally, differences in the erodibility and critical erosional strength have drastic effects on the amount of the eroded soil.

Although there is significant research work on isolating the effects of each individual key physical and biogeochemical parameters on overland flow and soil erosion, it is still unclear how the combined effects of these parameters, as well as their spatial distribution along the landscape, may ultimately affect rainfall-runoff and soil transport processes.

### 1.3 Effects of spatio-temporal hillslope heterogeneity on spatial and time lags

Landscape heterogeneity of the key physical and biogeochemical parameters may have a significant impact on the intermittent behavior of the runoff and soil delivery at the hill, expressed via spatial and temporal lag coefficients mathematically accounted in mass balance equations. The spatial and temporal lags express the “degree of readiness” of the hillslope system to respond immediately to changes in the runoff conditions, and specify a characteristic distance and time, respectively, for water drops and soil particles to adjust from non-equilibrium to equilibrium conditions. The effects of the lags triggered by the non-linear interactions of flow and soil have been off-set or “closed” mathematically by incorporating a lag coefficient,  $C_L$ , into the 1-D steady-state sediment continuity equation (e.g., Philips and Sutherland, 1989, 1990; Rahuel et al., 1989; Jain, 1992; Wu, 2007) such as:

$$\frac{\partial G(x)}{\partial x} = C_L (T_c - G(x)) \quad (1.1)$$

where,  $G(x)$  is the local soil particle discharge,  $T_c$  is transport capacity (i.e., the maximum amount of soil that the flow can “carry” without net deposition and erosion), and  $C_L$  is a spatial lag coefficient which has dimensions of reciprocal length. The inverse of  $C_L$  is a measure of the lag distance between the local and equilibrium soil/sediment transport rates and can vary from a couple of meters up to hundreds of meters depending on the applied flow conditions (Jain, 1992).

#### 1.4 Limitations of current models to reflect the effects of spatio- temporal hillslope heterogeneity

Current distributed parameter models use as inputs spatially variable physical and biogeochemical properties along the hillslope through the form of different Geographic Information System (GIS) layers (Cochrane and Flanagan, 1999; Vieux, 2004).

However, these models lack the physical processes in their formulation to account for the collective effects and interplay of key properties that vary in space and time within the hillslope continuum. One should consider that overland flows and constituent transport over erodible surfaces is challenging to model due to shallow flow environments, protruding effects of clods, surface tension, hyper-concentrated flows etc. Some notable limitations of modeling approaches which this dissertation addresses are that current models do not:

1. Handle numerical instabilities and shock waves introduced when simulating shallow flow conditions in conjunction with the presence of (i) discontinuities on the slope of the land surface topography and/or in the hydraulic roughness due to variability in LU/LC and (ii) sudden localized changes due to the presence of depressions. These numerical instabilities may cause violation of the flow continuity equation and lead to erroneous results (Borah et al., 1980; Jirka and Uijtewaal, 2004).

2. Adequately account for the role of turbulence on sediment movement. It is still unknown how turbulent flow characteristics may be affected by the soil surface micro-roughness and the hillslope curvature (e.g., Bell et al., 1989; Lu et al., 2001; Papanicolaou et al., 2004).

3. Account for the complexity in the overland flow hydraulics arising from the partial or marginal protrusion (i.e., partly or marginally submerged to the flow) of the aggregated clods or the vegetation, which affects flow frictional characteristics. Partial or marginal protrusion is more pronounced in the interrill areas where runoff “meanders” around soil clods, resulting in 2-d and 3-d sheet flow, whereas in the rills flow

concentrates in narrow micro-channels, resulting in 1-d and 2-d concentrated flow (e.g., Lawrence, 2000). Differences in the flow frictional characteristics between the interrill and rill areas affect the partitioning of flow and consequently the spatial variability of soil erosion processes over the hillslope (e.g., Kavvas et al., 2006).

4. Provide hydrographs as well as sedigraphs by accounting for the temporal variability of flow and soil erosion processes due to intra-storm flow dynamics. Most models do not account for the non-stationarity (or time lag) in the erosion process and use a steady-state form of the sediment continuity equation to describe the movement of sediment (e.g., Foster et al., 1995).

5. Simulate cohesive sediment transport, i.e., use of the appropriate formulas for determining (i) critical erosional strength, which is controlled by soil properties such as soil organic matter, clay mineralogy, soil water content, pH of the pore fluid; (ii) soil erodibility, which is affected by soil properties; (iii) sediment-transport capacity which are predominately developed for river flows and not for interrill or rill flows. The transport of cohesive sediment may increase the amounts of fine material, leading to a high suspended sediment concentration affecting the viscosity of the water-sediment mixture and the flow velocity.

6. Update the particle size distribution of the chemically-active fine sediment particles (i.e., % organics, clay, silt, sand) due to selective deposition of coarser particles and aggregates (e.g., Katopodes and Bradswa, 1999).



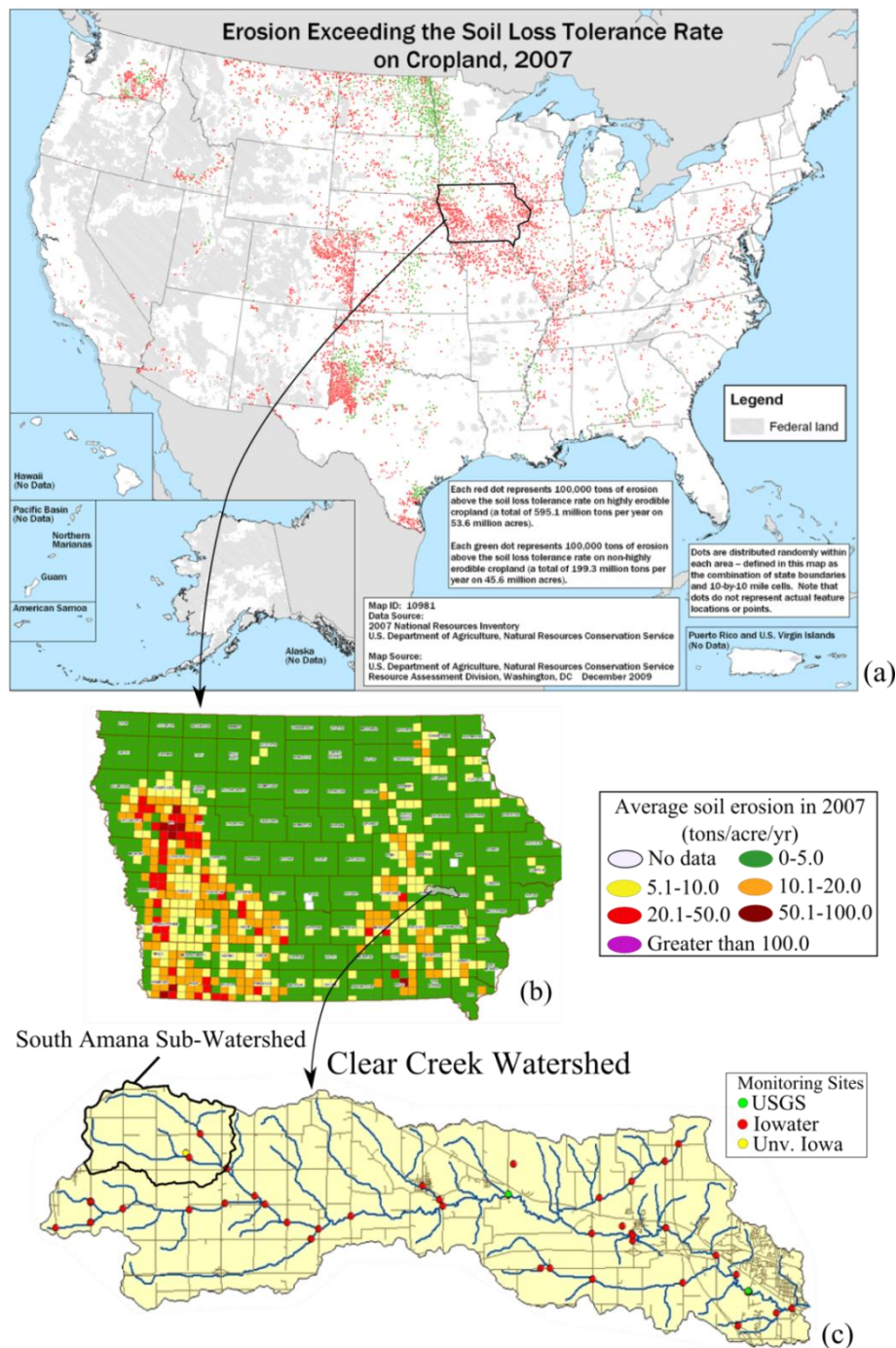


Figure 1.1 Maps of:

- (a) Locations exceeding soil tolerance rate in the U.S.;
- (b) Average soil erosion in the state of Iowa;
- (c) Monitoring stations within the Clear Creek Watershed, IA.

Source: USDA, 2009, *Summary Report: 2007 National Resources Inventory*, Ames, Iowa (Figure 1.1a); and Cox et al., 2011, *Losing ground*, Washington, DC (Figure 1.1b).

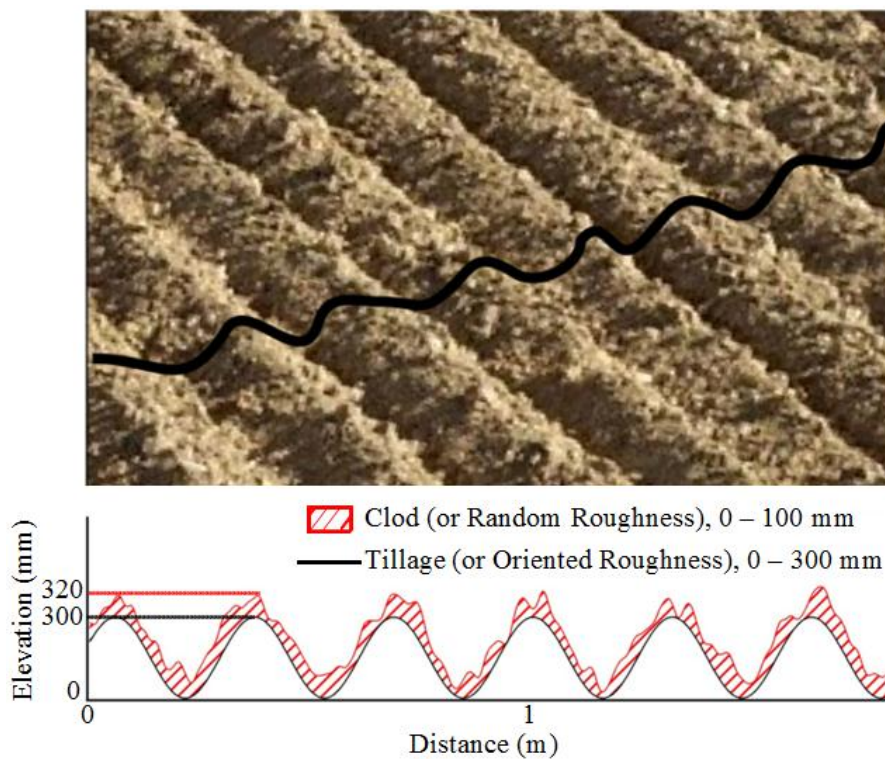


Figure 1.2 Definition sketch of surface micro-roughness types.

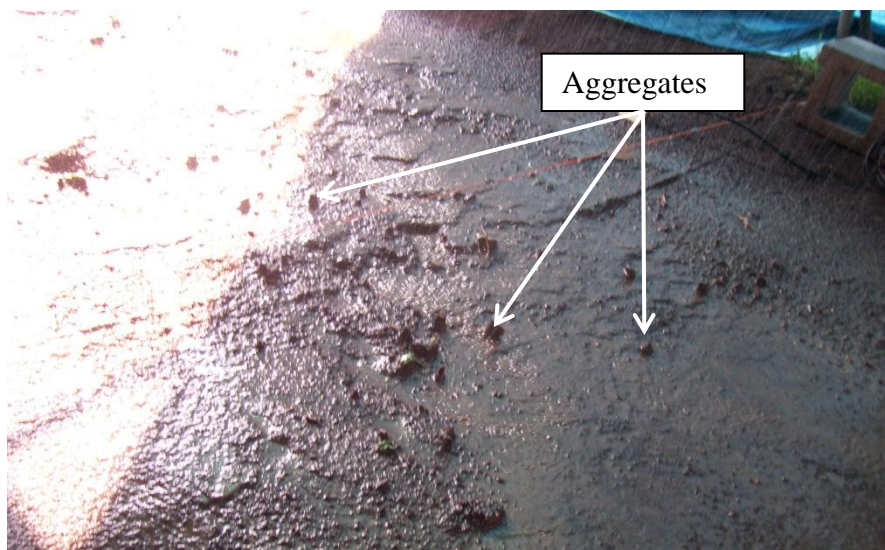


Figure 1.3 Soil aggregates.

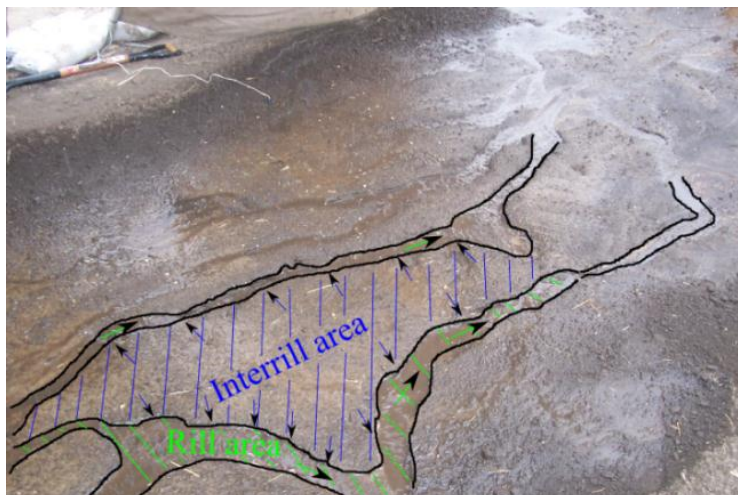


Figure 1.4 Rill and interrill areas during erosion experiments at the hillslope scale.

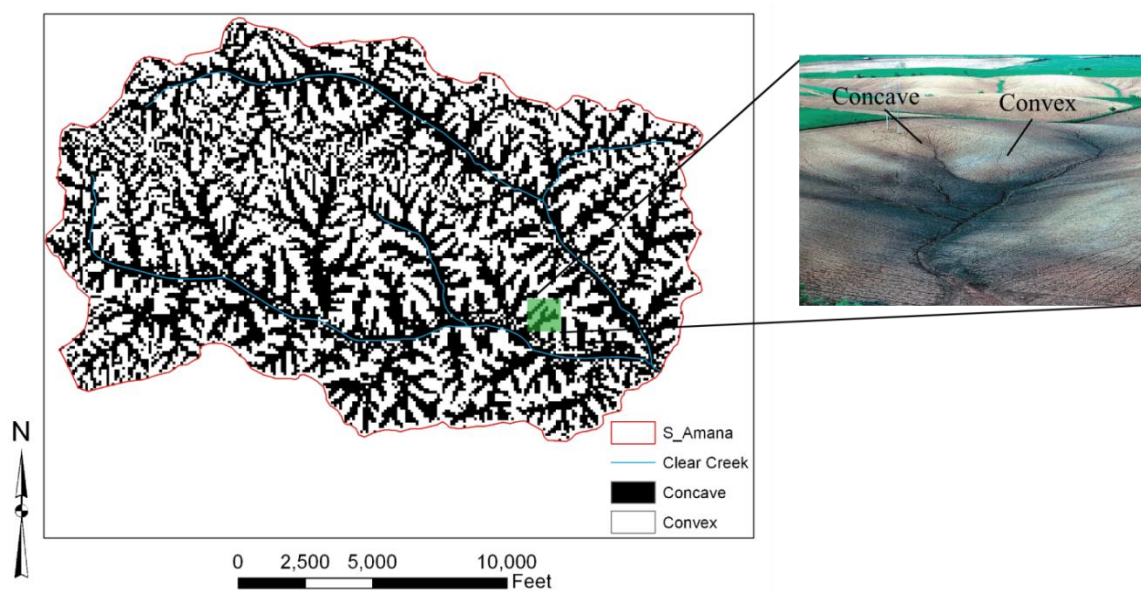


Figure 1.5 Curvature variability in the South Amana Sub-Watershed (SASW), IA.

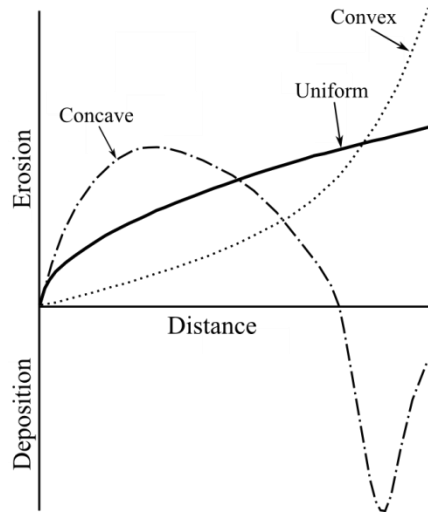


Figure 1.6 Qualitative sketches of curvature effects on the erosion/deposition patterns along the downslope distance of a hill.

---

Source: Toy et al., 2002, *Soil erosion: Processes, prediction, measurement, and control*, Wiley, New York.

## CHAPTER 2

### OBJECTIVES AND HYPOTHESIS

The overarching objective of this study is to develop and validate an improved watershed modeling framework that accounts for the effects of spatial heterogeneity on overland flow and erosion processes. The improved model overcomes some limitations of existing erosion models in terms of heterogeneity and it is computationally sound for shallow, overland flows with shock waves. If the physical processes of runoff are represented accurately at the hillslope scale, then by using an appropriate routing scheme of the flow and sediment within the stream network, it will be possible to scale-up the flow/sediment routing from the hillslope (small) to the watershed (large) scale without losing the degree of heterogeneity encapsulated from different hillslopes within the drainage network.

In the proposed study it is hypothesized that spatial heterogeneity of the landscape, in terms of the key physical and biogeochemical properties, affects the response of overland flow over erodible surfaces as well as the soil erosion rates through a cascade of different phase processes and interactions. The underlying assumption investigated herein is that the response and transport of overland flow and soil erosion depends on the degree of spatial heterogeneity exhibited by key properties at different locations along the hill (i.e., high roughness at the top vs. bottom of the hill) in concert to climatic drivers (i.e., low vs. high in magnitude storm event). Transport of water and its pollutants and their path-lines are strongly dependent on the probability of exceedance that climatic forcing exhibits in relation to thresholds of some of the key properties. If forcing barely supersedes the thresholds, then intermittent movement occurs. However, if the forcing is significantly greater than the thresholds, then general movement occurs as the lag times reduce considerably. To address this hypothesis two experiments were performed corresponding to intermittent and general movement.

## CHAPTER 3

### MODEL SELECTION AND LIMITATIONS

#### 3.1 Model availability and selection criteria

Numerous soil erosion models have been developed over past decades that simulate hydrologic and soil erosion processes at hillslope and watershed scales (Jetten et al., 1999; Aksoy and Kavvas, 2005). These models are based on an *empirical*, *conceptual*, or *physical* framework. Empirical models, such as the Universal Soil Loss Equation (USLE; Wischmeier and Smith, 1978) and Agricultural Nonpoint Source Pollution model (AGNPS; Young et al., 1989), are developed mainly from parametric analysis of hydrologic/erosion data. Conceptual models, such as the Simulator for Water Resources in Rural Basins (SWRRB; Arnold et al., 1990) and Large-Scale Catchment Model (LASCAM; Sivapalan et al., 2002), represent a watershed as a system of storage units. Finally, physically based models, such as the Kinematic Runoff and Erosion Model (KINEROS; Smith et al., 1995), Channel-Hillslope Integrated Landscape Development (CHILD; Tucker et al., 2001), and Cellular Automaton Evolutionary Slope and River model (CAESAR; Coulthard et al., 2007) employ fundamental, physical equations to simulate hydrologic and soil erosion processes.

Previous models that simulate erosion processes at the hillslope scale, which is the central theme in this thesis, include ones which simulate either interrill erosion (due to rainsplash and sheet flow) (e.g., Gilley et al., 1985; Hairsine and Rose, 1992a; Wicks and Bathurst, 1996 (SHESED); Gabet and Dunne, 2003; Jomaa et al., 2010); or rill erosion (due to concentrated flow) (e.g., Hairsine and Rose, 1992b; Lewis et al., 1994 (PRORIL); Favis-Mortlock et al., 1998 (RILLGROW); Nord and Esteves, 2007 (PSEM\_2D); Papanicolaou et al., 2010 (RILL1D)). Recently, there is a need to incorporate both interrill and rill flows and soil transport processes when simulating upland erosion at the hillslope scale (e.g., Flanagan and Nearing, 1995 (WEPP); Smith et

al., 1995 (KINEROS2); Thornes et al., 1996 (MEDALUS); Morgan et al., 1998 (EUROSEM); Di Stefano et al., 2000 (improved RUSLE); Tucker et al., 2001 (CHILD); Adams and Elliott, 2006 (SHETRAN); Kavvas et al., 2006 (WEHY); Liu et al., 2006; Bonilla et al., 2007 (PALMS); Tayfur, 2007; Deng et al., 2008; An and Liu, 2009). Table 3.1 provides a summary of some of the available erosion models and their capabilities.

One physical, upland erosion model that accounts for both rill and interill erosion processes and can provide, overall, a more accurate representation of the spatial heterogeneity within an agricultural setting is the Water Erosion Prediction Project model (WEPP version 2010.1; hereafter “WEPP-Original” model) (Flanagan and Nearing, 1995), initiated in August 1985 by the U.S. Department of Agriculture-Agricultural Research Service (USDA-ARS). Figure 3.1 provides a detailed schematic representation of the WEPP-Original model structure, including the model inputs, the processes, and the outputs. The WEPP-Original model was selected in the proposed study for the following reasons:

1. WEPP-Original is a physically based model that connects the temporal changes of soil properties and LU/LC with surface hydrology (rainfall interception by canopy cover, infiltration, rainfall excess, depression storage) and water balance calculations. For providing reliable estimates of the infiltration depth,  $F$ , the “effective” hydraulic conductivity of the soil,  $K_e$ , is considered in the Green-Ampt equation:

$$K_e t_c = F - \Psi \mathcal{G}_d \ln \left[ 1 + \frac{F}{\Psi \mathcal{G}_d} \right] \quad (3.1)$$

where,  $t_c$  is a corrected time to account for the difference between instantaneous and actual time to ponding,  $F$  is the cumulative infiltration depth,  $\mathcal{G}_d$  is the soil moisture deficit, and  $\Psi$  is the average capillary potential.  $K_e$  is the key hydro-pedo transfer parameter that facilitates the linkage between landscape properties and LU/LC with

hydrologic response, by accounting for both the intrinsic soil properties (such as soil texture, bulk density, organic matter) and extrinsic factors such as  $RR$ , surface crust, rainfall kinetic energy, and LU/LC (e.g., Onstad et al., 1984; Papanicolaou et al., 2008). Further, WEPP-Original has the capability to perform first order subsurface flow calculations to drain tiles or ditches based on the DRAINMOD model (Skaggs, 1978), thus, it is suitable for agricultural settings.

2. WEPP-Original accounts for micro-roughness and LU/LC effects on the overland flow frictional characteristics in both the rill and interrill areas. The friction factor is calculated separately for the rill ( $f_i$ ) and interrill ( $f_r$ ) areas as a summation of the friction factor for bare (baseline) soil conditions and the friction factor due to surface cover and vegetation. To perform overland flow hydraulics, WEPP-Original calculates an equivalent, area-weighted, average friction factor,  $f_{eq} = f_r A_r + f_i (1 - A_r)$ , where  $A_r$  is the fraction of the total area in rills. The  $f_{eq}$  is used via the Chezy coefficient,  $C = (8g/f_{eq})^{0.5}$ , for calculating the overland flow unit discharge,  $q$ , over a planar surface as:

$$q = CS_o^{0.5} h^{1.5} = \alpha h^{1.5} \quad (3.2)$$

where,  $CS_o^{0.5}$  is known as the kinematic depth-discharge coefficient,  $\alpha$ , and  $S_o$  is the slope of the planar surface.

Surface runoff relates to rainfall and infiltration through the continuity equation, written as:

$$\frac{\partial h}{\partial t} + \frac{\partial q}{\partial x} = v = r - f \quad (3.3)$$

where,  $h$  is the flow depth;  $x$  and  $t$  denote longitudinal direction and time, respectively;  $r$  is the rainfall rate;  $f$  is the infiltration rate;  $v$  is the rainfall excess rate. The rainfall excess



rate,  $r-f$ , is corrected for the effects of depression storage,  $S_d$ , which depends on  $RR$  and  $S_o$  of the planar surface, given as (Onstad, 1984)

$$S_d = 0.112 RR + 3.1 RR^2 - 1.2 RRS_o \quad (3.4).$$

Both  $RR$  and  $OR$  exponentially decay with the cumulative rainfall,  $R_c$ , based on a function proposed by Potter (1990):

$$RR_t = RR_i e^{-C_{br} \left[ \frac{R_c}{b} \right]^{0.6}} \quad (3.5)$$

where,  $RR_t$  is the random roughness at time  $t$ ,  $RR_i$  is the random roughness immediately after tillage,  $C_{br}$  is the adjustment factor for buried residue, and  $b$  is an empirical coefficient based on the soil organic matter and clay contents.

The system of equations (3.2) and (3.3) is solved for  $q$  and  $h$  using the method of characteristics, which involves re-writing these equations as ordinary differential equations on characteristic curves in the  $x-t$  plane (i.e., space-time computational domain) as follows:

$$\frac{dh}{dt} = r - f \quad (3.6a)$$

$$u = \text{wave speed} = \frac{dx}{dt} = 1.5CS_o^{0.5} h^{0.5} \quad (3.6b)$$

The wave speed in equation 3.6b is a key parameter for overland flow hydraulics as it affects the travel time of the flow, time for the system to reach equilibrium conditions (expressed via the time lag), and ultimately the shape of the hydrograph. The wave speed depends on the slope of the surface,  $S_o$ , the Chezy friction parameter,  $C$ , and the flow depth,  $h$ .

3. WEPP-Original, being a distributed-parameter model, allows the user to divide a hillslope into a number of sub-units (defined internally in the source code), known as Overland Flow Elements (OFEs) to describe the spatial heterogeneity of the governing soil parameters and LU/LC. Thus, each OFE includes information about hillslope gradient, LU/LC, and soil type.

4. The formulation of the sediment continuity equation in WEPP-Original for determining the rill sediment load,  $G_r$ , along the  $x$ -direction, accounts for the spatial-lag coefficient,  $C_L$ , discussed in section 1.3. Specifically, the sediment continuity equation in the WEPP-Original model is written as follows:

$$\frac{\partial G_r}{\partial x} = \frac{k_r(\tau_r - \tau_{c,r})}{T_{c,r}}(T_{c,r} - G_r) + D_i \quad (3.7)$$

where,  $\tau_r$  is the applied flow shear stress,  $\tau_{c,r}$  is the critical shear stress,  $T_{c,r}$  is the transport capacity,  $k_r$  is the rill erodibility, and  $D_i$  is the interrill erosion rate. By comparing equation 1.1 with WEPP-Original equation 3.7, it can be concluded that WEPP-Original accounts for the spatial lag coefficient,  $C_L$ , which is empirically lumped into the WEPP-Original sediment continuity equation 3.7 via the term:

$$C_L = \frac{k_r(\tau_r - \tau_{c,r})}{T_{c,r}} \quad (3.8).$$

Similarly to the effective hydraulic conductivity, WEPP-Original adjusts the rill erodibility to account for soil texture, buried residue, dead and live root, sealing and crusting, and freeze/thaw effects (Brown et al. 1989; Gimenez and Govers, 2008) and the  $\tau_{c,r}$  to account for soil texture, soil surface micro-roughness, sealing and crusting, and freeze/thaw affects.

5. WEPP-Original can update the size distribution of the fine sediment particles (i.e., organic matter, clay, silt, sand) and calculate the enrichment ratio.

6. WEPP-Original has been recently enhanced to utilize a geo-spatial interface (GeoWEPP) that enables inputs from airborne/spaceborne sensors about the micro-topography (i.e., at least *OR* with the 1-m and 0.3-m lidar resolution data), LU/LC, and soil type of the hills using GIS layers.

7. WEPP-Original is a well-established model that has been tested in many different countries and has been providing satisfactorily results (Flanagan et al., 2007).

### 3.2 WEPP model limitations

Despite the advantages of the WEPP-Original model for simulating overland flow and soil erosion processes at the hillslope scale, the model exhibits some key limitations outlined next:

1. WEPP-Original is not currently designed to handle kinematic shock waves introduced by the hillslope curvature. This is an inherent limitation due to the algorithm used for overland flow routing. For routing overland flow in concave or convex hillslopes, where the hill must be divided in different segments (OFEs) to account for curvature, the solution of the ordinary differential equations (3.6a) and (3.6b) may produce kinematic shock waves. Consequently, overland flow routing in WEPP-Original is performed assuming a single, planar OFE, neglecting curvature effects to the flow. For demonstration purposes, Figure 3.2 provides the results from three hypothetical, single storm, hillslope-scale, WEPP-Original simulations performed for three different hillslope profile curvatures (i.e., concave, uniform, convex) having the same average gradient, climate, LU/LC, and soil type. The WEPP-Original model results show that the runoff volume and peak runoff rates are identical for all three cases, independently of the curvature of the hill, which contradicts experimental measurements (Rieke-Zapp and

Nearing, 2005). It is evident that the error in the determination of the runoff hydrograph for the concave and convex hillslopes will propagate in the hillslope erosion simulations.

2. Similarly to the first limitation, the WEPP-Original model does not account for spatial heterogeneity on overland flow routing in terms of LU/LC and soil type along different OFEs. Instead, the WEPP-Original model utilizes the equilibrium storage concept developed by Wu et al. (1978) to transform multiple OFEs into a single uniform OFE. This method computes an aggregate kinematic depth-discharge coefficient which will give the same equilibrium discharge rate at the outlet of a single OFE that disaggregated depth-discharge coefficients give at the bottom-most OFE of a series of OFEs (Stone et al., 1995). Also, infiltration on multiple OFEs is computed using the OFE length-weighted average Green-Ampt parameters of the multiple OFEs under consideration. Spatial heterogeneity of LU/LC and soil type may affect the surface micro-roughness, friction factor, canopy and surface cover, hydraulic conductivity and may lead to the formation of shock waves, similarly to the profile curvature. The conditions for the shock formation are discussed in detail on chapter 4.

3. WEPP-Original assumes steady-state conditions when simulating erosion processes, thus, no sedigraph is produced at the outlet of the hillslope. For solving the steady-state equation, WEPP-Original considers a constant peak runoff rate and adjusts the runoff duration accordingly to maintain the same total runoff with the one determined in the overland flow simulation. Thus, WEPP-Original does not account for the temporal lag for the soil particles to adjust from the non-equilibrium to equilibrium conditions. However, it should be noted that WEPP-Original considers the effects of the curvature in the soil erosion calculations by using the local gradient,  $S_o(x)$ , in the determination of the applied flow shear stress,  $\tau_f$ , along the hill.

Table 3.1 Summary of existing soil erosion models.

Model	Lumped/ Distribu- ted <sup>a</sup>	Stochastic/ Determi- nistic <sup>b</sup>	1-D/ 2-D	Steady/ Unsteady <sup>c</sup>	Event/ Continuous <sup>d</sup>	Rilled/ Unrilled <sup>e</sup>
ANSWERS	D	D	1-D	S	E	U
LISEM	D	D	1-D	S	E	R
CREAMS	D	D	1-D	S	E	R
WEPP	D	D	1-D	S/U	E/C	R
EUROSEM	D	D	1-D	U	E	U
KINEROS	D	D	1-D	U	E	U
RUNOFF	D	D	1-D	U	E	U
SEM	D	D	2-D	U	C	U
SHESED	D	D	2-D	U	C	U

<sup>a</sup>D = distributed

<sup>b</sup>D = deterministic

<sup>c</sup>S = steady, U = unsteady

<sup>d</sup>E = event, C = continuous

<sup>e</sup>R = rilled, U = unrilled

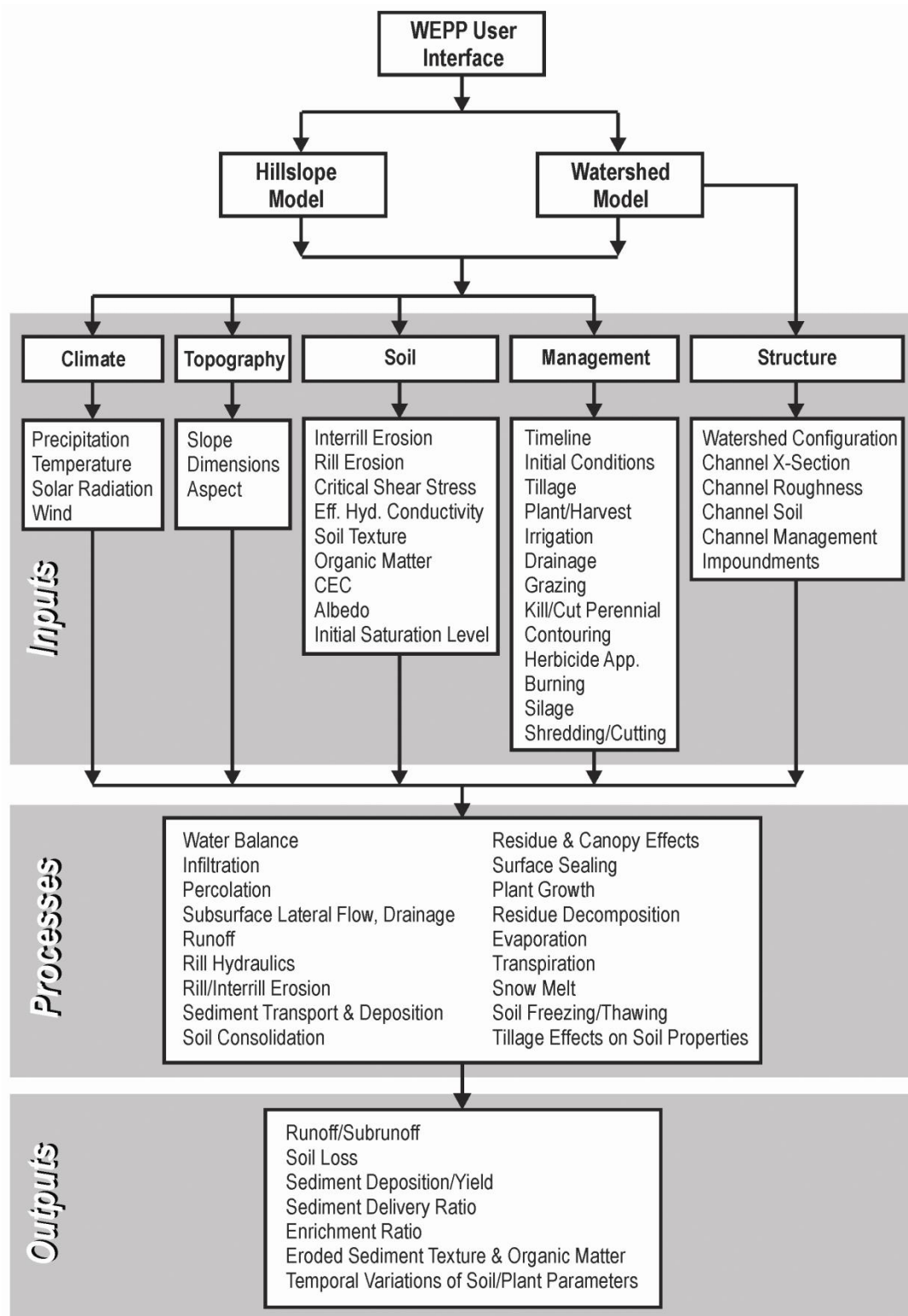


Figure 3.1 Schematic representation of WEPP-Original components.

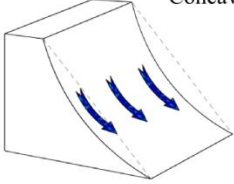
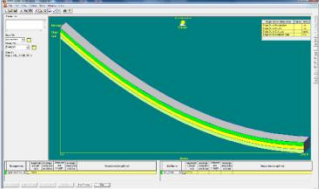
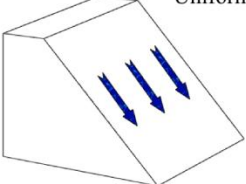
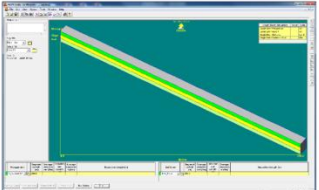
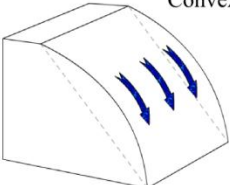
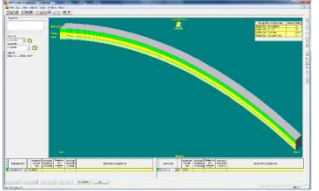
Hillslope Topography	WEPP model	WEPP Results
<p>Concave</p> 		<p>Runoff volume = 2.15 m<sup>3</sup>  Peak runoff rate = 11.9 mm/hr  Sediment yield = 0.83 kg</p>
<p>Uniform</p> 		<p>Runoff volume = 2.15 m<sup>3</sup>  Peak runoff rate = 11.9 mm/hr  Sediment yield = 16.7 kg</p>
<p>Convex</p> 		<p>Runoff volume = 2.15 m<sup>3</sup>  Peak runoff rate = 11.9 mm/hr  Sediment yield = 75.6 kg</p>

Figure 3.2 WEPP-Original results from hypothetical, single storm, hillslope-scale simulations highlighting model's limitations for accounting curvature effects.

## CHAPTER 4

## WEPP MODEL IMPROVEMENTS AND IMPLEMENTATION

4.1 Overland flow routing and shock formation criteria

Overland flow routing involves solving the kinematic wave equations (KWE) (see Equations 3.6a and 3.6b) with respect to the overland flow depth,  $h$ , and unit runoff discharge,  $q$ , as it was presented in chapter 3. WEPP-Original utilizes the method of characteristics (MOC) to solve numerically the KWE and route the rainfall excess,  $r-f$ , along the hillslope (Stone et al., 1995). Utilization of the MOC in solving the KWE allows the formulation of a semi-analytical solution, which is currently adopted in the WEPP-Original model and has two advantages (e.g., Borah et al., 1980): (1) eliminates the wave celerity dampening usually introduced by numerical schemes; and (2) results in faster computational procedures.

The use of a semi-analytical solution for overland flow routing along a hill is restricted for the case of a single OFE, for which there is no downslope variability in terms of topography, LU/LC and soil type. However, in the case of multiple OFE's it has been documented that shock waves may be generated during overland flow routing, as a result of the spatial heterogeneity of the key physical and biogeochemical characteristics along the hillslope (e.g., Kibler and Woolhiser, 1972). These shock waves represent discontinuities in the flow field and produce near-vertical fronts in the outflow hydrographs (Kibler and Woolhiser, 1972) (Figure 4.1), thus, affecting the magnitude of both the overland flow depth and runoff discharge.

Kinematic wave shocks arise when an upper OFE<sub>1</sub> has a depth-discharge coefficient,  $\alpha$  (see equation 3.2), larger than the lower OFE<sub>2</sub>, i.e.,

$$\alpha_{OFE_1} > \alpha_{OFE_2} \Rightarrow \sqrt{\frac{8g}{f_{e(OFE_1)}}} S_{o(OFE_1)}^{0.5} > \sqrt{\frac{8g}{f_{e(OFE_2)}}} S_{o(OFE_2)}^{0.5} \quad (\text{criterion - 1}) \quad (4.1).$$



According to criterion-1, formation of shock waves depends on the slope of the OFEs,  $S_o$ , and the equivalent friction factor,  $f_{eq}$  (see section 3.1), thus, it is a landscape topographical (micro-roughness and curvature) related criterion.

Additionally, according to Borah et al. (1980), a shock occurs between two consecutive characteristics  $c_1$  and  $c_2$  within an OFE, when the following criterion is satisfied:

$$\left[ q^{(c2)} \right]^{1/1.5} - \left[ q^{(c1)} \right]^{1/1.5} > \alpha_{OFE}^{1/1.5} q_l \Delta t \quad (\text{criterion} - 2) \quad (4.2)$$

where,  $q_l$  is the rainfall excess equal to  $r-f$  (see right hand side of equation 3.3).

According to criterion-2, the characteristics originating along the rising limb of the hydrograph may intersect and a shock will form, depending upon the relative magnitude of the variables appearing in criterion-2. Criterion-2 is both a landscape topographical and hydrological related criterion.

#### 4.2 Shock-capturing schemes

To incorporate the effects of spatial heterogeneity for multiple OFEs, in terms of topography, LU/LC, and soil type on the overland flow routing algorithm, two numerical, shock-capturing schemes were tested. The first was developed by Borah et al. (1980) and it is based on the MOC, similarly to the numerical scheme adopted in WEPP-Original. The second is based on finite differences using the TVD-MacCormack scheme, which is an expansion of the widely used MacCormack scheme (MacCormack, 1969).

#### 4.2.1 Method of characteristics: Borah et al. (1980)

Borah et al. (1980) proposed a propagating shock-fitting scheme (PSF) applicable for multiple OFEs, which preserved the effects of the shocks, without introducing additional computational complication. Borah et al. (1980) used an analytical solution to the kinematic wave model, by utilizing the MOC and discretizing equations (3.6a) and (3.6b), between two consecutive points, e.g.,  $A(x_{i-1}, t_{j-1})$  and  $B(x_i, t_j)$  along a characteristic path (Figure 4.2):

$$h_{i,j} = h_{i-1,j-1} + q_{lj} \Delta t_j \quad (4.3)$$

$$q_{i,j} = q_{i-1,j-1} + q_{lj} \Delta x_i \quad (4.4)$$

$$\Delta x_i = \frac{\alpha}{q_{lj}} \left[ (q_{lj} \Delta t_j + h_{i-1,j-1})^{1.5} - h_{i-1,j-1}^{1.5} \right] \quad (4.5)$$

$$\Delta t_j = \frac{1}{q_{lj}} \left[ \left( \frac{q_{lj}}{\alpha} \Delta x_i + h_{i-1,j-1}^{1.5} \right)^{1/1.5} - h_{i-1,j-1} \right] \quad (4.6)$$

where,  $\Delta x_i = x_i - x_{i-1}$ ,  $\Delta t_j = t_j - t_{j-1}$ ,  $q_l = r-f$ , and  $\alpha$  is the depth-discharge coefficient. Equations (4.5) and (4.6) are used to trace the characteristic path by considering either  $\Delta x_i$  or  $\Delta t_j$  as a dependent variable and choosing a suitable value for the other.

In the case where a shock occurs (i.e., see Figure 4.2 where two characteristics intersect), tracing of the shock path is performed by considering two consecutive points, e.g.,  $C(x_{i-1}, t_{j-1})$  and  $D(x_i, t_j)$  along a shock trajectory  $S$  and calculating the space and time increments,  $\Delta x_i$  and  $\Delta t_j$ , respectively, as:

$$\Delta x_i = \frac{\alpha}{2.5 q_l (h_{i-1,j-1}^{bh} - h_{i-1,j-1}^{ah})} \left\{ [q_l \Delta t_j + h_{i-1,j-1}^{bh}]^{2.5} - [q_l \Delta t_j + h_{i-1,j-1}^{ah}]^{2.5} - (h_{i-1,j-1}^{bh})^{2.5} + (h_{i-1,j-1}^{ah})^{2.5} \right\} \quad (4.7)$$

$$\Delta t_j = \frac{1.5\alpha}{2.5q_l(q_{i-1,j-1}^{bh} - q_{i-1,j-1}^{ah})} \left\{ \left[ \frac{q_l}{\alpha} \Delta x_i + h_{i-1,j-1}^{bh} \right]^{1.67} - \left[ \frac{q_l}{\alpha} \Delta x_i + (h_{i-1,j-1}^{ah})^{1.5} \right]^{1.67} - (h_{i-1,j-1}^{bh})^{2.5} + (h_{i-1,j-1}^{ah})^{2.5} \right\} \quad (4.8)$$

where, *ah*, *bh* denote the location ahead and behind the shock, respectively. Similar to the routing of the characteristics,  $\Delta t_j$  is taken as the independent variable. Then, equation (4.3) is used to compute  $h_{i,j}^{ah}$  and  $h_{i,j}^{bh}$ , and using their values in equation  $q = \alpha h^{1.5}$ ,  $q_{i,j}^{ah}$  and  $q_{i,j}^{bh}$  are determined. Lastly, equation (4.7) is used to compute  $\Delta x_i$ .

In the same manner that shocks arise from the intersection of characteristic waves, they can also meet with other shocks to form new shocks downhill. In addition, shocks introduced in the shock-forming zone of a given OFE (Figure 4.2) will propagate into the downstream OFEs, interacting with each other and creating new shocks. The PSF scheme proposed by Borah et al. (1980) treats shocks arising from the intersection between two characteristic waves, i.e., it tracks one shock wave at a time. Thus, it cannot handle the interaction between multiple shock waves. For example, Figure 4.3 illustrates the characteristics ( $x, t$ ) for the uniform hillslope topography presented in Figure 4.1 (b), but with different management practices for the 2 OFEs, such as the rainfall excess in OFE<sub>2</sub> is less than OFE<sub>1</sub>. Under hydrologic conditions where there is much less rainfall excess on the second OFE, this scenario is likely to occur and the PSF scheme may not work well as shown in Figure 4.3.

#### 4.2.2 Finite difference: TVD-MacCormack scheme

Due to the limitation of the Borah et al. (1980) method to handle interaction of multiple shock waves, the method of finite differences was utilized next to solve numerically the kinematic wave equations (3.6a) and (3.6b). The TVD-MacCormack numerical scheme is an expansion of the widely used MacCormack scheme (MacCormack, 1969). The scheme is suitable for implementation in an explicit time-

marching algorithm and involves a two-step procedure known as the “predictor-corrector” algorithm (Garcia-Navarro et al., 1992). To solve the kinematic wave equations, the computational domain is discretized as  $x_i = i\Delta x$  and  $t_j = j\Delta t$ , where  $i$  and  $j$  denote space and time, respectively, and  $\Delta x$ ,  $\Delta t$  denote the size of the uniform mesh and time step, respectively. Based on Tseng (2010), the one-dimensional kinematic wave equations can be written using the MacCormack scheme as follows:

*Predictor Step:*

$$\Delta A_i^p = -\frac{\Delta t}{\Delta x} (Q_{i+1} - Q_i) + q_i \Delta t \quad (4.9)$$

$$A_i^p = A_i + \Delta A_i^p \quad (4.10)$$

$$Q_i^p = \alpha A_i^{p1.5} \quad (4.11)$$

*Corrector Step:*

$$A_i^c(t + \Delta t) = A_i(t) - \frac{\Delta t}{\Delta x} (Q_i^p - Q_{i-1}^p) + q_i \Delta t \quad (4.12)$$

where, the subscript  $p$  and  $c$  stands for the predictor and corrector steps, respectively,  $A$  denotes the cross-sectional area,  $Q$  is the flow discharge, and  $\alpha$  is the depth-discharge coefficient. It should be noted that in the above equations 4.9-4.12 the flow discharge,  $Q$ , and cross-sectional area,  $A$ , are the unknowns vs. the unit discharge,  $q$ , and flow depth,  $h$ , in the Borah et al. (1980) method.

The revised TVD-MacCormack scheme includes a shock-capturing method (resolve discontinuous solutions) with a second order of accuracy, capable of rendering the solution oscillation free (e.g., Davis, 1984; Garcia-Navarro et al., 1992; Mingham et al., 2001), without introducing any additional difficulty for the treatment of the rainfall

excess rate,  $q_i$  (source term). For implementing the TVD-MacCormack scheme, a dissipative term is used to provide oscillation free solution, denoted as  $TVD_i$ , given as:

$$TVD_i = G(r_i)(A_{i+1} - A_i) - G(r_{i-1})(A_i - A_{i-1}) \quad (4.13)$$

where,

$$G(r_i) = 0.5 \cdot C(Cr_i) \cdot (1 - \varphi(r_i)) \quad (4.14)$$

where,  $\varphi(r_i)$  is the flux limiter function given as:

$$\varphi(r_i) = \begin{cases} \min(2r_i, 1), & r_i < 0 \\ 0, & r_i \geq 0 \end{cases} \quad (4.15)$$

and  $r_i$  is the ratio of successive gradients equal to

$$r_i = \frac{A_i - A_{i-1}}{A_{i+1} - A_i} \quad (4.16)$$

In equation 4.17, the parameter  $C(Cr_i)$  is a function of the local courant number,  $Cr_i$ , and is given as:

$$C(Cr_i) = \begin{cases} 0.25, & Cr_i > 0.5 \\ Cr_i(1 - Cr_i), & Cr_i \leq 0.5 \end{cases} \quad (4.17)$$

The courant number,  $Cr_i$ , is calculated as follows:

$$Cr_i = \left( \frac{Q_i}{A_i} + 1.5aA_i^{0.5} \right) \frac{\Delta t}{\Delta x} \quad (4.18)$$

The TVD-MacCormack scheme must satisfy the Courant-Friedrich-Lewy (CFL) criterion at each cell in order to be stable. The CFL criterion is defined as:

$$Cr_i = \frac{\Delta t}{\Delta x} (|u_i| + c_i) \leq 1 \quad (4.19)$$

where,  $u_i$  is the velocity at cell  $i$  calculated as  $Q_i/A_i$  and  $c_i$  is the wave celerity. At the end of a time step  $j$ , after averaging the predicted and corrected values (equations 4.11 and 4.15) and by adding the  $TVD_i$  term, the final values for the cross-sectional flow area and flow discharge are given as:

$$A_i = \underbrace{\frac{1}{2}(A_i^p + A_i^c)}_{\text{predictor-corrector terms}} + \underbrace{TVD_i}_{\text{TVD dissipation term}} \quad (4.20)$$

$$Q_i = \alpha A_i^{1.5} \quad (4.21)$$

### 4.3 WEPP-Improved model implementation

The WEPP-Improved model “calls” 18 out of the 221 pre-existing subroutines found in the WEPP-Original model related to surface hydrology, infiltration, and water balance. In addition, 6 new subroutines have been added in the WEPP-Improved model using Visual Fortran for incorporating the TVD-MacCormack numerical scheme. The WEPP-Improved model is computationally efficient, since one simulation for a single storm event in a hillslope comprised of 2 OFE’s, requires fractions of a second to complete. Main outputs from WEPP-Improved include the flow hydrograph at the exit of each OFE and at the hillslope outlet, as well as the flow depths along the hill at different time steps per user’s request. It should be noted that all other calculations (e.g., sediment routing, residue decomposition) are performed by WEPP-Original, producing the

common WEPP output files such as soil loss, sediment deposition/yield, sediment delivery ratio, enrichment ratio, temporal variations of soil/plant parameters (see Figure 3.1).

Below a description is provided of the WEPP-Improved model implementation. Assuming, for example, that overland flow is routed along a hillslope profile ABC, as shown in Figure 4.4, the steps to be followed are:

*Step 1:* The examined, natural, hillslope profile is split into multiple OFE's to account for the spatial heterogeneity in terms of topography, LU/LC, and soil type. For this step, WEPP-Original is called to create the input files for each OFE. Each OFE has a uniform slope, as well as a unique LU/LC (e.g., in terms of micro-roughness, vegetation) and soil type (e.g., in terms of erodibility, saturated hydraulic conductivity). In general, the physical and/or biogeochemical properties may vary along the hill, which will affect the number of OFE's to be considered.

*Step 2:* Infiltration calculations are performed per OFE using the Green-Ampt model (see equation 3.1). This step is different from WEPP-Original, where infiltration is computed using the OFE length-weighted average Green-Ampt Mein-Larson parameters of the 2 OFEs under consideration.

*Step 3:* Rainfall excess,  $v$ , is calculated for each OFE (e.g.,  $v_1$  and  $v_2$  for OFE<sub>1</sub> and OFE<sub>2</sub>, respectively) as the difference between the rainfall,  $r$ , and infiltration rate,  $f$  (see equation 3.3). The amount of rainfall excess,  $v$ , is corrected for the depression storage (see equation 3.4).

*Step 4:* The corrected rainfall excess,  $v_1$  is routed along OFE<sub>1</sub>, from location A to location B, using the TVD-MacCormack scheme, thus producing a hydrograph at location B. Next, the hydrograph at location B is routed downhill OFE<sub>2</sub> along with the rainfall excess,  $v_2$ , using the TVD-MacCormack scheme.

Step 4 is a key difference between WEPP-Improved and WEPP-Original. In WEPP-Original, overland flow routing is performed by calculating an aggregated, kinematic, depth-discharge coefficient which gives the same equilibrium discharge rate at the outlet of a single OFE that disaggregated depth-discharge coefficients give at the bottom-most OFE of the multiple OFEs. Due to this limitation, kinematic wave shocks and their propagation cannot be modeled with WEPP-Original.



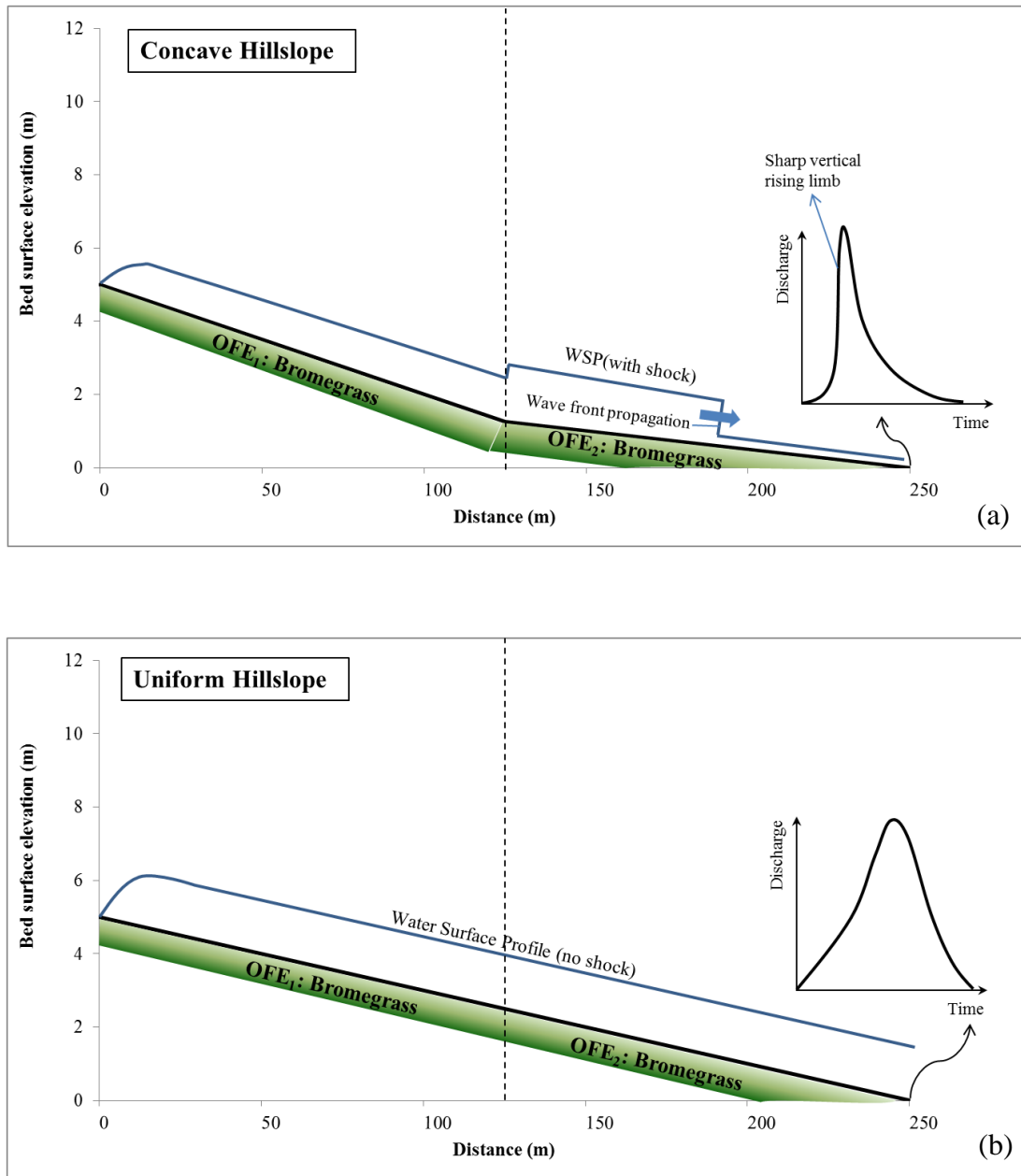


Figure 4.1 Qualitative sketch of the outflow hydrograph and water surface profile (WSP) of a hill showing (a) formation of a shock due to the concave hillslope profile and (b) non-formation of shocks due to uniform hillslope.

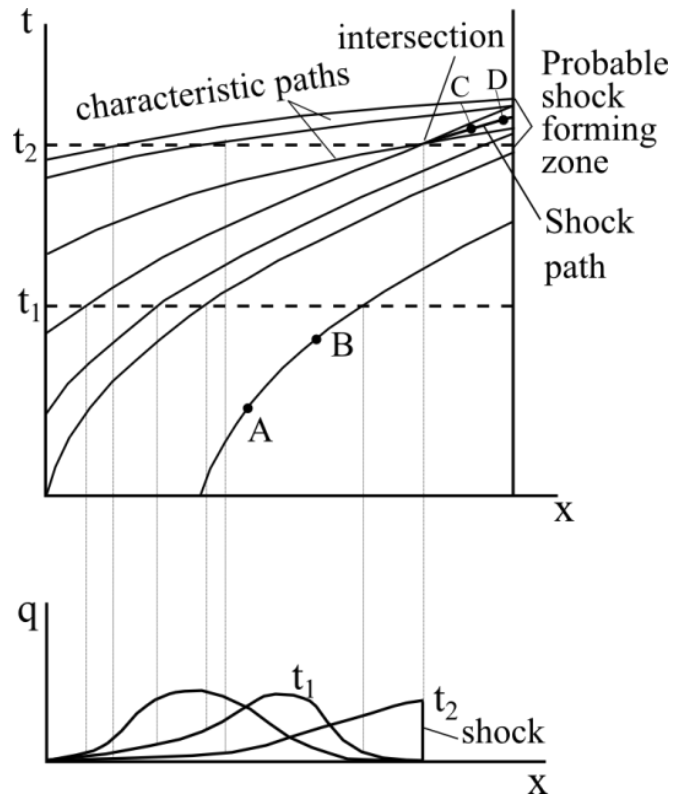


Figure 4.2 Example of shock formation.

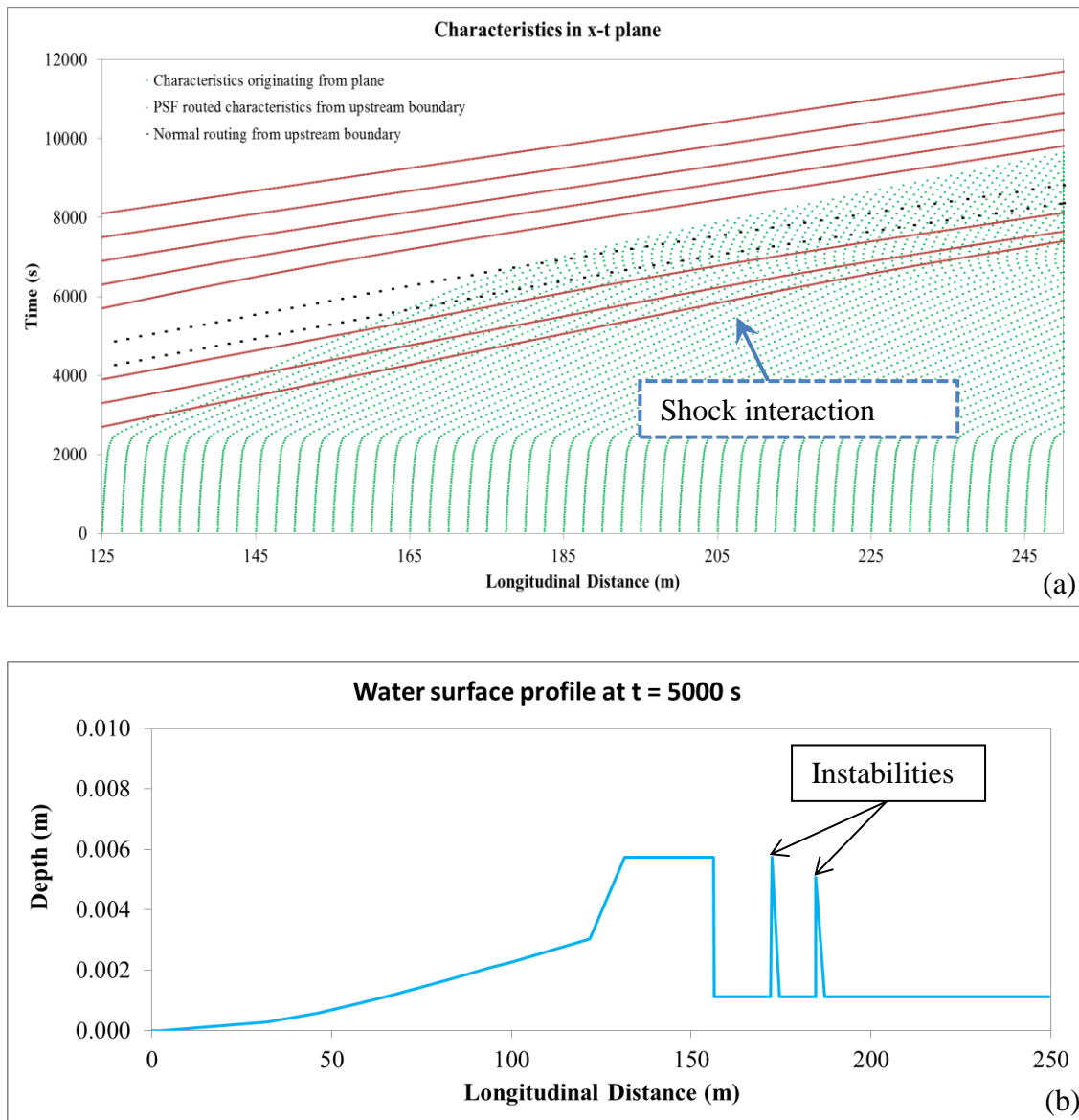


Figure 4.3 (a) Shock wave interaction in the space-time domain using the MOC and (b) instabilities in the simulated outlet hydrograph at the outlet of the uniform hilslope profile shown in Figure 4.1b having different management practices.

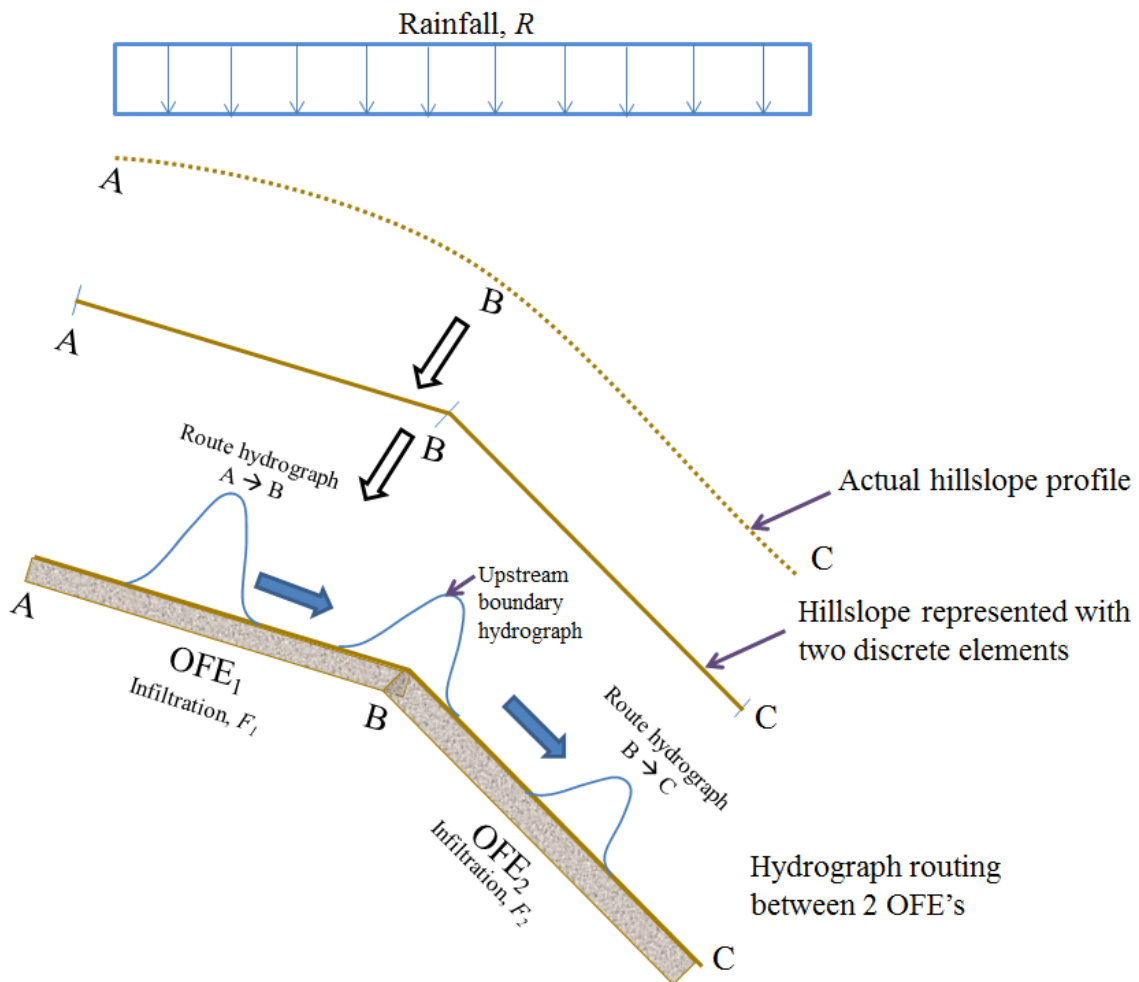


Figure 4.4 WEPP-Improved model implementation: routing of the overland flow.

## CHAPTER 5

### FIELD EXPERIMENTS IN THE SOUTH AMANA SUB-WATERSHED

#### 5.1 Reasoning for the experimental study

Detailed field experiments were performed in an instrumented plot scale, designed to test the WEPP-Improved model's capability to (1) predict the runoff hydrograph and sediment transport rates at the outlet of the plot and (2) provide the water depth distribution within the plot at different time steps and for various hydrologic conditions, management practices, roughness, and curvature.

Preliminary reconnaissance experiments were conducted during fall 2011 at the South Amana Sub-Watershed (SASW), a headwater system of Clear Creek, IA, within the IIHR-experimental station (Figure 5.1). The experimental station is located near the floodplain of Clear Creek and is comprised of mostly the Colo soil series (fine-silty, mixed, superactive, mesic Cumulic Endoaquoll). The preliminary experiments were carried out mainly to test the equipment, experimental set-up and the experimental procedure to be followed in the final experiments performed during summer 2012. The preliminary experiments provided also an insight for the time to equilibrium for flow and sediment, which varied between 1 and 4 hrs, respectively. This was important information to obtain, even at a qualitative sense, as WEPP-Original solves the unsteady form of the kinematic wave equation of the flow component (see equation 3.6a and 3.6b), whereas only the steady state of a simplistic version of the general Exner equation is solved for the sediment component (see equation 3.7). The final experiments were performed during July 2012 on a concave-shaped plot, after a succession of several preliminary runs, for a low and high in magnitude single storm event (i.e., 2 experiments). The concave slope was constructed by two-linearly shaped slopes, having different longitudinal gradient (steep to mild slope). Due to the time required to set-up and conduct these experiments, no runs were performed for different management

practices and curvature types. Instead, the focus was centered around the effects of rainfall intensity on a bare soil, for testing the behavior of WEPP-Improved in isolating the effects of high and low intensity storms and testing the hypothesis. The two experiments were performed for identical conditions other than the precipitation intensity, which was selected to represent conditions corresponding to low and high storm intensities encountered in Iowa for intermittent and general movement. Next, a description is provided of the main equipment used during the experiments.

## 5.2 Experimental set-up and instrumentation

### 5.2.1 Rainfall simulators

Two different constant rainfall intensities (i.e., 30 mm/hr and 60 mm/hr, corresponding to representative low and high magnitude storm events in the region, respectively as seen from the tipping bucket rain gauge data nearby the experimental station in Figure 5.2) were applied to a concave plot (i.e., ~ 7 m long, 2 m wide) using Norton Ladder Multiple Intensity Rainfall Simulators (dimension of 2.5 x 1.5 x 2.7 m), designed by the USDA-ARS National Erosion Research Laboratory in W. Lafayette, IN (Norton, 2006). Specifically, three rainfall simulators in series were mounted ~ 2.5 m above the plot (Figure 5.3) and a uniform rainfall was applied by oscillating VeeJet type nozzles, providing spherical drops with a median drop size of 2.25 mm and a terminal velocity of 6.8 m/s (Elhakeem and Papanicolaou, 2009). The size distribution of the raindrops generated by the rainfall simulators for the selected intensities agreed well with the Marshall-Palmer distribution, which is commonly accepted distribution for natural raindrop sizes (Marshall and Palmer, 1948). The distance of ~ 2.5 m was selected so that the terminal velocities of almost all drops from the Veejet nozzle were nearly equal to the terminal velocities of those from natural rainstorms. The simulators were equipped with storage tanks (total capacity of 1,500 gal) (Figure 5.4) and a water pump connected to a system of valves that allowed internal water pressure to be adjusted for each simulator

independently. Water pressure in the pipes for each simulator was frequently checked during the experiment via the pressure gages attached on each simulator (Figure 5.5). More details of the set-up, the use of the rainfall simulators, as well as the agreement between the rainfall simulator's raindrop distribution and the Marshall-Palmer distribution are provided in Elhakeem and Papanicolaou (2009). Rainfall was applied for a sufficient amount of time (at least 4 hrs as determined by the preliminary experiments in fall 2011) in order to be certain that equilibrium conditions have been reached for both water and sediment.

### 5.2.2 Soil moisture probes

Soil moisture was recorded via the CS625 Water Content Reflectometers manufactured by Campbell Scientific, Inc., which provided continuous measurements during the experiments. The water content reflectometer consists of two stainless steel rods connected to a printed circuit board (Figure 5.6). A shielded four-conductor cable is connected to the circuit board to supply power, enable the probe, and monitor the pulse output. High-speed electronic components on the circuit board are configured as a bistable multivibrator. The output of the multivibrator is connected to the probe rods which act as a wave guide. The travel time of the signal on the probe rods depends on the dielectric permittivity of the material surrounding the rods and the dielectric permittivity depends on the water content. Therefore, the oscillation frequency of the multivibrator is dependent on the water content of the media being measured. Digital circuitry scales the multivibrator output to an appropriate frequency for measurement with a datalogger. The water content reflectometer output is essentially a square wave. The probe output period ranges from about 14 microseconds with rods in air to about 42 microseconds with the rods completely immersed in typical tap water. A calibration equation was developed for SASW that converts period to volumetric water content.

### 5.2.3 Mapping of micro-topography

The micro-topography of the soil surface before and after each experiment was recorded during the night by using a state-of-the-art instantaneous surface-profile laser scanner (0.5 mm elevational accuracy) developed by USDA–ARS National Soil Erosion Research Laboratory (Darboux and Huang, 2003). Dark conditions were required to discern and record the laser activity. The system is comprised of two laser diodes, mounted 40 cm apart, generating a 3.60-mW, single, 0.5 mm thick, laser beam on the targeted surface at 635 nm (red) (Figure 5.7). An 8-bit monochrome, high resolution, progressive scan CCD (charge-coupled device) camera manufactured by Basler (model A102k) (Figure 5.8) with 1030 rows x 1300 columns and a 9-mm lens is used to detect the laser beam (Figure 5.7). The CCD camera is interfaced to external circuitry via two connectors located on the back of the camera (Figure 5.8b): (1) a 26-pin connector used to transmit image data and control signals and configuration commands; and (2) a 6-pin connector to provide power to the camera. The camera is connected to a portable desktop computer through the custom-built electronic board R3-CL (Figure 5.9), manufactured by Bitflow for image acquisition (frame grabber). The lasers and camera are mounted on a 5-m long carriage assembly (Figure 5.10).

Before using the laser system to scan the area of interest, the system was calibrated. The calibration consists of measuring a set of points of known  $(x, y, z)$  coordinates located on the laser plane (see Figure 5.7). For this reason a light-bar with LED's (light-emitting diode) of known distance is placed on a calibrating fixture (Figure 5.11a) and the camera records the location  $(x, y, z)$  of the LED's (Figure 5.11b). By moving the light-bar up at different slots on the calibration fixture, calibration points are obtained within the area of view of the camera. After the calibration process, the laser system is used to scan the plot area. The aligned laser diodes generate a bright line on the soil surface and the shape of this line, digitized by the camera from an oblique angle, changes depending on the surface micro-topography (Figure 5.11c). Because of the fixed



camera-laser positioning, the surface roughness height is estimated using a simple calibration procedure. A built-in computer program, namely “Scan”, is used to control the movement of the laser system and specifically to define the travel distance of the laser system, i.e., the designated scanning length. Once the output file from the laser scanner data for the whole area is processed using the resulted polynomials from the calibration process, a set of (x, y, z) coordinates is obtained that can be used to construct the Digital Elevation Model (DEM) of the scanned area. From the initial and final scans, the random roughness  $RR$  (see definition in section 1.2) is determined via statistical analysis, known as the variogram (e.g., Vazquez et al., 2005; Strom and Papanicolaou, 2008).

#### 5.2.4 Measurement of flow and sediment transport rates

For determining the water and sediment concentrations throughout the duration of the experiment, a V-notch weir (20° opening angle) was installed at the outlet of each plot to facilitate the collection of water/sediment samples (catch samples) during the experiments (Figure 5.12). Flow discharge at the outlet of the plot was determined using the calibration-equation for the V-notch weir (Brater et al., 1996):

$$Q = 1.55 \tan\left(\frac{\theta_w}{2}\right) H_w^{2.5} \quad (5.1)$$

where,  $H_w$  is the flow depth recorded at the weir and  $\theta_w$  is the angle opening. A measured tape was mounted on the weir to enable quick reading of the flow depth (Figure 5.12). For comparison purposes, flow (and suspended sediment) discharge was also calculated from discrete sampling, i.e., by determining the volume of water (and suspended sediment) collected at the plot outlet over a specific period of time varied between 1 – 10 sec.

Upstream of the weir section and immediately downstream of the plot exit a plywood board of triangular shape was installed. The board was placed to facilitate and encourage the unimpeded delivery of water and sediment to the V-notch weir and provide easy access for the discrete sampling. The board side walls (Figure 5.13), also, ensured that the incoming from the plot water and its sediment will be redirected to the V-notch weir. To minimize the likelihood that water will not seep through the seam at the interface between the plot soil and the board entrance, a thin strip of the entrance was covered with sprinkles of Portland concrete cement which matched the micro-roughness of the experiment plot (Figure 5.14).

#### 5.2.5 Measurement of flow depth

Flow depth within the plot area was measured using a telescopic rod with a bubble (for leveling) and a ruler equipped with a flat pad at its end to prevent submersion into the wet soil and minimize the experimental error. The ruler was attached at the end of the rod (Figure 5.15) and measurements were taken through the coordinated effort of two people. The first one was holding the rod leveled while placing the ruler on the soil surface. The second one was reading the flow depth value with the ruler using binoculars and recorded the value in the field book. To determine the flow depth within the plot, measurements of the flow depth were obtained at 6 different cross-sections (namely sections A, B, C, D, E, F from the top to the bottom of the plot) spaced 1-m apart (see Figure 5.16). For each cross-section, flow depth measurements were taken every 0.3 m in the transverse direction (see Figure 5.16), resulting in 6 point measurements per cross section (i.e., total number of 36 measurement points within the plot area).

#### 5.2.6 Tracers and other recordings

In order to measure the travel time of the flow two tracers were used: (1) rhodamine pills placed at different cross-sections (e.g., Figure 5.17) (Tauro et al., 2012) and (2) milk released from the top of the plot (used also for visualization purposes). The

travel time of the tracers to reach the plot outlet and the distance from their initial position to the plot outlet were also recorded.

A regular, 30 frames per second, digital, video camera was used to monitor the plot activity and provide view of the test section (Figure 5.18). To attain better visualization of the rate of transport of the soil particles during the experiment, the soil surface was spray-painted before the experiment with different colors at three locations in the plot (red-summit, white-backslope, blue-toeslope) (Figure 5.16). Spray-painted areas were recorded throughout the duration of the experiment using a high definition digital Canon camera (Figure 5.19).

### 5.3 Experimental procedure

The preparation involved for each of the two experiments was laborious and time consuming. Each experiment required 2-days of advance preparation of the plot bed condition, laser pre-scans, sensor set-up, and acquisition of supplies such as water to fill the tanks and other miscellaneous things. The preparatory steps included (in chronological order): a) preparation of the soil bed surface; b) calibration of the laser scanner and pre-scanning of the bed surface; c) preparation of the experimental plot and recordings during the experimental run; d) termination of the experiment and post-scanning of the bed surface.

a) Preparation of the soil bed surface.

The soil bed surface was reworked to attain a concave shape using a 1.5 Hp Honda tiller (Figure 5.20). As it was previously mentioned, no vegetation was present as the experiments were performed under bare soil conditions. The concave slope was constructed by two, linearly shaped, slopes having different longitudinal gradient (from ~ 12 % steep to ~ 6 % mild slope). After re-working the soil, the soil surface was tapped using a plywood board to create a smooth surface, thus minimizing the effects of the initial soil surface micro-roughness, which may introduce an experimental error.

b) Calibration of the laser scanner and pre-scanning of the bed surface.

The calibration and pre-scanning of the soil surface was performed during the previous night before the actual experiment to reduce any glare from the surrounding environment. In order to scan the whole plot area 3 scan swaths were acquired.

c) Preparation of the experimental plot and recordings during the experimental run.

The following day, the final preparation for the experimental run was conducted and included: (1) assignment of the 6 cross-sections for obtaining the flow depth measurements; (2) placement of the eight soil moisture probes within the soil column, along the perimeter of the plot (Figure 5.21); and (3) spray-painting of the soil surface at 3 different locations along the plot. The locations of the cross-sections, soil moisture probes and spraying areas were the same in both experiments. During the experiment: (1) flow and sediment catch-samples were collected at the weir outlet and the water level was recorded every 5-10 mins; (2) flow depth measurements were measured continuously throughout the duration of the experiment in the 36 pre-defined points as well as at random locations based on the observed flow patterns; (3) tracer experiments were performed using the rhodamine pills and milk; (4) still pictures of the spray painted areas were taken frequently to observe the rate of transport of the soil particles.

A general view of the set-up before starting an experiment is presented in Figure 5.21. The experimental plot and the instrumentation were covered with a tarp to protect them for the case of natural rainfall during the experiment (Figure 5.22).

d) Termination of the experiment and post-scanning of the bed surface.

Each experiment was terminated about 1-2 hrs after the flow depth in the weir reached approximately a constant level (e.g., Mancilla, 2004; Jomaa et al., 2012). This additional time was required to allow the sediment rate to approach an equilibrium condition. Other indicators were also considered for assessing when equilibrium conditions in terms of sediment movement were reached, such as the changes in the plot topography between the upper and lower-linearly shaped slopes of the plot, features such

as spacing of headcuts and plunging pools, as well as the changes in the spray-painted areas with time. Post-scanning of the final bed elevation was performed during the night, as it was described earlier.

It should be noted that each experiment required the involvement of 8 people in order to: (1) record the flow depth within the plot area; (2) collect samples at the plot outlet and record the flow depth at the weir; (3) acquire still pictures of the plot during the experiment; (4) perform the tracer experiments; (5) check the pumps operating the rainfall simulators, pressure at the nozzles of the rainfall simulators, and other miscellaneous tasks.

#### 5.4 Results

The results from the two field experiments are organized as follows. First, the time series of the flow rates and sediment discharge at the plot outlet are presented, as well as the time series of the volumetric water content determined via the soil moisture probes. Second, a comparison is performed between the measured and predicted (via the WEPP-Improved model) flow and sediment rates at the plot outlet as well as the flow depth within the plot. Third, the results from the tracer experiments are presented along with representative pictures of the spray-painted areas at different times during the experiments.

##### 5.4.1 Time series for flow rates, sediment discharges, and soil moisture

Figures 5.23(a) and 5.24(a) provide the time series of the flow rates at the plot outlet for the low (hereafter “Exp-1”) and high (hereafter “Exp-2”) constant rainfall intensity events, respectively. Flow rates were calculated via the two methods; (1) using the calibrated-weir equation 5.1; and (2) by determining the volume of water collected using discrete sampling within a specific time interval. For Exp-1, the results from the two methods are relatively close. However, for Exp-2 there is difference on the flow

rates between the two methods, which is mainly attributed to the higher amount of deposited soil upstream of the weir comparatively to Exp-1, affecting the reading of the flow depth at the weir. Further, the lower rainfall intensity increased the time to runoff (i.e., time between the beginning of rainfall and the start of first outflow at the weir), which was ~ 30 min for Exp-1 and ~ 7 min for Exp-2. Additionally, the time series of the flow rate for the two experiments revealed that there is a characteristic time for rain drops to adjust from non-equilibrium to equilibrium conditions (i.e., time lag, as defined in section 1.2.1), which is ~ 150 min for Exp-1 and ~ 90 min for Exp-2.

Figures 5.23b and 5.24b present the time series of the volumetric soil water content for the two experiments. The initial soil moisture content for Exp-1 varied between 27-31 %, whereas for Exp-2 varied between 30-31 %. This difference is attributed to the fact that the experiments were not performed at the same time of the day (Exp-1 started around 1 pm whereas Exp-2 around 9 am). Although the initial moisture levels were different between the two experiments, the trends of the time series during the experiments were approximately the same. In both experiments, soil moisture increased with time until it reached a constant rate, when the soil became fully saturated. Results for the time series of the soil moisture are in agreement with the results for the flow rates. The time for the flow rates to reach equilibrium conditions coincided roughly with the time that the soil becomes fully saturated.

Figures 5.23c and 5.24c illustrate the time series of the sediment rates (i.e., sedigraph) for Exp-1 and Exp-2, respectively. The sedigraph for Exp-1 reveals two distinct periods within the experiment dominated by different erosion mechanisms. The first period, which lasted about 90 min from the beginning of Exp-1, is dominated by splash erosion (Figure 5.25). As Exp-1 progresses, incision starts to occur in response to increased runoff, as the soil moisture approaches saturation conditions (see Figure 5.23b). Due to incision, the sediment transport rates increases considerably and peaks around 135 min. After the sediment transport rate peaked, the sediment discharge declined over a

period of ~120 min until it reached an equilibrium state due to limited availability of material and/or decline in the sediment carrying capacity. Thus, the time lag for the sediment to reach equilibrium conditions was ~ 250 min. For Exp-2, the runoff volume was much higher than Exp-1 and the main erosion mechanism was interrill/rill erosion (i.e., no opportunity for splash erosion to dominate). Thus, incision was the key process in Exp-2 affecting the soil material exiting the plot. Conversely to Exp-1, in Exp-2 flow was stronger and the sediment supply was unlimited. The sediment flux rose to an equilibrium rate over a period of 60 min (time lag for sediment) and there was no subsequent decline in the sediment flux due to sediment availability. In the case of higher rainfall intensity it is believed that the hydraulic forcing exceeded significantly the threshold for the soil particle movement, resulting in the reduction of the time lag. In each experiment, the hydrograph and sedigraph peaked at almost the same time. However, the time to peak was shorter in Exp-2 (~ 1 hr) than in Exp-1 (~ 2.25 hrs) due to larger volume of rainfall and higher initial soil moisture content in the former experiment. Lastly, it is evident that due to larger volume of runoff water, sediment transport rates in Exp-2 were greater (up to 3 times) than Exp-1.

#### 5.4.2 Measured vs. predicted flow rates, sediment transport rates, and flow depths

A comparison was performed between the experimental data and the simulated data from the WEPP-Improved model. In order to run the WEPP-Improved model the following input data were required: (1) climate information (precipitation and duration of the single storm event); (2) topography of the hill; (3) soil type; and (4) the initial conditions input regarding the “existing state” of the hillslope in terms of initial micro-roughness, soil moisture content, residue cover, bulk density etc.

Figures 5.26 and 5.27 provide a comparison between the measured flow rates vs. the simulated ones using the WEPP-Improved model for Exp-1 and Exp-2, respectively.

It is clear that there is very good agreement between the measured and modeled data for Exp-1 and fairly good agreement for the Exp-2. In both experiments, the WEPP-Improved model could simulate the “degree of readiness” of the plot system expressed via the time lag, corresponding to the time required for the plot system to reach equilibrium conditions. According to WEPP-Improved, the time lag for Exp-1 was ~ 150 – 200 min and for Exp-2 ~ 100 min, which is in close agreement with the values of ~ 150 min and ~ 90 min determined via the measured data.

Figures 5.28 and 5.29 show the comparison between the measured vs. simulated sediment rates for Exp-1 and Exp-2, respectively. Measured data for both experiments illustrate the unsteadiness in the sediment transport rates, which is a result of the flow unsteadiness as presented in Figures 5.26 and 5.27. As expected, WEPP-Improved provided only a steady-state sediment transport rate (i.e., constant over time) and could not capture the increase on the sediment transport rate (see equation 3.7). Nonetheless, for Exp-1 the simulated steady-state sediment transport rate agreed well with the measured, steady-state sediment transport rate. However, for Exp-2, the WEPP-Improved model underestimated the value of the steady state sediment flux (i.e.,  $\sim 4 \times 10^{-3}$  vs.  $\sim 1.2 \times 10^{-3}$  kg/s for the measured vs. simulated steady state sediment flux).

Table 5.1 provides the measured and simulated flow depths within the plot during the time to equilibrium. In order to compare the measured vs. simulated flow depths, the measured flow depths, taken at 6 point locations in the transverse direction for each cross section (i.e., cross sections A, B, C, D, E, F), were averaged per cross-section. This averaging of the measured flow depths was performed since the simulated results from the WEPP-Improved model were determined along the longitudinal direction of the plot (i.e., 1-D unsteady flow equation), thus, the model did not provide information on the transverse flow depth. It should be noted that the simulated results in Table 5.1 are presented in a form of a range of values of the flow depth.



According to the results in Table 5.1, for Exp-1 the measured flow depths in the upper parts of the plot was larger, overall, than the corresponding flow depths for Exp-2, whereas in the lower parts of the plot the opposite behavior occurred. It is believed that in Exp-2, deeper and more incised micro-channel (rills) were formed at the toeslope comparatively to Exp-1 due to higher runoff volume, resulting to higher flow depths at the lower sections of the plot. Further, the simulated flow depths along the longitudinal direction of the plot were lower in magnitude than the measured flow depths, thus WEPP-Improved under-predicted the values of the flow depth. One of the reasons for this difference is the fact that the WEPP-Improved model does not partition the flow into interrill and rill areas and calculates only an averaged flow depth along the plane using the equivalent friction factor (see section 3.1). It is believed that differences in the flow frictional characteristics between the interrill and rill areas affected the partitioning of flow (Baird et al. 1992). Consequently, there is a need to improve in the future the flow component to account for flow decomposition between the rills and interills, which will also affect the sediment calculations in the model.

#### 5.4.3 Tracer experiments and other recordings

Figures 5.30 and 5.31 illustrate a picture of the rhodamine pills and the milk, respectively, used during the progression of the experiment. Table 5.2 summarizes the travel time, travel distance, and mean velocity for each of the tracers placed at a specific cross-section along the plot and at a certain time. For Exp-1, it took ~ 240 sec for a rhodamine pill, placed at cross-section D, to travel to the end of the plot when ponding began (~ 35 min after the commencement of the experiment). In contrast, it took an average of 45 sec for the rhodamine placed at cross-section A to travel to the end of the plot when flow was at equilibrium, even though cross-section A is located 3 m upstream of the cross section D. These times are consistent with the explanation of the splash-dominated period of erosion (initial period of Exp-1) where there was little runoff, and

the rill-dominated period of erosion (later period of Exp-1) where there was increased runoff. The milk tracer was released slowly during the “transition” phase (before equilibrium) and it took ~ 60 sec to travel to the end of the plot. This travel time of the milk tracer (~ 60 sec) was comparable to the travel time of the rhodamine that was placed during the equilibrium stage (~ 40 – 50 sec).

For Exp-2, the travel times for flow were much lower than the ones for Exp-1. Specifically, it took ~ 16 sec for a rhodamine pill, placed at cross-section D, to travel to the end of the plot ~ 35 min after the commencement of the experiment vs. the travel time of ~ 240 sec determined for Exp-1. Along the same lines, the results for the milk show that during equilibrium conditions the travel time of the flow for Exp-2 was ~ 50.5 sec vs. the travel time of ~ 26 sec for Exp-1.

Lastly, Figure 5.32 provides snapshot pictures of the spray-painted areas for different times during the Exp-1, where runoff was first seen at the top half of the plot. The steeper slope in addition to the increased energy per unit area resulted in higher splash effects at the top half of the plot. Consequently, the red particles travelled to the end of the plot at an average velocity twice as fast as the blue particles (0.004 m/s vs. 0.002 m/s). The white particles, which originated between the red and the blue particles travelled at a mean velocity of 0.003 m/s. The aforementioned speeds correspond to the period during which splash erosion dominated and runoff was low. Also, from Figure 5.32, it is evident that after a while there was not significant changes in the sprayed areas, illustrating that equilibrium conditions were reached (at least in a qualitative sense). At the equilibrium stage, most of the particles had already being eroded from the spray painted areas and transported/deposited downstream or exited the plot.

The trend was different for the Exp-2, where the blue particles travelled faster than the red particles (0.013 m/s vs. 0.007 m/s). This was attributed to the fact that rill erosion was dominant throughout the duration of Exp-2. More flow in the lower parts of the plot meant higher flow depths (and consequently higher sediment discharge), which

can explain the higher flow depths in Exp-2 vs. Exp-1 at the lower part of the plot as presented in Table 5.1.

Table 5.1 Flow depth measurements within the plot.

		Exp-1		Exp-2	
Cross-section	Distance from the top of the plot (m)	Measured flow depth (mm)	Simulated flow depth (mm)	Measured flow depth (mm)	Simulated flow depth (mm)
A	1	4.8	1.0 - 2.0	2.3	1.9 - 3.3
B	2	4.5		2.7	
C	3	6.3		3.4	
D	4	7.0		3.5	
E	5	5.0		7.0	
F	6	5.7		6.5	

Table 5.2 Results from the tracer tests (Exp-1).

Time after start of experiment (min)	Tracer	Tracer location (cross-section)	Travel time to end of plot (s)	Approximate travel distance (m)	Mean velocity (m/s)
28	Rhodamine	D	240	3.0	0.01
105	Milk	A	59.0	6.0	0.10
251	Milk	A	26.1	6.0	0.23
273	Rhodamine	A	41.1	6.0	0.15
283	Rhodamine	A	51.6	6.5	0.13
293	Rhodamine	A	40.3	6.0	0.15

Table 5.3 Results from the tracer tests (Exp-2).

Time after start of experiment (min)	Tracer	Tracer location (cross-section)	Travel time to end of plot (s)	Approximate travel distance (m)	Mean velocity (m/s)
14	Rhodamine	D	15.95	3.0	0.19
87	Milk	A	53.31	6.0	0.11
91	Milk	A	47.42	6.0	0.12
167	Milk	A	50.53	6.0	0.12

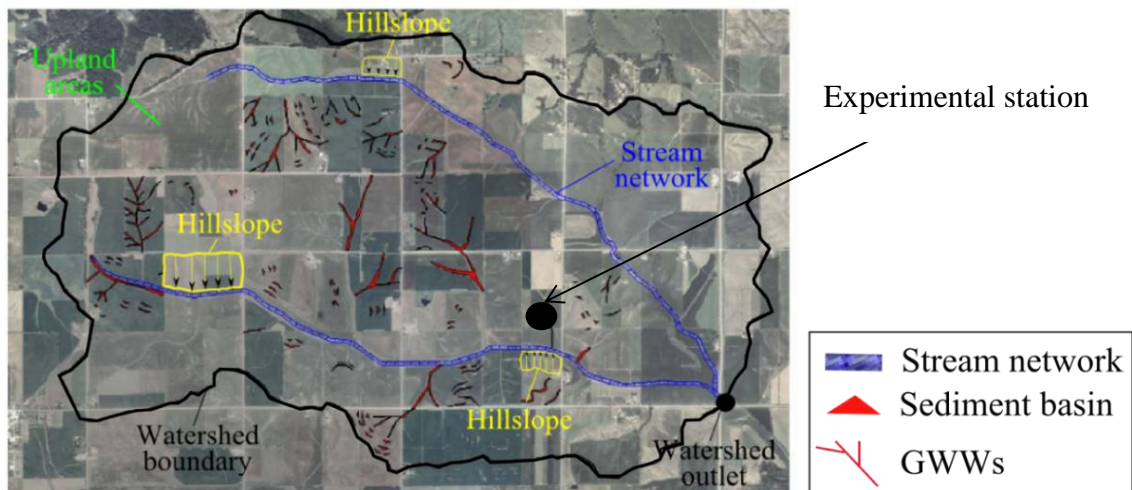


Figure 5.1 The experimental station within the South Amana Sub-Watershed located in the Clear Creek watershed, IA.

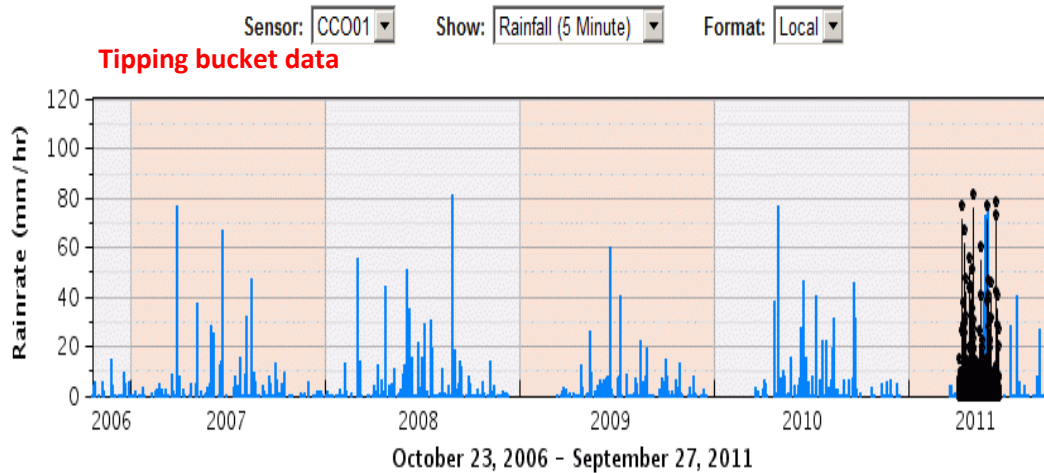


Figure 5.2 The time series of the tipping bucket data located nearby the experimental station within the South Amana Sub-Watershed located in the Clear Creek watershed, IA.



Figure 5.3 The 3 rainfall simulators placed in series located in the experimental station.



Figure 5.4 Water tanks used to store the excess water from the return pipe in the rainfall simulator.



Figure 5.5 Checking the pressure in the pipes during the experiment using binoculars.

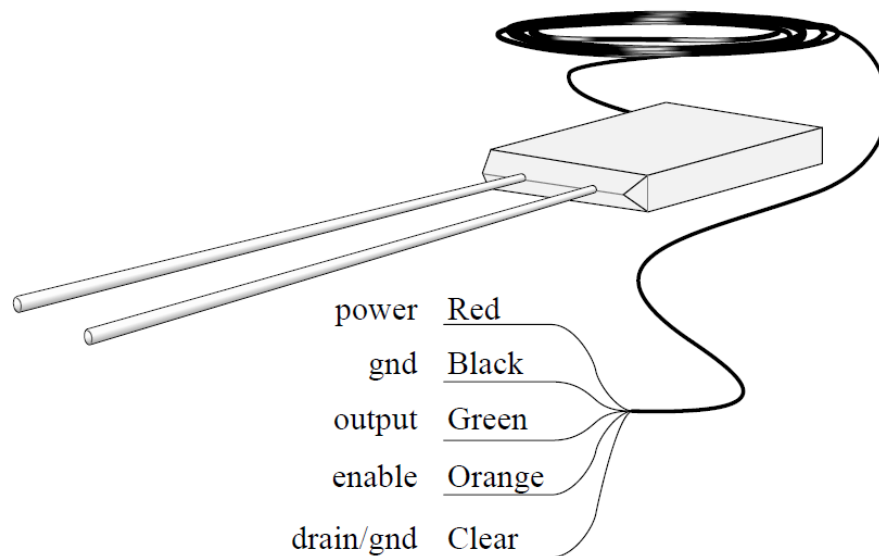


Figure 5.6 Water content reflectometer.



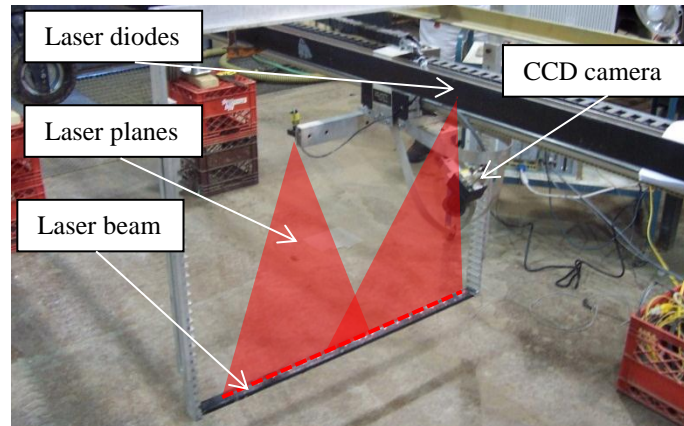


Figure 5.7 The two laser diodes (due to the camera area of view only one is shown in the picture) generating a single beam on the surface (see red dashed line).

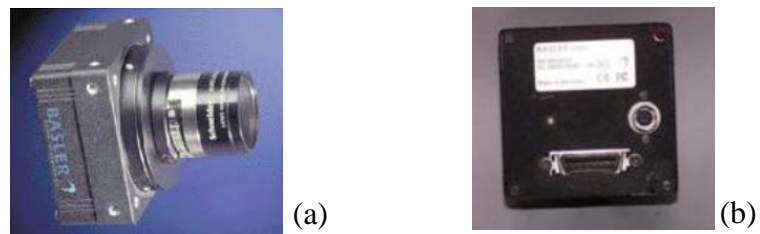


Figure 5.8 (a) The camera used in the laser system; (b) the connectors in the back of the camera.



Figure 5.9 The R3-CL frame grabber board.



Figure 5.10 The laser carriage.

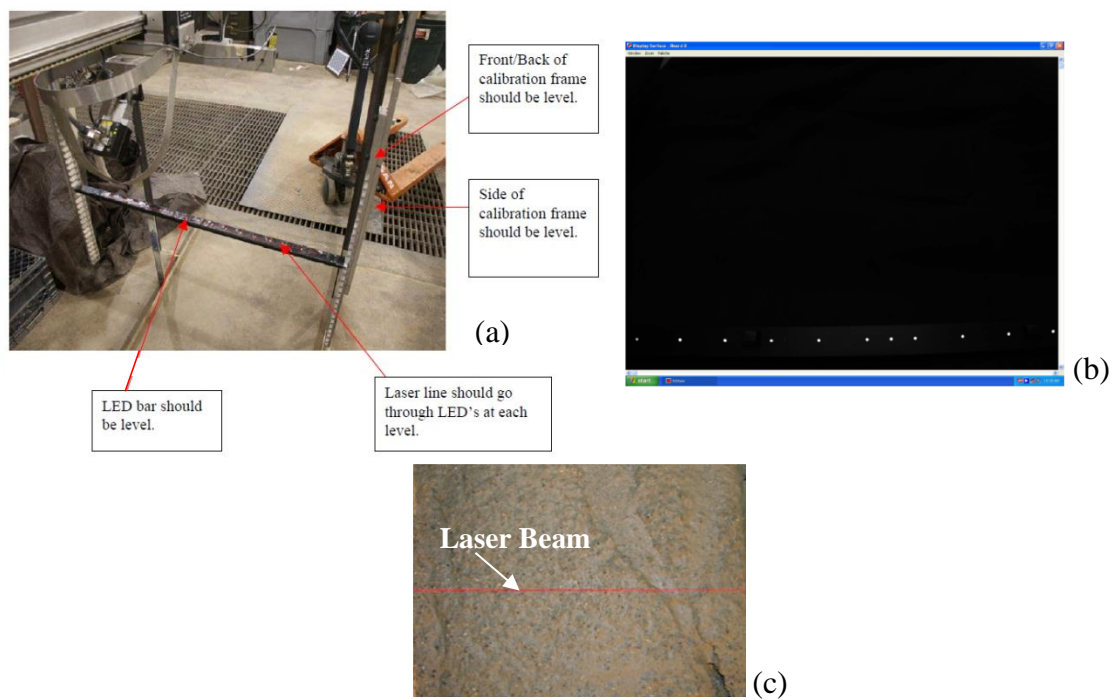


Figure 5.11(a) Calibration fixture with the LED light-bar; (b) camera view of the LED's in the light-bar; (c) laser beam projected on the soil surface.

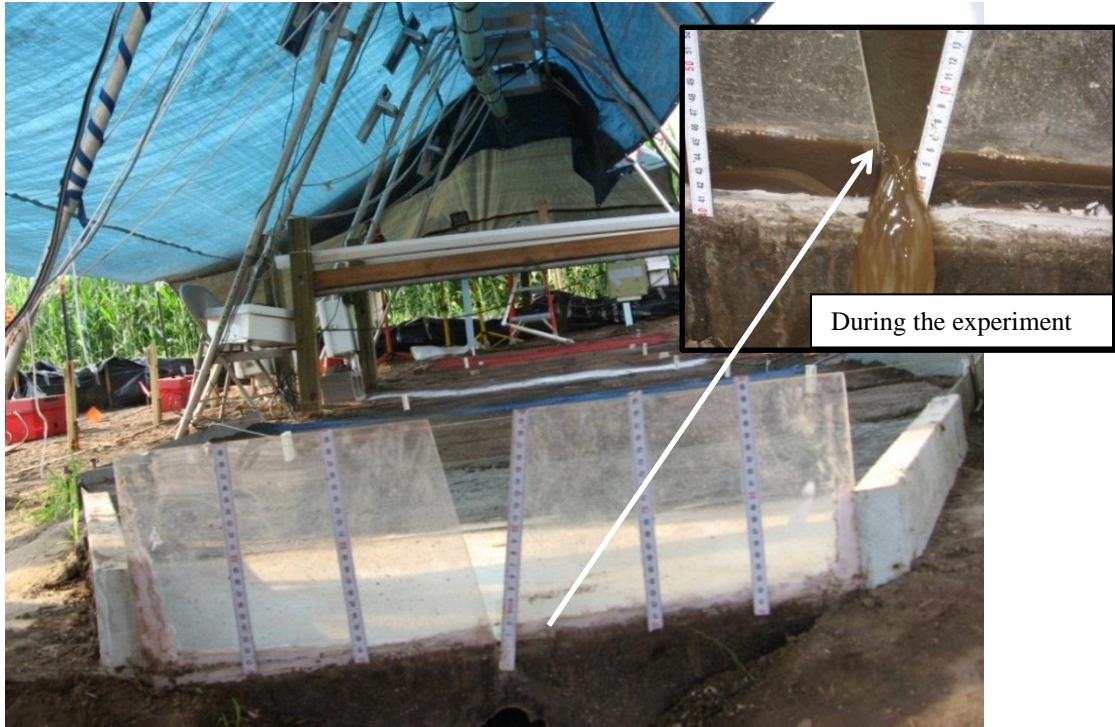


Figure 5.12 The weir at the plot outlet with the measured tapes to record the flow depth. Figure at the top right corner illustrates the flow depth at the weir during the experiment.



Figure 5.13 The board side walls along the perimeter of the plot.



Figure 5.14 A thin strip of the entrance covered with sprinkles of Portland concrete cement.

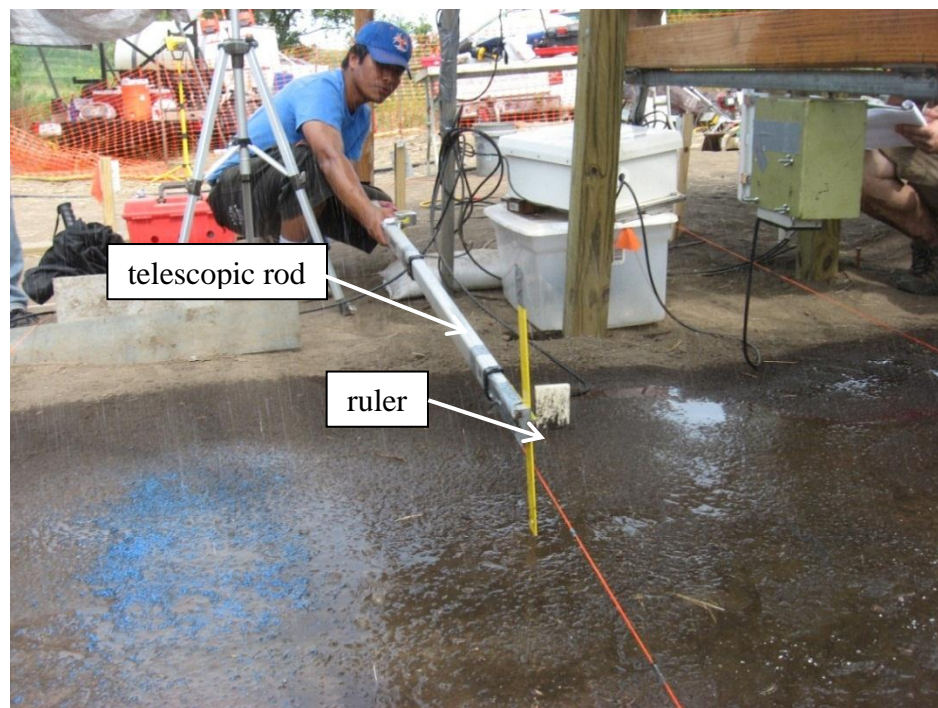


Figure 5.15 Flow depth measurements during the experiment.

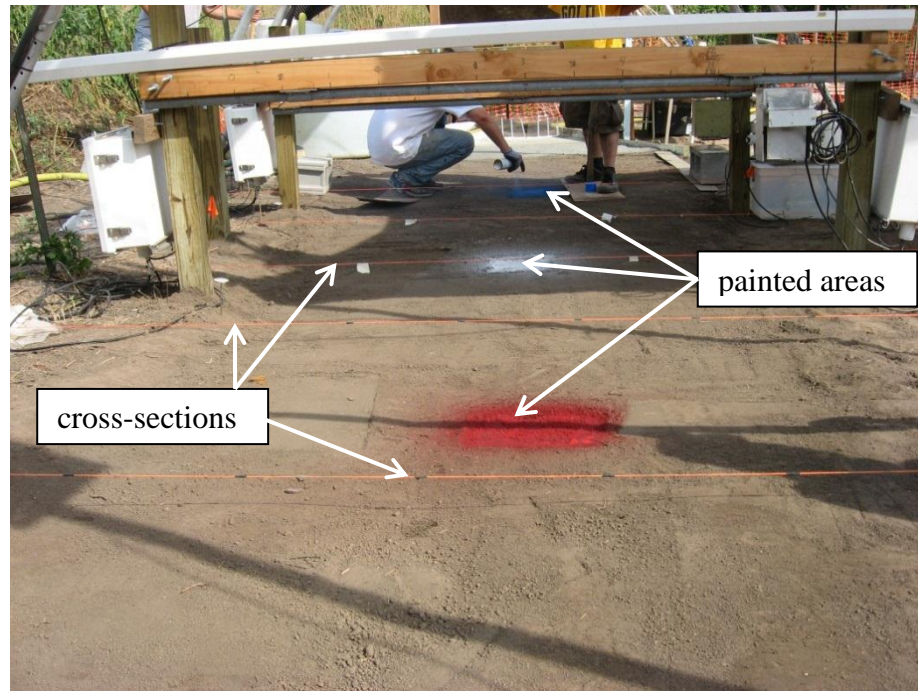


Figure 5.16 The spray painted areas (red, white, blue) and the cross-sections (orange rope) indicating the locations for the flow depth measurements (looking downslope).

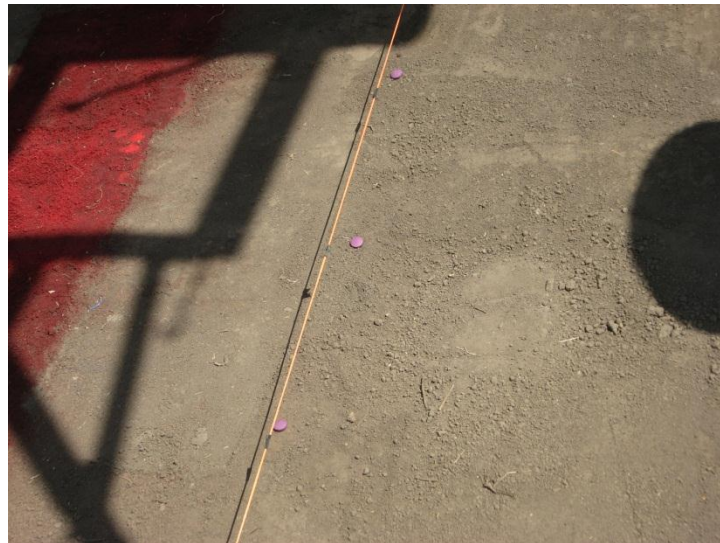


Figure 5.17 The rhodamine pills used as tracers.



Figure 5.18 Video recording of the experiments via a video-camera placed at the plot outlet.



Figure 5.19 Still images taken during the experiments.



Figure 5.20. The Honda 1.5 Hp tiller used to till the soil.



Figure 5.21 The plot set-up before the beginning of the experiment.



Figure 5.22 The experimental plot covered with a tarp.

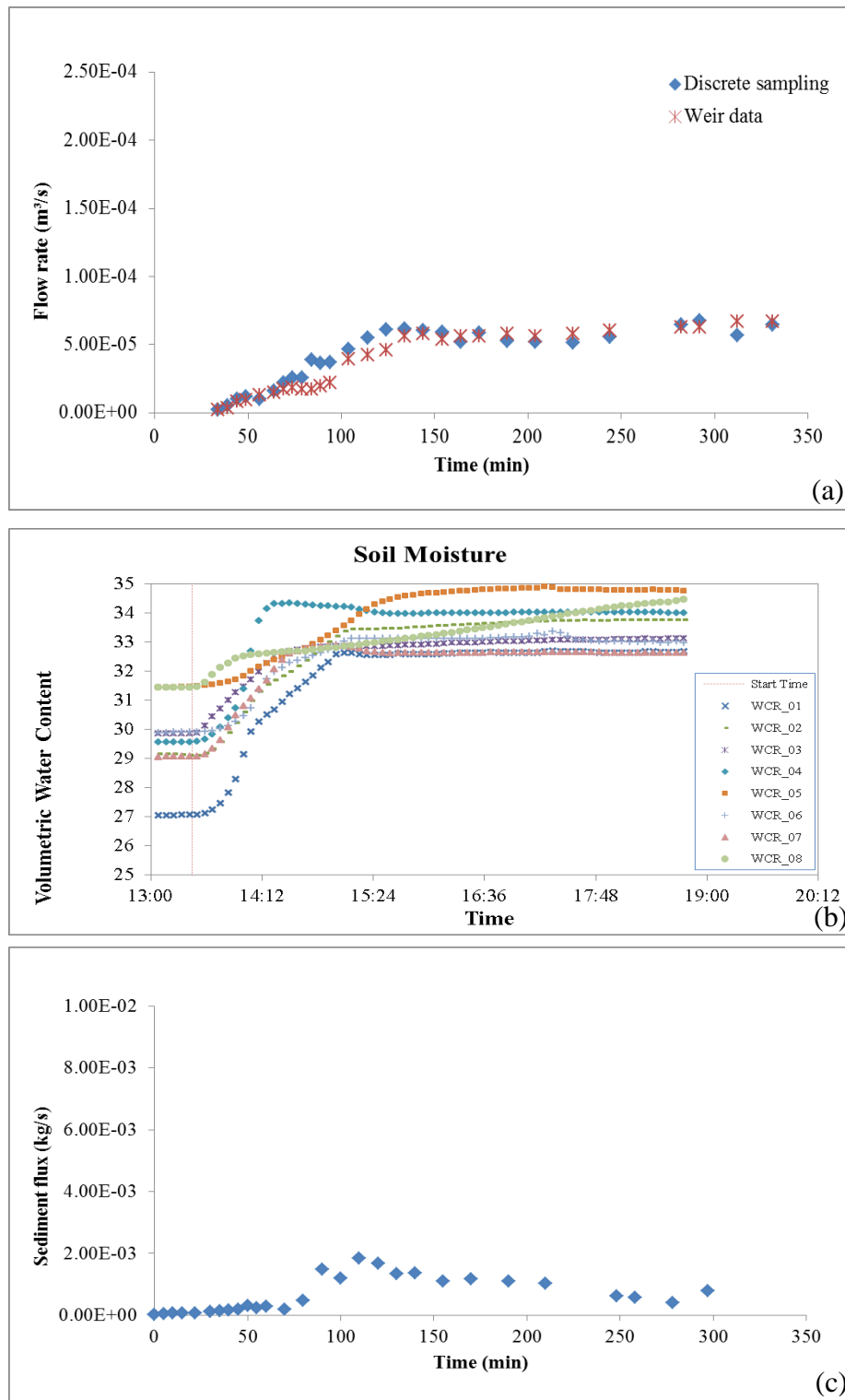


Figure 5.23 Time series results for (a) flow rate, (b) soil moisture and (c) sediment flux for Exp-1 (low rainfall intensity).



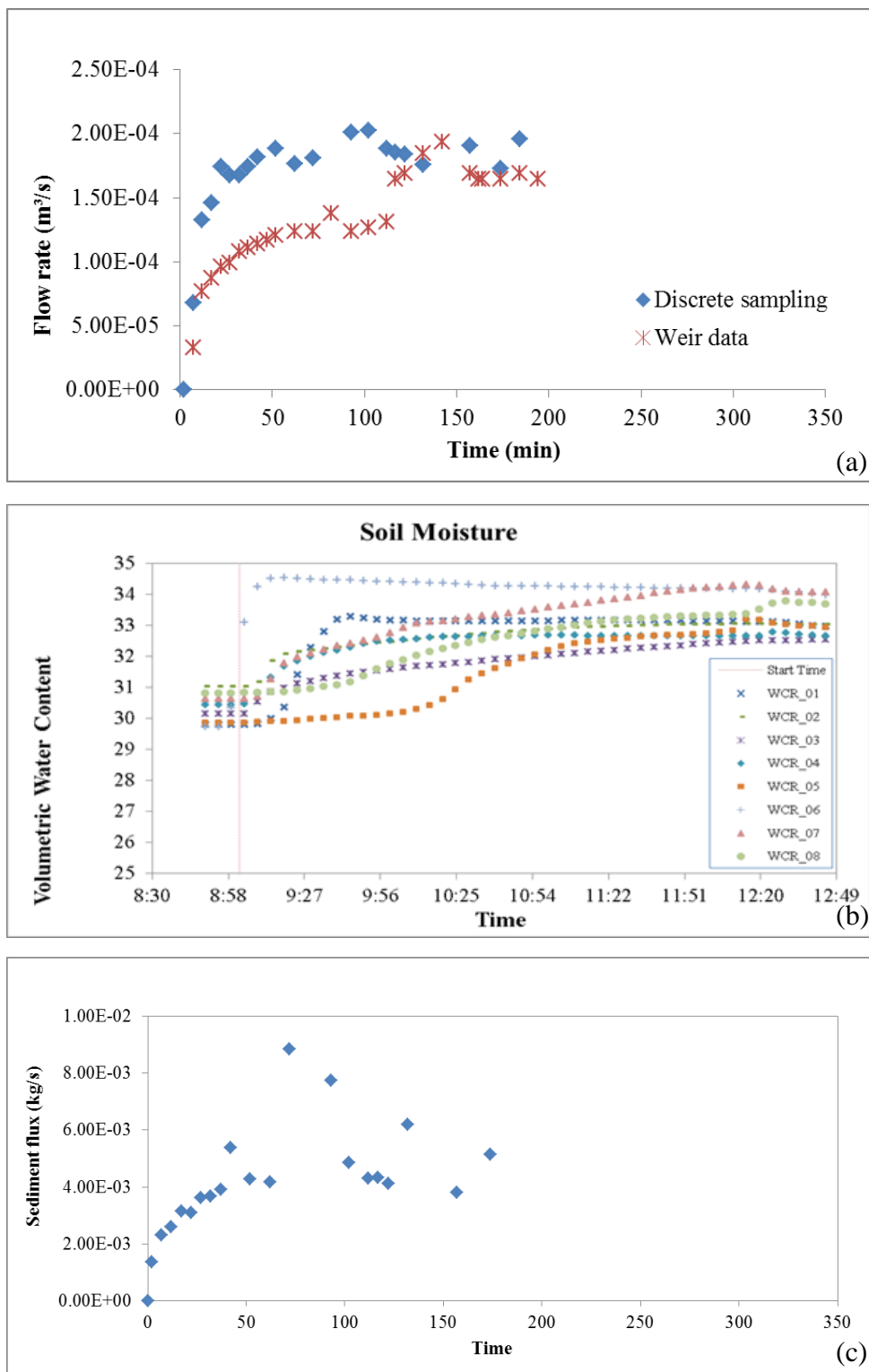


Figure 5.24 Time series results for (a) flow rate, (b) soil moisture and (c) sediment flux for Exp-2 (high rainfall intensity).



Figure 5.25 Splash erosion.

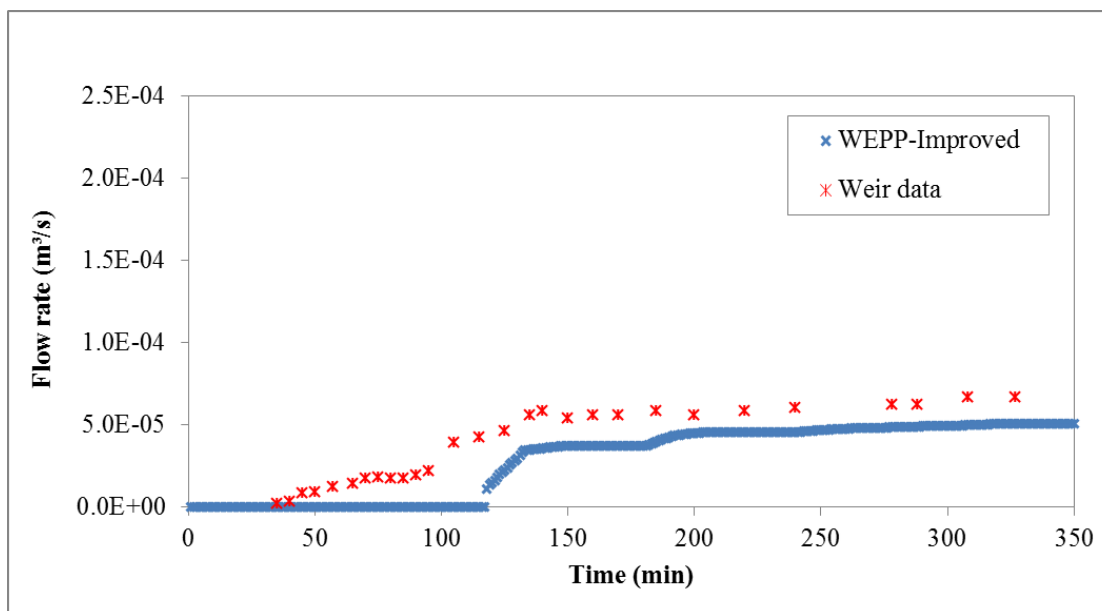


Figure 5.26 Comparison of the flow rates between measured vs. WEPP-Improved model for Exp-1 (low rainfall intensity).

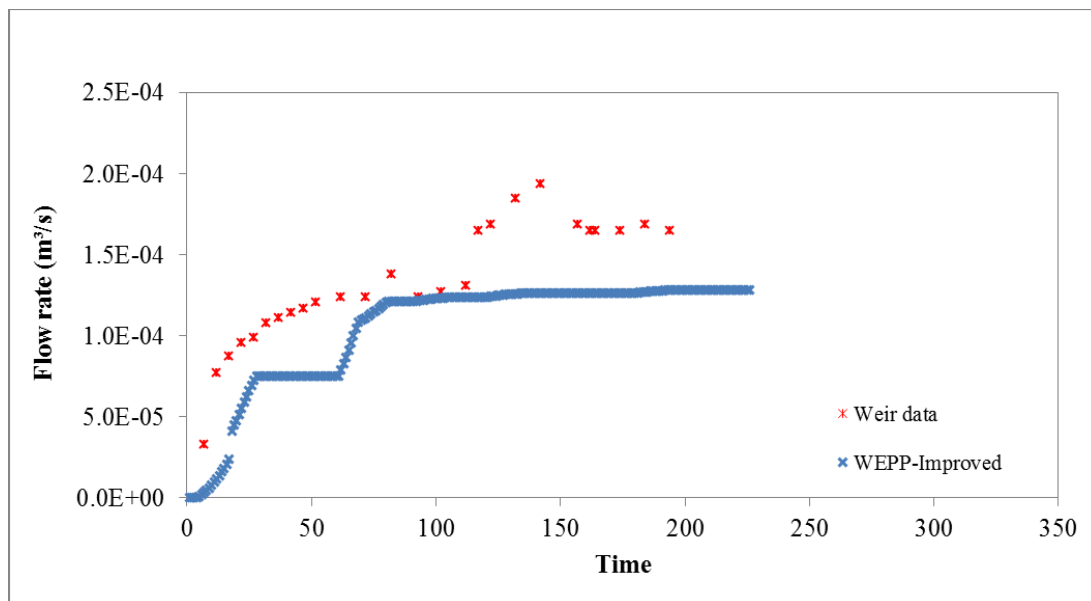


Figure 5.27 Comparison of the flow rates between measured vs. WEPP-Improved model for Exp-2 (high rainfall intensity).

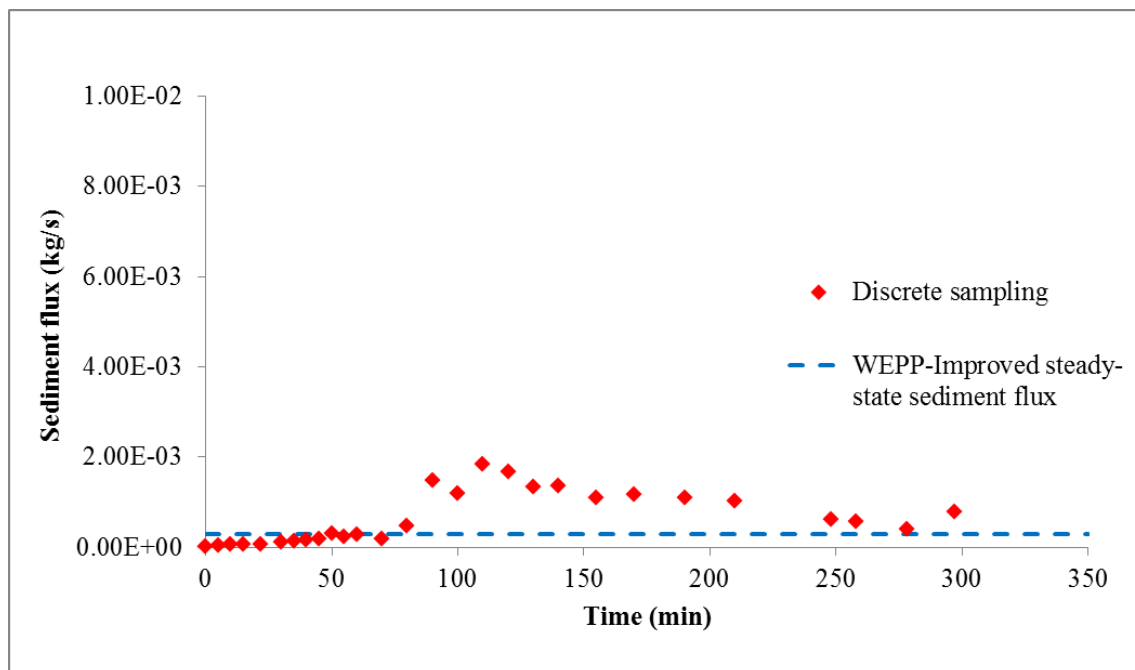


Figure 5.28 Comparison of the sediment fluxes between measured vs. WEPP-Improved model for Exp-1 (low rainfall intensity).

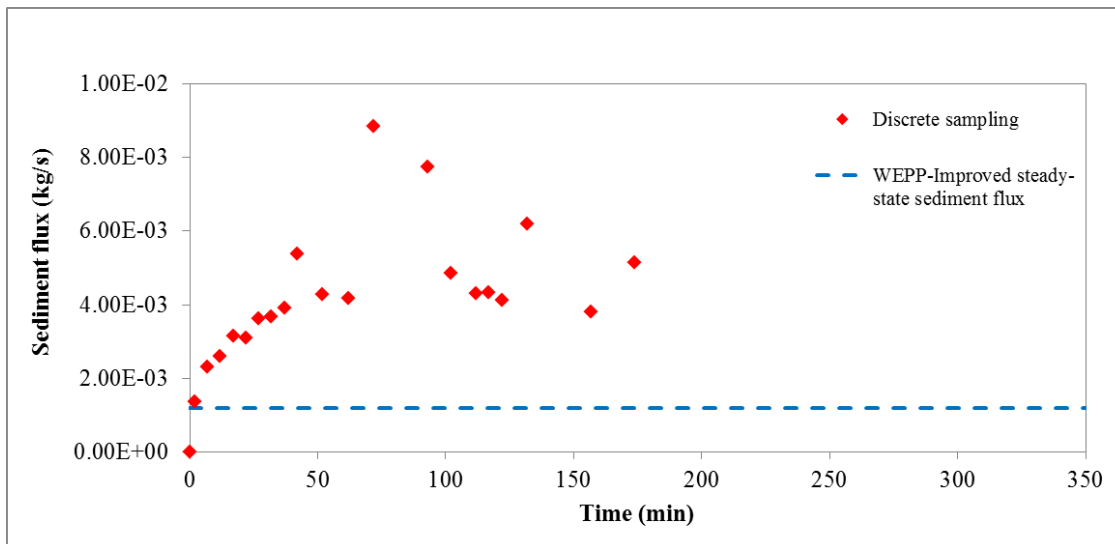


Figure 5.29 Comparison of the sediment fluxes between measured vs. WEPP-Improved model for Exp-2 (high rainfall intensity).



Figure 5.30 Rhodamine pills used during the experiment.



Figure 5.31 Milk dye tracer applied during the progression of the experiment.



Figure 5.32 Illustration of spray-painted areas during Exp-1 (red-summit, white-backslope, blue-toeslope).

## CHAPTER 6

### GENERIC SIMULATIONS TO TEST THE PERFORMANCE OF THE WEPP- IMPROVED MODEL

The goal of the generic simulations was to demonstrate the performance of the WEPP-Improved model under a wide range of climatic, topographic, LU/LC, and soil type conditions. Although the field experiments presented in chapter 5 provided insight into the flow and soil erosion processes along the hill, as well as the required data to test WEPP-Improved, these experiments were limited primarily due to time constraints. For this reason, 48, generic, single-storm simulations were performed at the hillslope scale to test the ability of WEPP-Improved to account for the effects of spatial heterogeneity (in terms of topography, LU/LC, and governing soil parameters at different OFEs) in both the spatial and temporal distribution of overland flow (runoff). By utilizing the TVD-MacCormack numerical scheme (e.g., Davis, 1984) to solve the kinematic wave equations, WEPP-Improved was able to capture sudden changes in the flow conditions (i.e., runoff depth) and simulate the propagation of sharp water fronts (shocks) formed due to spatial heterogeneity along the hill. For comparison purposes, the 48 numerical simulations were repeated using WEPP-Original.

#### 6.1 Selection of the input parameters

Basic input requirements for the WEPP-Improved (and WEPP-Original) model include climate, topography, LU/LC, and soil type. For the climate, 15-min resolution breakpoint rainfall input data were required for performing the single-storm simulations. The chosen rainfall events were representative of the study area in the SASW (see description in Chapter 5), based on an 11-year (1997-2007) NCEP Stage IV dataset of hourly precipitation measurements, and included a low and high in magnitude storm event (i.e., 2 single-storm events) from the summers of 2007 and 2008 (Figure 6.1).

With respect to the topography, the hillslope profiles had a fixed length of 250 m for all generic simulations, which is typical for hills found in the southeast Iowa (Dermisis et al., 2010). All the simulated hillslope profiles consisted of 2 OFEs having equal length of 125 m and all simulations were performed per unit width of the hill. The gradient of each OFE depended on the examined profile curvature, i.e., uniform, concave, or convex (Figure 6.2). For the uniform profile both OFEs had the same gradient of 2 %. For the concave profile the upstream OFE (i.e., OFE<sub>1</sub>) had a gradient of 3 % and the downstream OFE (i.e., OFE<sub>2</sub>) 1 %, whereas for the convex profile OFE<sub>1</sub> had a gradient of 1 % and OFE<sub>2</sub> 3 %. It should be noted that the average gradient of the simulated hillslope was selected to be 2 % in all 3 profile curvatures, which falls within the range of 0.5 % to 8 % found for hills in the southeast Iowa (Dermisis et al., 2010). The study by Dermisis et al. (2010) has shown that for the low magnitude storm events, as the average gradient of the typical hillslope increased above 3 %, the depth of runoff decreased to a point where the transport capacity equations (Yalin, 1963) used in WEPP-Original produced erroneous results. As a result, an average gradient towards the lower end of the typical range (0.5 – 8 %) was chosen.

With respect to the LU/LC, two land management types were selected; the 2-yr no till corn–fall till bean (NTC-FTB) crop rotation and the prairie Bromegrass (*Bromus wildenowii*) for Conservation Reserve Program (CRP). The NTC-FTB rotation has been previously found to be the most intense land use in terms of tillage operations comparatively to other crop rotations (Abaci and Papanicolaou, 2009), whereas the Bromegrass has demonstrated distinct differences from other crop rotations in terms of sediment delivery and runoff. Table 6.1 provides detailed information regarding the initial condition parameters used for the two management practices at the beginning of the simulated single-storm events. One key difference between the initial conditions for the two management practices is the rill and interrill cover (i.e., percent of the rill and interrill surface area, respectively, with surface cover on it) as well as the canopy cover.

Bromegrass has significantly larger percent of both canopy and rill/interill surface cover than the NTC-FTB, which ultimately affects rainfall interception, effective hydraulic conductivity, infiltration and runoff rates.

The soil types were selected to be TAMA (fine-silty, mixed, superactive, mesic Typic Argiudoll) or DOWNS (fine-silty, mixed, superactive and mesic Mollic Hapludalf), which are prominent in southeast Iowa (e.g., Abaci and Papanicolaou, 2009). Table 6.2 provides information regarding the input parameters for the two soil types. Also, the initial soil moisture was considered to be 73 % for the TAMA soil and 50 % for the DOWNS due to differences in the soil texture. The antecedent soil moisture content can significantly affect the time to runoff, the amount of runoff generated during a storm event, as well as soil erosion rates and sediment delivery ratios (e.g., Truman and Bradford, 1990; le Bissonnais et al., 1995; Abaci and Papanicolaou, 2009; Jomaa et al., 2012).

#### 6.2 First set of scenarios: spatial heterogeneity of curvature and LU/LC

For the first set of scenarios, both OFEs consisted of TAMA soil in order to isolate the effects of climate, topography and LU/LC on overland flow hydraulics. For the selected LU/LC (i.e., NTC-FTB and Bromegrass) there were 4 different scenarios depending on their location along the hill: (Sc-1) OFE<sub>1</sub> = NTC-FTB, OFE<sub>2</sub> = NTC-FTB; (Sc-2) OFE<sub>1</sub> = Bromegrass, OFE<sub>2</sub> = Bromegrass; (Sc-3) OFE<sub>1</sub> = NTC-FTB, OFE<sub>2</sub> = Bromegrass; (Sc-4) OFE<sub>1</sub> = Bromegrass, OFE<sub>2</sub> = NTC-FTB. Baseline conditions with respect to land management were considered the ones where the LU/LC was the same for both OFEs (i.e., Sc-1 and Sc-2). However, to account for the effects of the spatial heterogeneity in terms of LU/LC, different land management practices were applied for each OFE (i.e., Sc-3 and Sc-4). For each of the scenarios above, uniform, concave, and convex hillslope profiles were considered (see Figure 6.2) and the simulations were



performed for both the low and high magnitude single-storm events. Table 6.3 provides a summary of the conditions used in the first set of scenarios (Sc-1–Sc-4). Overall, 24 simulations were performed using the WEPP-Improved model and were repeated using the WEPP-Original model. The results from the first set of simulations are presented in Figures 6.3-6.10; Figures 6.3-6.6 provide the results for the low rainfall event and Figures 6.7-6.10 the ones for the high rainfall event. The plots in Figures 6.3-6.10 include (1) the simulated runoff hydrographs (and associated peak runoff rates,  $Q_{peak}$ ) of WEPP-Original and WEPP-Improved models at the outlet of the hillslope (i.e., point C in Figure 6.2) and (2) the simulated runoff hydrograph with WEPP-Improved at the mid-point of the hill (i.e., point B in Figure 6.2). It should be noted that WEPP-Original does not provide the hydrograph at the mid-point location and it is not plotted herein.

#### 6.2.1 Homogeneous baseline conditions

Figure 6.3 illustrates the results of the simulated runoff hydrographs for Sc-1 (i.e., low rainfall event conditions and NTC-FTB crop rotation for both OFEs) and for the 3 representative hillslope profiles (i.e., convex, uniform and concave). Due to homogeneity in terms of the LU/LC (i.e., NTC-FTB) and soil type (i.e., TAMA) between the 2 OFE's, any differences between the simulated runoff hydrographs are attributed to the effects of topographical heterogeneity, i.e., topographic curvature.

The comparison between the runoff hydrographs at point C, determined using WEPP-Original and WEPP-Improved, shows small differences in the shape of the hydrographs and associated  $Q_{peak}$  for the concave and convex hillslope profiles. The percent difference between  $Q_{peak}$  estimated from the two models is calculated hereafter as:

$$\% \text{ difference} = \frac{Q_{peak,WEPP-Improved} - Q_{peak,WEPP-Original}}{Q_{peak,WEPP-Original}} \quad (6.1)$$

Positive difference means that WEPP-Original predicted lower values of  $Q_{peak}$  than the WEPP-Improved, whereas negative means the opposite. For Sc-1, the percent difference in the predicted  $Q_{peak}$  between the WEPP-Improved and WEPP-Original models is approximately equal to 8 % and -4 % for the convex and concave profiles, respectively. The differences between the  $Q_{peak}$  diminish for the case of uniform hillslope profile and the simulated runoff hydrographs between the two models coincide.

Figure 6.4 presents the results for Sc-2 (i.e., low rainfall event conditions and Bromegrass for both OFEs) and for the 3 curvature profiles. Due to higher infiltration rates in the case of Bromegrass, the simulated runoff rates at the hillslope outlet are smaller in magnitude (range of  $0.0-1.0 \times 10^{-4} \text{ m}^3/\text{s}$ ) compared to the ones for the NTC-FTB crop rotation (range of  $0.0- 3.7 \times 10^{-4} \text{ m}^3/\text{s}$ ). Similar to Sc-1, the differences between the predicted  $Q_{peak}$  from the WEPP-Improved and WEPP-Original models are more prominent for the convex and concave curvature profiles and equal to 3 % and 62 %, respectively. Also, the predicted shapes of the hydrographs at point C for the concave hillslope profile are significantly different between the two models; the WEPP-Improved model predicted a bimodal runoff hydrograph (i.e., double peaks), whereas the WEPP-Original model predicted a unimodal runoff hydrograph (i.e., one peak; flat-topped hydrograph).

### 6.2.2 Spatially heterogeneous hillslope conditions

The results presented in Figures 6.5 and 6.6 demonstrate the effects of heterogeneity introduced by differences in the LU/LC between the 2 OFE's (i.e., NTC-FTB vs. Bromegrass). A general observation from these two figures is that spatial heterogeneity due to LU/LC affects significantly the shape and  $Q_{peak}$  of the hydrographs.

Figure 6.5 shows the predicted hydrographs for Sc-3 (i.e., low rainfall event conditions) for the 3 curvature types when the Bromegrass is introduced at the bottom OFE<sub>2</sub>. A comparison of the magnitude of the predicted  $Q_{peak}$  between the WEPP-Original

and WEPP-Improved models indicates that the WEPP-Original model under-predicts the  $Q_{\text{peak}}$  for the specified conditions. Specifically, the predicted values of  $Q_{\text{peak}}$  using the WEPP-Improved model were ~70 % – 170 % higher than the ones predicted by the WEPP-Original model, with the most prominent difference being the one for the concave hillslope profile.

In the case of the uniform and concave hillslope profiles, the WEPP-Improved model predicted bimodal runoff hydrographs at locations B and C. According to the results from the WEPP-Improved model, the first wave reaches location B at ~ 2,700 sec and the second wave peaks at ~ 8,100 sec for both the concave and uniform hillslopes. The two waves propagate downstream along OFE<sub>2</sub> and reach the hillslope outlet (location C) at times ~8,200 and ~11,200 sec for the uniform hillslope and ~ 8,700 and ~12,000 sec for the concave hillslope. The speed of the wave depends on the hillslope gradient and flow frictional characteristics (see equation 3.6b). Since the LU/LC in OFE<sub>2</sub> is Bromegrass for all three curvature profiles (i.e., same friction), any difference in the wave speed is attributed to changes in slope. As a result, the wave speed reduces for the concave slope due to the lower gradient of OFE<sub>2</sub>, a reduction which is captured by the WEPP-Improved model. In contrast, the WEPP-Original model predicts unimodal hydrographs at location C for both uniform and concave hillslope profiles. As discussed in section 3.2, the WEPP-Original model uses the equivalent plane approach when routing overland flow hydraulics in multiple OFE's. Consequently, the WEPP-Original model cannot capture discrepancies in the wave speeds amongst different OFEs due to different flow frictional characteristics, topographical features, and rainfall excess rates.

In the case of the convex hillslope profile (Figure 6.5), the WEPP-Improved model predicted a unimodal runoff hydrograph at locations B and C, which contradicts with the observations of the bimodal hydrograph for the uniform and concave hillslope profiles. Bimodality in runoff hydrographs may be preserved or lost depending on both the time to equilibrium and the speed of the successive waves. In other words, successive

waves may catch up with and overlap the first wave, resulting in a single wave (i.e., unimodal hydrograph), or propagate separately (i.e., bimodal or multimodal hydrograph). The existence of a single  $Q_{\text{peak}}$  for the convex hillslope profile at location B is associated with the wave speed in OFE<sub>1</sub>. Since the LU/LC in OFE<sub>1</sub> is NTC-FTB for all three curvature profiles (i.e., same friction), the wave speed in OFE<sub>1</sub> for the convex profile is higher than the one for the uniform and concave hillslope profiles. As a result, it is believed that the successive waves from OFE<sub>1</sub> in the convex profile overlapped, resulting to the unimodal hydrograph.

Figure 6.6 shows the results for Sc-4, where Bromegrass is introduced in the top OFE<sub>1</sub>. Similar to Sc-3, spatial heterogeneity of the LU/LC affected both the shape of the hydrograph and the associated  $Q_{\text{peak}}$ . For Sc-4, the WEPP-Original model over-predicted the values of  $Q_{\text{peak}}$  at point C, which is in contrast with the previous finding for Sc-3. The reason is that the WEPP-Original model calculates the rainfall volume lost due to canopy and surface residue cover interception based on the LU/LC of the bottom OFE<sub>2</sub>, which affects the water balance calculations and eventually the runoff volume and  $Q_{\text{peak}}$  as it is shown in Table 6.4. Based on the WEPP-Original model, in Sc-3 the amount of water intercepted due to canopy cover is controlled by the Bromegrass (i.e., higher canopy cover) leading to less runoff, whereas in Sc-4 canopy cover interception is controlled by the NTC-FTB (i.e., less canopy cover) resulting to higher runoff. For Sc-4 the difference in the magnitude of the  $Q_{\text{peak}}$  between the WEPP-Original and WEPP-Improved models ranges between -10% to -25 % depending on the hillslope profile curvature, with the most significant difference being the one for the concave profile. In the WEPP-Improved model the intercepted rainfall volume due to canopy and surface residue cover interception is determined by summing the intercepted volumes for the individual OFEs along the hill. Based on these calculations of the intercepted rainfall volume, the water balance was satisfied in all the examined scenarios using the WEPP-Improved model

with errors < 0.2 %, whereas using the WEPP-Original model the errors varied between 0.1-6.5 %.

Further, for Sc-4, the WEPP-Improved model predicted unimodal hydrographs at mid-point B for all hillslope profiles. However, at the hillslope outlet C bimodal hydrographs were predicted for the convex and uniform hillslope profiles. In this case it is believed that the waves leaving OFE<sub>1</sub> (and entering OFE<sub>2</sub>) propagate slower than the waves produced at OFE<sub>2</sub> due to higher friction (i.e., Bromegrass) and smaller hillslope gradient in OFE<sub>1</sub> (i.e., 1 % and 2 % for convex and uniform profiles, respectively- see Figure 6.2). Also, the waves at OFE<sub>2</sub> move faster than OFE<sub>1</sub> due to less infiltration and higher runoff rates (i.e., NTC-FTB in OFE<sub>2</sub> vs. Bromegrass in OFE<sub>1</sub>), thus the generated waves from the 2 OFEs never merge (bimodal hydrograph). In contrast, for the concave profile the speed of the waves entering OFE<sub>2</sub> were higher in magnitude than the ones in the convex and uniform profiles due to steeper gradient in the OFE<sub>1</sub> (i.e., 3 %- see Figure 6.2). Thus, the waves entering OFE<sub>2</sub> overlap the waves generated at OFE<sub>2</sub> (i.e., unimodal hydrograph).

Table 6.5 provides a summary of the results presented above from the first set of simulations and includes the examined scenario, the type of the outlet hydrograph (unimodal vs. bimodal) and the differences in the  $Q_{\text{peak}}$  for the different curvature profiles. Substantial differences in the water budget have been also reported by Roth and Capel (2012) for different LU/LC (e.g., scrub, prairie grass, strip cropping, conventional vs. non-conventional tillage practices).

### 6.2.3 Effects of climatic conditions

Figures 6.7-6.10 present the predicted runoff hydrographs for Sc-1–4 for the high storm event. As expected, these hydrographs exhibit larger values of runoff rates and  $Q_{\text{peak}}$  than the ones for the low storm event presented in Figures 5.3-5.6. It is a common characteristic that for the high storm event the percentage differences on the runoff

volumes and  $Q_{\text{peak}}$  are not significant between the WEPP-Improved and WEPP-Original models. The maximum difference on the  $Q_{\text{peak}}$  is observed for Sc-3 (i.e., OFE<sub>1</sub> = NTC-FTB; OFE<sub>2</sub> = Bromegrass), ranging between 5-17 %, and it is more pronounced for the concave hillslope profile.

### 6.3 Second set of scenarios: spatial heterogeneity of curvature and soil type

The second set of scenarios examined the effects of the spatial heterogeneity in terms of soil type on overland flow hydraulics. As discussed earlier, two representative soil types found in southeast Iowa were selected (TAMA and DOWNS). Since the high storm event did not show significant differences on the predicted runoff rates between WEPP-Original and WEPP-Improved models based on the first set of scenarios, herein only the low event simulations were performed. To isolate the effects of soil type on runoff rates, the same LU/LC was selected for both OFEs (either NTC-FTB or Bromegrass). Similarly to the first set of scenarios, baseline conditions with respect to soil type were considered the ones where the soil type was the same for both OFEs. However, spatial heterogeneity was introduced by considering different soil types for each OFE. For the selected soil types there were 4 different scenarios depending on their location along the hill: (Sc-5) OFE<sub>1</sub> = TAMA, OFE<sub>2</sub> = TAMA; (Sc-6) OFE<sub>1</sub> = DOWNS, OFE<sub>2</sub> = DOWNS; (Sc-7) OFE<sub>1</sub> = TAMA, OFE<sub>2</sub> = DOWNS; (Sc-8) OFE<sub>1</sub> = DOWNS, OFE<sub>2</sub> = TAMA. The simulations for Sc-5–Sc-8 were performed first by assuming NTC-FTB along the 2 OFE's and then repeated using Bromegrass. Table 6.6 provides a summary of the conditions used in the second set of scenarios. Overall, 24 runs were performed using the WEPP-Improved model and repeated using the WEPP-Original model. Since the LU/LC was the same for both OFE's, the amount of rainfall volume intercepted by the canopy cover was also the same. Consequently, WEPP-Original and

WEPP-Improved models provide the same amount of intercepted water volume for all scenarios 5-8 (see Table 6.7).

Figures 6.11 and 6.12 illustrate the runoff hydrographs for the case of homogeneous TAMA and DOWNS soil, respectively, having NTC-FTB as the crop rotation. Note that the results for the homogeneous TAMA soil type in Figure 6.11 are the same with the ones presented in Figure 6.3 since the simulated scenarios are the same. Similarly to the first set of simulations, topography affects the shape and magnitude of the runoff rates especially for the case of the convex and concave profiles. The difference in the predicted  $Q_{\text{peak}}$  between the WEPP-Improved and WEPP-Original models for homogeneous soil type ranges between ~1-19 %. By introducing soil type heterogeneity along the hill, the difference in  $Q_{\text{peak}}$  between the two models vary between 5-21% (see Figures 6.13 and 6.14)

Along the same lines, Figures 6.15-6.18 provide the results of Sc-5–Sc-8 when Bromegrass is used in both OFEs. Due to higher infiltration rates comparatively to the case of NTC-FTB, the runoff rates are significantly lower. In this case, the difference between the  $Q_{\text{peak}}$  is more pronounced compared to the case of NTC-FTB crop rotation and varies between 2%-200%, with the highest difference being the one for the concave profile.

Tables 6.8 and 6.9 provide a summary of the results presented above for the second set of simulations considering NTC-FTB and Bromegrass as the LU/LC, respectively, and includes the examined scenario, the type of the outlet hydrograph (unimodal vs. bimodal) and the differences in the  $Q_{\text{peak}}$  for the different curvature profiles.

#### 6.4 Shock formation and propagation

To better understand the differences in the predicted runoff rates between the WEPP-Improved and WEPP-Original model, the water surface profiles along the

longitudinal direction are plotted for selected scenarios. These scenarios are chosen based on the criteria for the formation of the shock presented in section 4.1 and are summarized below:

Criterion-1a:  $S_{o(OFE_1)} > S_{o(OFE_2)}$  (related to the profile curvature);

Criterion-1b:  $f_{e(OFE_1)} < f_{e(OFE_2)}$  (related to the micro-roughness);

Criterion-2:  $[q^{(c2)}]^{1/1.5} - [q^{(c1)}]^{1/1.5} > \alpha^{1/1.5} q_i \Delta t$  (related to hydrologic conditions, curvature, micro-roughness).

For criterion-1a, the water surface profile for Sc-2 is plotted for the low storm event and for the concave hillslope profile. Figure 6.19 presents the water surface profile (hereafter WSP) along the longitudinal direction of the hill using the WEPP-Improved model. Based on the simulated WSP, the WEPP-Improved model can capture the sudden change in the overland flow depth occurring at location B due to the abrupt change in the gradient between the 2 OFEs. In addition, one can observe the formation of a sharp, wave front moving from location  $\sim 150$  m at 6,300 sec to  $\sim 170$  m at 7,200 sec, which is numerically captured using the TVD-MacCormack scheme. In contrast, the WEPP-Original model uses the equivalent plane approach, thus, it is not developed to handle the formation and propagation of shocks (Stone et al. 1995) and the WSP is determined for the uniform slope having average gradient of 2 % as shown in Figure 6.20. The formation of a shock for the homogeneous (in terms of LU/LC and soil type) concave hillslope profile explains the significant difference in the shape of the hydrographs and the magnitude of  $Q_{\text{peak}}$  observed for Sc-1, 2 and Sc-5, 6.

To further illustrate the conditions under which a shock may form, the WSP is plotted for Sc-2 in Figure 6.21 and for the convex hillslope profile. Although there is a sudden change in the slope between the 2 OFEs, a shock does not form at OFE<sub>2</sub> since criterion-1a is not satisfied for this type of curvature profile.

For satisfying criterion-1b the WSP for Sc-3 is plotted (low event, uniform slope profile, OFE<sub>1</sub> = NTC-FTB; OFE<sub>2</sub> = Bromegrass). Similarly to the WSP for the concave



hillslope profile in Figure 6.19, a significant change in the flow depth occurs at location B due to sudden change in micro-roughness and surface/canopy cover between the 2 OFEs (i.e., different LU/LC), as it is clearly shown in Figure 6.22. The shock is located ~ 200 m from the top of the hill at 6,300 sec and arrives ~ 225 m downhill at 7,200 sec, having an average speed of ~ 0.028 m/s. The shock eventually reaches the outlet of the hill at ~ 8,100 sec, which coincides with the time to peak (see Figure 6.5)

In contrast to the previous case, the WSP for Sc-4 (low event, uniform slope profile, OFE<sub>1</sub> = Bromegrass, OFE<sub>2</sub>= NTC-FTB) is plotted in Figure 6.23. The change in the spatial distribution of the LU/LC resulted in the absence of shock at OFE<sub>2</sub>. Moreover, by comparing the runoff hydrographs for Sc-3 and Sc-4, presented in Figures 6.5 and 6.6, the effects of the shock formation in Sc-3 are pronounced in the predicted value of  $Q_{\text{peak}}$ . Specifically, the difference in the  $Q_{\text{peak}}$  is ~ 100 % between the WEPP-Improved and WEPP-Original models when a shock is formed, whereas this difference drops to ~ 20 % when no shock occurs.

Finally, for criterion 2 the WSP for Sc-7 is plotted in Figure 6.24 for the case of uniform slope and Bromegrass along the entire hill. In this case the difference in the soil type between the OFEs is associated with difference in the baseline hydraulic conductivity and antecedent soil moisture content which affects the infiltration rate and the rainfall excess  $q_l$  (see equations 3.1 and 3.3). According to Figure 6.23 a shock is formed at OFE<sub>2</sub> and propagates downhill. Further, one can observe from the WSP that the WEPP-Improved model is able to simulate the propagation of a shock wave over a barely “dry” bed, as it is illustrated by the very small flow depth (~ 0.0) after the location of the shock (at ~150 m). By plotting the WSP for Sc-8 in Figure 6.25, where TAMA soil type occurs in OFE<sub>2</sub> and DOWNS in OFE<sub>1</sub>, it is evident that no shock occurs since criterion-3 is not met. TAMA soil has greater hydraulic conductivity than DOWNS (0.74 vs. 0.83 mm/hr) and one would expect smaller runoff depth in the case of TAMA soil comparatively to the one for DOWNS. However, the two soil types have different initial

soil moisture contents, thus, different water storage capacities (defined as the total amount of water that is stored within the soil column). Since TAMA soil has greater soil moisture content than DOWNS, the former has less available storage for water, resulting to smaller infiltration rates as well as higher runoff rates and flow depths. Consequently, the right hand side term in criterion-2 is larger in the case of the TAMA soil and the criterion is more likely to be satisfied in the case of the DOWNS soil type, resulting to the formation of a shock.

Table 6.1 Input data for the 2 LU/LC.

Parameter / Land use	CRP	NTC-FTB
Initial Plant	Bromegrass	Soybean
Bulk density after last tillage (g/cm <sup>3</sup> )	1.37	1.31
Initial canopy cover (0-100%)	100.00	13.22
Days since last tillage (days)	10000	111
Days since last harvest (days)	10000	323
Initial frost depth (cm)	0	0
Initial interrill cover (0-100%)	99.9	30.76
Cumulative rainfall since last tillage (mm)	1.00E+05	561.2
Initial ridge height after last tillage (cm)	0	2.5
Initial rill cover (0-100%)	99.9	30.8
Initial roughness after last tillage (cm)	0.3	0.6
Rill spacing (cm)	100	100
Initial snow depth (cm)	0	0
Initial depth of thaw (cm)	0	0
Depth of secondary tillage layer (cm)	0	7.62
Depth of primary tillage layer (cm)	0	22.86
Initial rill width (cm)	26.18	13.31
Initial total dead root mass (kg/m <sup>2</sup> )	1.00E-05	9.57E-02
Initial total submerged residue mass (kg/m <sup>2</sup> )	1.00E-05	4.60E-01

Table 6.2 Compositions of TAMA and DOWNS soil types.

Soil Type (-)	Layer ---	Depth (cm)	Sand (%)	Clay (%)	Silt (%)	SOM (%)	K <sub>b</sub> (mm/hr)
Tama	1	20.32	5	26	68	4.4	0.83
	2	45.72	5	26	68	3.0	
	3	81.28	4	31	64	1.5	
	4	152.4	3	25	70	0.25	
Downs	1	20.32	3	22	73	3.1	0.74
	2	43.18	3	22	73	1.0	
	3	99.06	3	30	64	0.75	
	4	152.4	5	24	70	0.25	

Table 6.3 The first set of simulations to address the effects of LU/LC heterogeneity.

Scenario	Climate	Hillslope profile	LU/LC	Soil type	No. of simulations
1	Low	Convex	OFE <sub>1</sub> =NTC-FTB OFE <sub>2</sub> =NTC-FTB	TAMA	6
		Uniform			
	High	Concave			
2	Low	Convex	OFE <sub>1</sub> =Bromegrass OFE <sub>2</sub> =Bromegrass	TAMA	6
		Uniform			
	High	Concave			
3	Low	Convex	OFE <sub>1</sub> =NTC-FTB OFE <sub>2</sub> = Bromegrass	TAMA	6
		Uniform			
	High	Concave			
4	Low	Convex	OFE <sub>1</sub> = Bromegrass OFE <sub>2</sub> = NTC-FTB	TAMA	6
		Uniform			
	High	Concave			

Table 6.4 Water balance for first set of scenarios.

	Scenario	Topo- graphy	Rainfall (m <sup>3</sup> )	WEPP-Original					WEPP-Improved				
				CI (m <sup>3</sup> )	I (m <sup>3</sup> )	R (m <sup>3</sup> )	$Q_{peak}$ $\times 10^{-4}$ (m <sup>3</sup> /s)	E (%)	CI (m <sup>3</sup> )	I (m <sup>3</sup> )	R (m <sup>3</sup> )	$Q_{peak}$ $\times 10^{-4}$ (m <sup>3</sup> /s)	E (%)
Low Event	NTC-FTB, Bromegrass	Convex	6.01	0.65	3.85	1.32	1.31	3.1	0.34	3.92	1.75	2.22	0.0
		Uniform		0.65	3.85	1.26	1.12	4.2	0.34	3.92	1.75	2.27	0.0
		Concave		0.65	3.85	1.10	0.86	6.7	0.34	3.92	1.75	2.58	0.0
	Bromegrass, NTC-FTB	Convex		0.03	4.02	1.92	3.08	0.7	0.34	3.92	1.75	2.77	0.0
		Uniform		0.03	4.02	1.90	3.08	1.0	0.34	3.92	1.75	2.57	0.0
		Concave		0.03	4.02	1.87	2.77	1.5	0.34	3.92	1.75	2.08	0.0
	NTC-FTB, NTC-FTB	Convex		0.03	3.73	2.21	3.52	0.7	0.03	3.73	2.25	3.79	0.0
		Uniform		0.03	3.73	2.20	3.48	0.8	0.03	3.73	2.25	3.48	0.0
		Concave		0.03	3.73	2.16	3.41	1.5	0.03	3.73	2.25	3.26	0.0
	Bromegrass, Bromegrass	Convex		0.65	4.11	1.07	0.99	3.0	0.65	4.11	1.25	1.02	0.0
		Uniform		0.65	4.11	1.01	0.85	4.0	0.65	4.11	1.25	0.85	0.0
		Concave		0.65	4.11	0.86	0.65	6.5	0.65	4.11	1.24	1.05	0.2

Table 6.4 Continued.

	Scenario	Topo- graphy	Rainfall (m <sup>3</sup> )	WEPP-Original					WEPP-Improved				
				CI <sup>a</sup> (m <sup>3</sup> )	I <sup>b</sup> (m <sup>3</sup> )	R <sup>c</sup> (m <sup>3</sup> )	Q <sub>peak</sub> x10 <sup>-4</sup> (m <sup>3</sup> /s)	E <sup>d</sup> (%)	CI (m <sup>3</sup> )	I (m <sup>3</sup> )	R (m <sup>3</sup> )	Q <sub>peak</sub> x10 <sup>-4</sup> (m <sup>3</sup> /s)	E (%)
High Event	NTC-FTB, Bromegrass	Convex	15.33	0.65	8.33	6.32	7.09	0.2	0.34	8.50	6.48	7.41	0.1
		Uniform		0.65	8.33	6.32	6.90	0.2	0.34	8.50	6.48	7.40	0.1
		Concave		0.65	8.33	6.30	6.21	0.3	0.34	8.49	6.47	7.30	0.1
	Bromegrass, NTC-FTB	Convex		0.03	8.65	6.63	8.03	0.1	0.34	8.49	6.49	8.21	0.1
		Uniform		0.03	8.65	6.63	7.90	0.1	0.34	8.50	6.48	7.91	0.1
		Concave		0.03	8.65	6.60	7.73	0.3	0.34	8.50	6.48	7.51	0.1
	NTC-FTB, NTC-FTB	Convex		0.03	8.14	7.13	8.34	0.2	0.03	8.14	7.16	8.54	0.0
		Uniform		0.03	8.14	7.13	8.22	0.2	0.03	8.14	7.16	8.17	0.0
		Concave		0.03	8.14	7.10	8.03	0.4	0.03	8.14	7.15	7.80	0.1
	Bromegrass, Bromegrass	Convex		0.65	8.86	5.80	6.80	0.1	0.65	8.86	5.80	6.49	0.1
		Uniform		0.65	8.86	5.80	6.54	0.1	0.65	8.86	5.80	6.52	0.1
		Concave		0.65	8.86	5.77	5.76	0.3	0.65	8.86	5.79	6.34	0.2

<sup>a</sup>CI= Cover interception

<sup>b</sup>I= Infiltration & dep. storage

<sup>c</sup>R= Runoff

<sup>d</sup>E= Continuity deficit error

Table 6.5 Summary table for the first set of scenarios (low rainfall intensity).

Low Event	Outlet hillslope hydrograph		% $Q_{\text{peak}}$ difference
	WEPP-Original	WEPP-Improved	
Scenario 1 OFE <sub>1</sub> : NTC-FTB OFE <sub>2</sub> : NTC-FTB	CX <sup>a</sup> : Unimodal U <sup>b</sup> : Unimodal CV <sup>c</sup> : Unimodal	CX: Bimodal U: Unimodal CV: Unimodal	CX: +8.0 % U: 0.0 % CV: -4.0 %
Scenario 2 OFE <sub>1</sub> : Bromegrass OFE <sub>2</sub> : Bromegrass	CX: Unimodal U: Unimodal CV: Unimodal	CX: Unimodal U: Unimodal CV: Unimodal	CX: +3% U: 0.0 % CV: +62 %
Scenario 3 OFE <sub>1</sub> : NTC-FTB OFE <sub>2</sub> : Bromegrass	CX: Unimodal U: Unimodal CV: Unimodal	CX: Unimodal U: Bimodal CV: Bimodal	CX: +70 % U: +103 % CV: +170 %
Scenario 4 OFE <sub>1</sub> : Bromegrass OFE <sub>2</sub> : NTC-FTB	CX: Unimodal U: Unimodal CV: Unimodal	CX: Bimodal U: Bimodal CV: Unimodal	CX: -10% U: -17 % CV: -25 %

<sup>a</sup>CX = convex hillslope profile

<sup>b</sup>U = uniform hillslope profile

<sup>c</sup>CV = concave hillslope profile

Table 6.6 The second set of scenarios to address the effects of soil type heterogeneity.

Scenario	Hillslope profile	LU/LC	Soil type	Climate	No. of simulations
5	Convex	OFE <sub>1</sub> =NTC-FTB OFE <sub>2</sub> =NTC-FTB	OFE <sub>1</sub> = TAMA OFE <sub>2</sub> = TAMA	Low	6
	Uniform				
	Concave	OFE <sub>1</sub> =Bromegrass OFE <sub>2</sub> =Bromegrass			
6	Convex	OFE <sub>1</sub> =NTC-FTB OFE <sub>2</sub> =NTC-FTB	OFE <sub>1</sub> = DOWNS OFE <sub>2</sub> = DOWNS	Low	6
	Uniform				
	Concave	OFE <sub>1</sub> =Bromegrass OFE <sub>2</sub> =Bromegrass			
7	Convex	OFE <sub>1</sub> =NTC-FTB OFE <sub>2</sub> =NTC-FTB	OFE <sub>1</sub> = TAMA OFE <sub>2</sub> = DOWNS	Low	6
	Uniform				
	Concave	OFE <sub>1</sub> =Bromegrass OFE <sub>2</sub> =Bromegrass			
8	Convex	OFE <sub>1</sub> =NTC-FTB OFE <sub>2</sub> =NTC-FTB	OFE <sub>1</sub> = DOWNS OFE <sub>2</sub> = TAMA	Low	6
	Uniform				
	Concave	OFE <sub>1</sub> =Bromegrass OFE <sub>2</sub> =Bromegrass			



Table 6.7 Water balance for second set of scenarios.

	Scenario	Topography	Rainfall (m <sup>3</sup> )	WEPP-Original					WEPP-Improved				
				CI (m <sup>3</sup> )	I (m <sup>3</sup> )	R (m <sup>3</sup> )	$Q_{peak}$ $\times 10^{-4}$ (m <sup>3</sup> /s)	E (%)	CI (m <sup>3</sup> )	I (m <sup>3</sup> )	R (m <sup>3</sup> )	$Q_{peak}$ $\times 10^{-4}$ (m <sup>3</sup> /s)	E (%)
NTC -FTB	TAMA, TAMA	Convex	6.01	0.03	3.73	2.21	3.52	0.7	0.03	3.73	2.25	3.79	0.0
		Uniform		0.03	3.73	2.20	3.48	1.0	0.03	3.73	2.25	3.48	0.0
		Concave		0.03	3.73	2.16	3.41	1.5	0.03	3.73	2.25	3.26	0.0
	DOWNS, DOWNS	Convex		0.03	4.54	1.40	2.41	0.7	0.03	4.54	1.44	2.37	0.0
		Uniform		0.03	4.54	1.39	2.28	1.0	0.03	4.54	1.44	2.28	0.0
		Concave		0.03	4.54	1.35	1.75	1.5	0.03	4.54	1.44	2.08	0.0
	TAMA, DOWNS	Convex		0.03	4.16	1.78	1.78	0.7	0.03	4.13	1.85	3.13	0.0
		Uniform		0.03	4.16	1.76	1.76	0.8	0.03	4.13	1.85	2.68	0.0
		Concave		0.03	4.16	1.72	1.72	1.5	0.03	4.13	1.85	2.59	0.0
	DOWNS, TAMA	Convex		0.03	4.16	1.78	1.78	0.7	0.03	4.13	1.85	3.18	0.0
		Uniform		0.03	4.16	1.75	1.75	1.0	0.03	4.13	1.84	3.18	0.0
		Concave		0.03	4.16	1.72	1.72	1.5	0.03	4.13	1.84	3.01	0.0

Table 6.7 Continued.

	Scenario	Topo- graphy	Rain- fall (m <sup>3</sup> )	WEPP-Original					WEPP-Improved				
				CI <sup>a</sup> (m <sup>3</sup> )	I <sup>b</sup> (m <sup>3</sup> )	R <sup>c</sup> (m <sup>3</sup> )	Q <sub>peak</sub> x10 <sup>-4</sup> (m <sup>3</sup> /s)	E <sup>d</sup> (%)	CI (m <sup>3</sup> )	I (m <sup>3</sup> )	R (m <sup>3</sup> )	Q <sub>peak</sub> x10 <sup>-4</sup> (m <sup>3</sup> /s)	E (%)
Brome- grass	TAMA, TAMA	Convex	6.01	0.65	4.11	1.07	0.99	3.0	0.65	4.11	1.25	1.02	0.0
		Uniform		0.65	4.11	1.01	0.85	4.0	0.65	4.11	1.25	0.85	0.0
		Concave		0.65	4.11	0.86	0.65	6.2	0.65	4.11	1.24	1.05	0.2
	DOWNS, DOWNS	Convex		0.65	4.91	0.27	0.22	3.0	0.65	4.91	0.45	0.23	0.0
		Uniform		0.65	4.91	0.24	0.18	4.0	0.65	4.91	0.45	0.19	0.0
		Concave		0.65	4.91	0.18	0.14	6.2	0.65	4.90	0.45	0.23	0.0
	TAMA, DOWNS	Convex		0.65	4.53	0.65	0.54	3.0	0.65	4.51	0.84	0.67	0.0
		Uniform		0.65	4.53	0.58	0.46	4.0	0.65	4.51	0.85	0.85	0.0
		Concave		0.65	4.53	0.47	0.35	6.5	0.65	4.50	0.85	1.05	0.0
	DOWNS, TAMA	Convex		0.65	4.53	0.65	0.54	3.0	0.65	4.50	0.85	1.02	0.0
		Uniform		0.65	4.53	0.59	0.46	3.5	0.65	4.51	0.85	0.85	0.0
		Concave		0.65	4.53	0.47	0.35	4.5	0.65	4.51	0.84	0.63	0.2

<sup>a</sup>CI= Cover interception

<sup>b</sup>I= Infiltration & dep. storage

<sup>c</sup>R= Runoff

<sup>d</sup>E= Continuity deficit error

Table 6.8 Summary table for the second set of scenarios (LU/LC = NTC-FTB).

Low Event	Outlet hillslope hydrograph		% $Q_{\text{peak}}$ difference
	WEPP-Original	WEPP-Improved	
Scenario 1 OFE <sub>1</sub> : TAMA OFE <sub>2</sub> : TAMA	CX <sup>a</sup> : Unimodal U <sup>b</sup> : Unimodal CV <sup>c</sup> : Unimodal	CX: Bimodal U: Unimodal CV: Unimodal	CX: +8.0 % U: 0.0 % CV: -4.0 %
Scenario 2 OFE <sub>1</sub> : DOWNS OFE <sub>2</sub> : DOWNS	CX: Unimodal U: Unimodal CV: Unimodal	CX: Bimodal U: Bimodal CV: Bimodal	CX: -2.0% U: 0.0 % CV: +19 %
Scenario 3 OFE <sub>1</sub> : TAMA OFE <sub>2</sub> : DOWNS	CX: Unimodal U: Unimodal CV: Unimodal	CX: Unimodal U: Bimodal CV: Bimodal	CX: +8.0 % U: -8.0 % CV: +5.0 %
Scenario 4 OFE <sub>1</sub> : DOWNS OFE <sub>2</sub> : TAMA	CX: Unimodal U: Unimodal CV: Unimodal	CX: Bimodal U: Bimodal CV: Unimodal	CX: +10 % U: + 9.0 % CV: +22 %

<sup>a</sup>CX = convex hillslope profile

<sup>b</sup>U = uniform hillslope profile

<sup>c</sup>CV = concave hillslope profile

Table 6.9 Summary table for the first set of scenarios (LU/LC = Bromegrass).

Low Event	Outlet hillslope hydrograph		% $Q_{\text{peak}}$ difference
	WEPP-Original	WEPP-Improved	
Scenario 1 OFE <sub>1</sub> : TAMA OFE <sub>2</sub> : TAMA	CX <sup>a</sup> : Unimodal U <sup>b</sup> : Unimodal CV <sup>c</sup> : Unimodal	CX: Bimodal U: Unimodal CV: Unimodal	CX: +3.0 % U: 0.0 % CV: +62 %
Scenario 2 OFE <sub>1</sub> : DOWNS OFE <sub>2</sub> : DOWNS	CX: Unimodal U: Unimodal CV: Unimodal	CX: Unimodal U: Unimodal CV: Unimodal	CX: +5.0 % U: 0.0 % CV: +66 %
Scenario 3 OFE <sub>1</sub> : TAMA OFE <sub>2</sub> : DOWNS	CX: Unimodal U: Unimodal CV: Unimodal	CX: Unimodal U: Bimodal CV: Bimodal	CX: +24 % U: +86 % CV: +200 %
Scenario 4 OFE <sub>1</sub> : DOWNS OFE <sub>2</sub> : TAMA	CX: Unimodal U: Unimodal CV: Unimodal	CX: Bimodal U: Bimodal CV: Unimodal	CX: +89 % U: +85 % CV: +79 %

<sup>a</sup>CX = convex hillslope profile

<sup>b</sup>U = uniform hillslope profile

<sup>c</sup>CV = concave hillslope profile

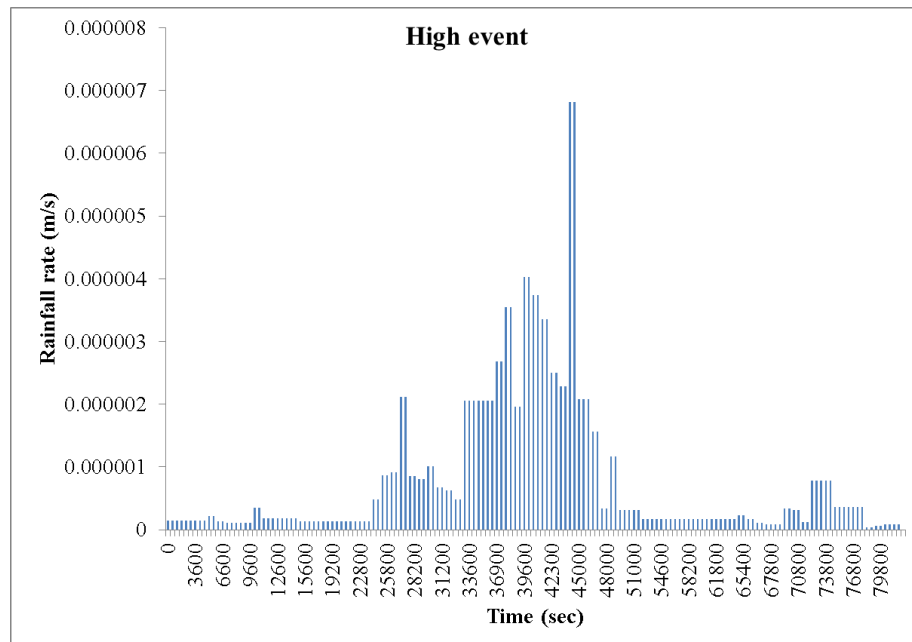
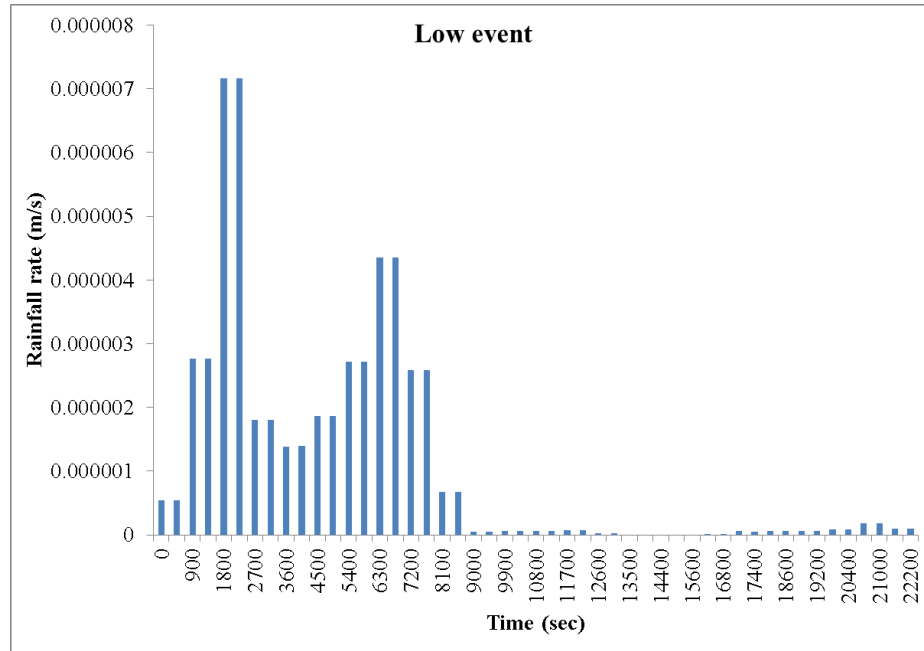


Figure 6.1 The low (top) and high (bottom) single storm events used in the generic simulation.

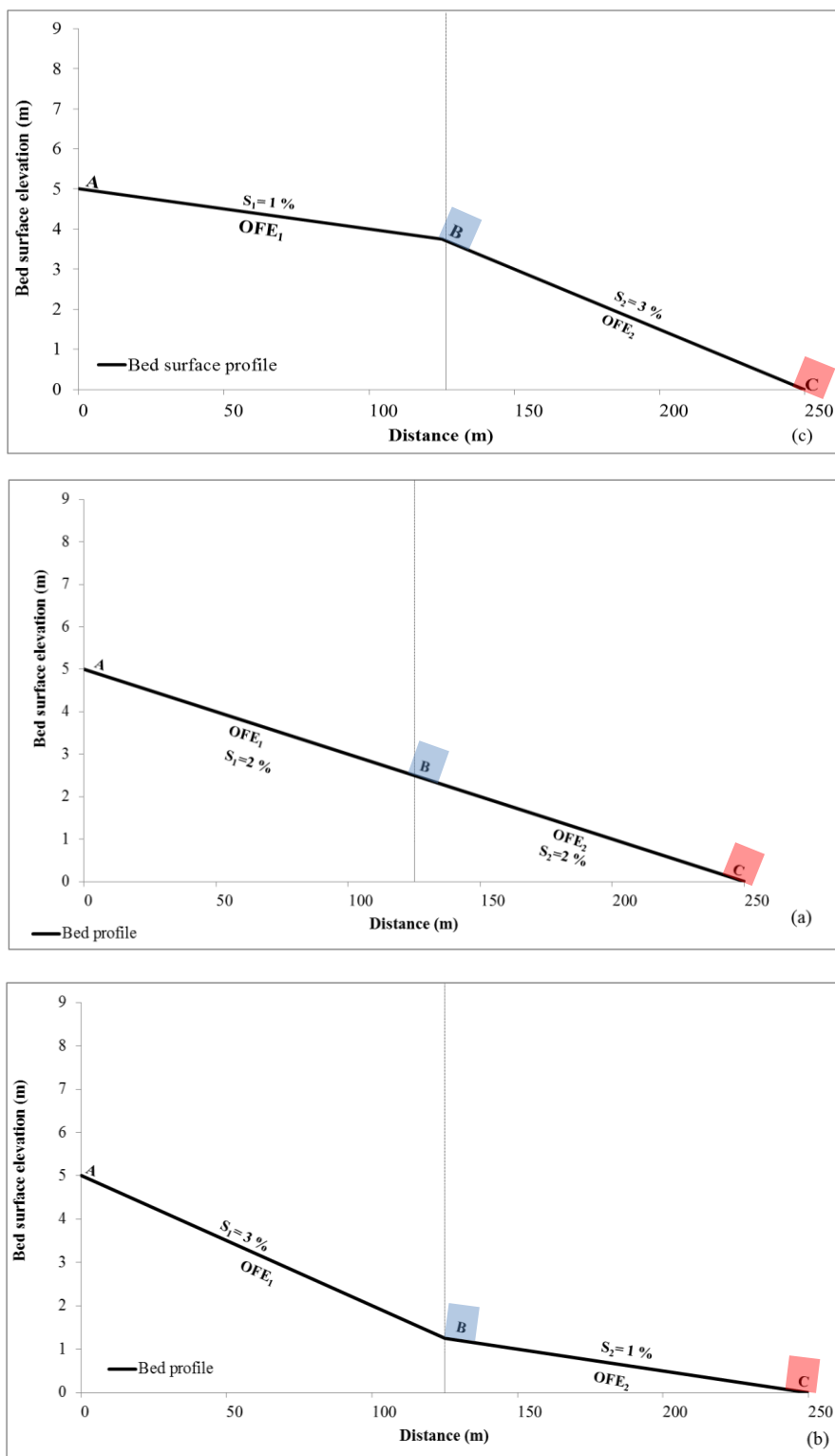


Figure 6.2 The examined hillslope profiles: (a) uniform; (b) concave; (c) convex. The colors at location B, C match the colors of the hydrographs in figures 6.3-6.18.

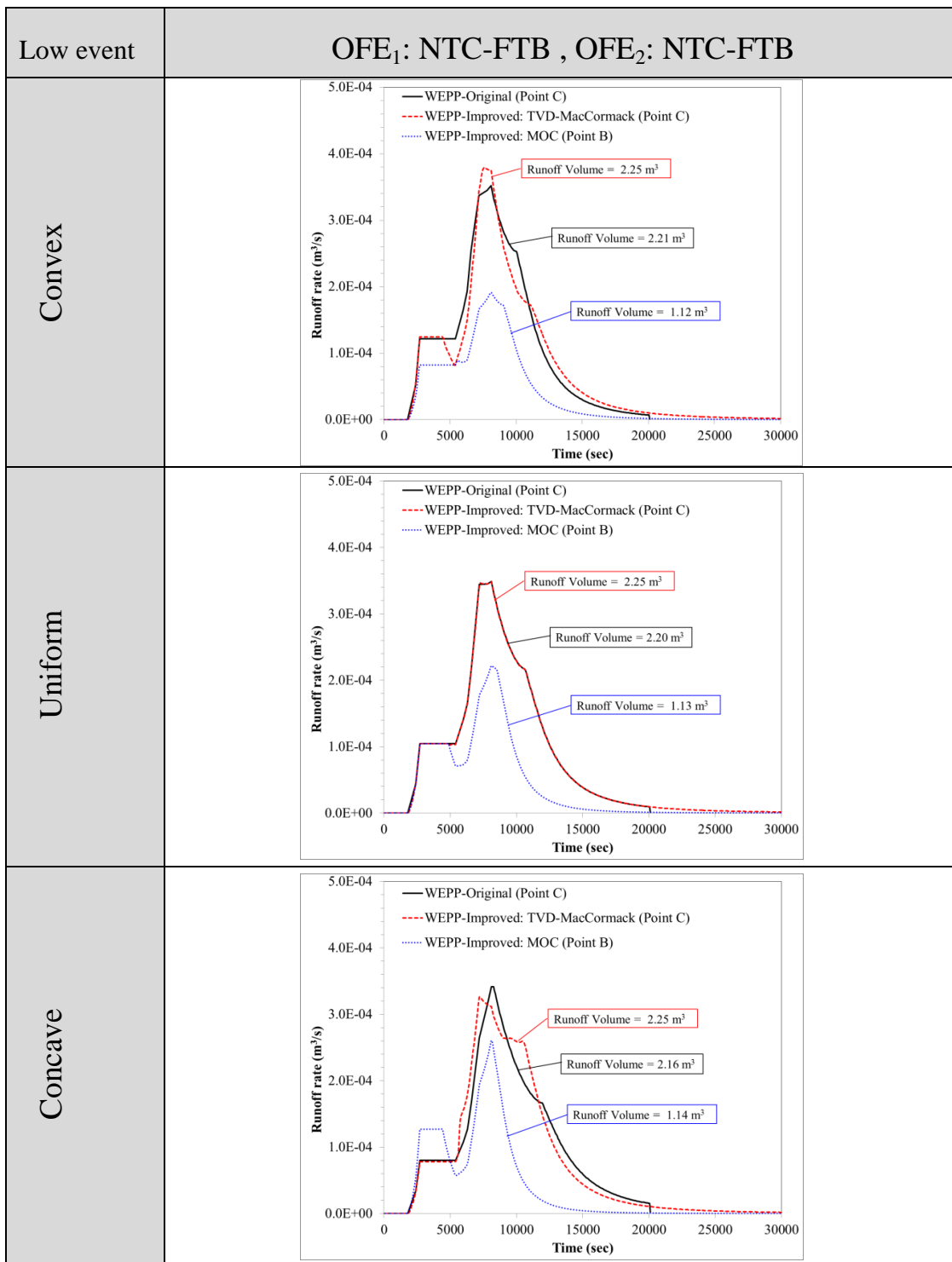


Figure 6.3 Runoff hydrographs for Sc-1 (OFE<sub>1</sub>: NTC-FTB, OFE<sub>2</sub>: NTC-FTB) for the low rainfall event and for the convex, uniform, and concave hillslopes.

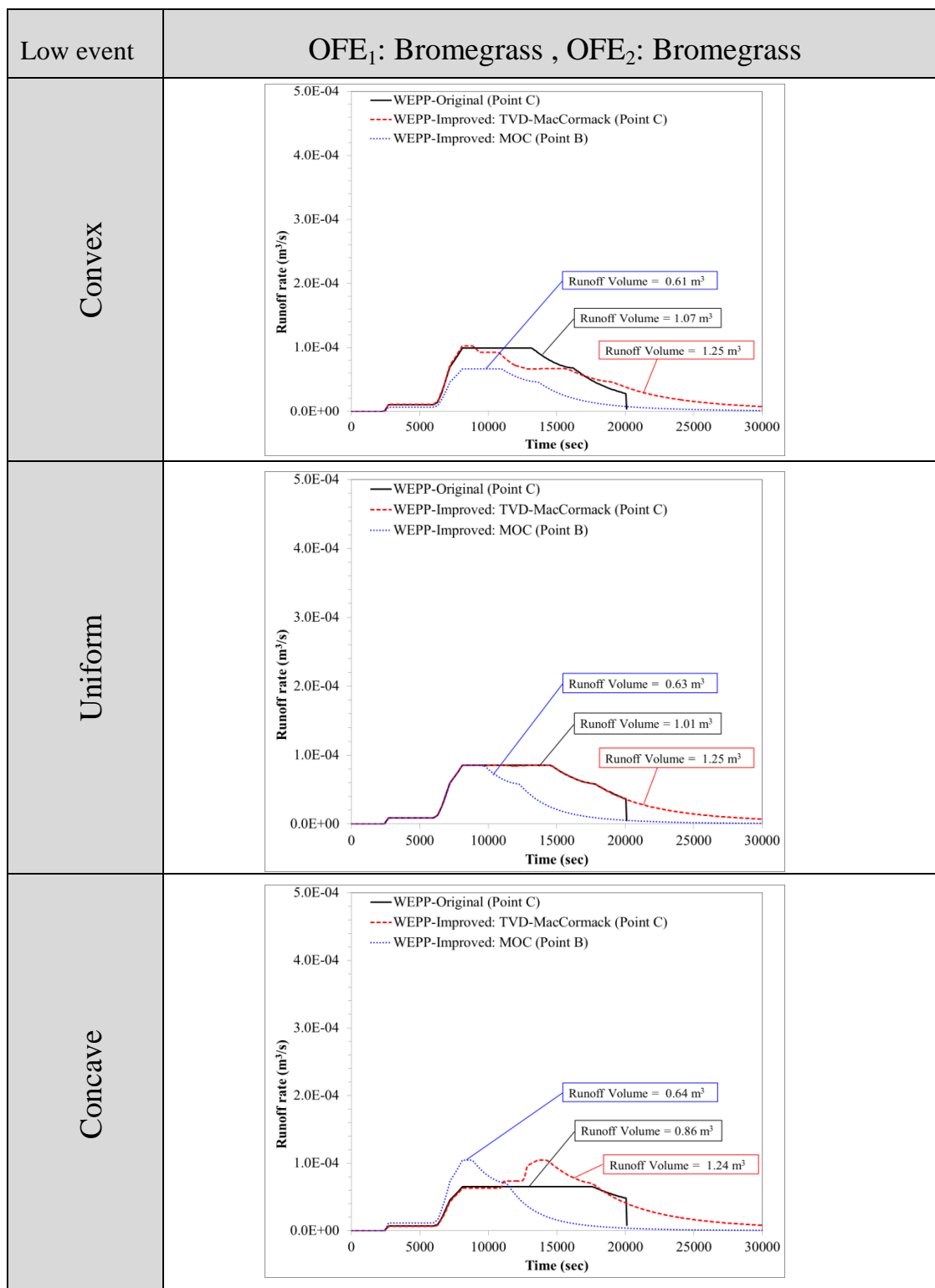


Figure 6.4 Runoff hydrographs for Sc-2 (OFE1: Bromegrass, OFE2: Bromegrass) for the low rainfall event and for the convex, uniform, and concave hillslopes.



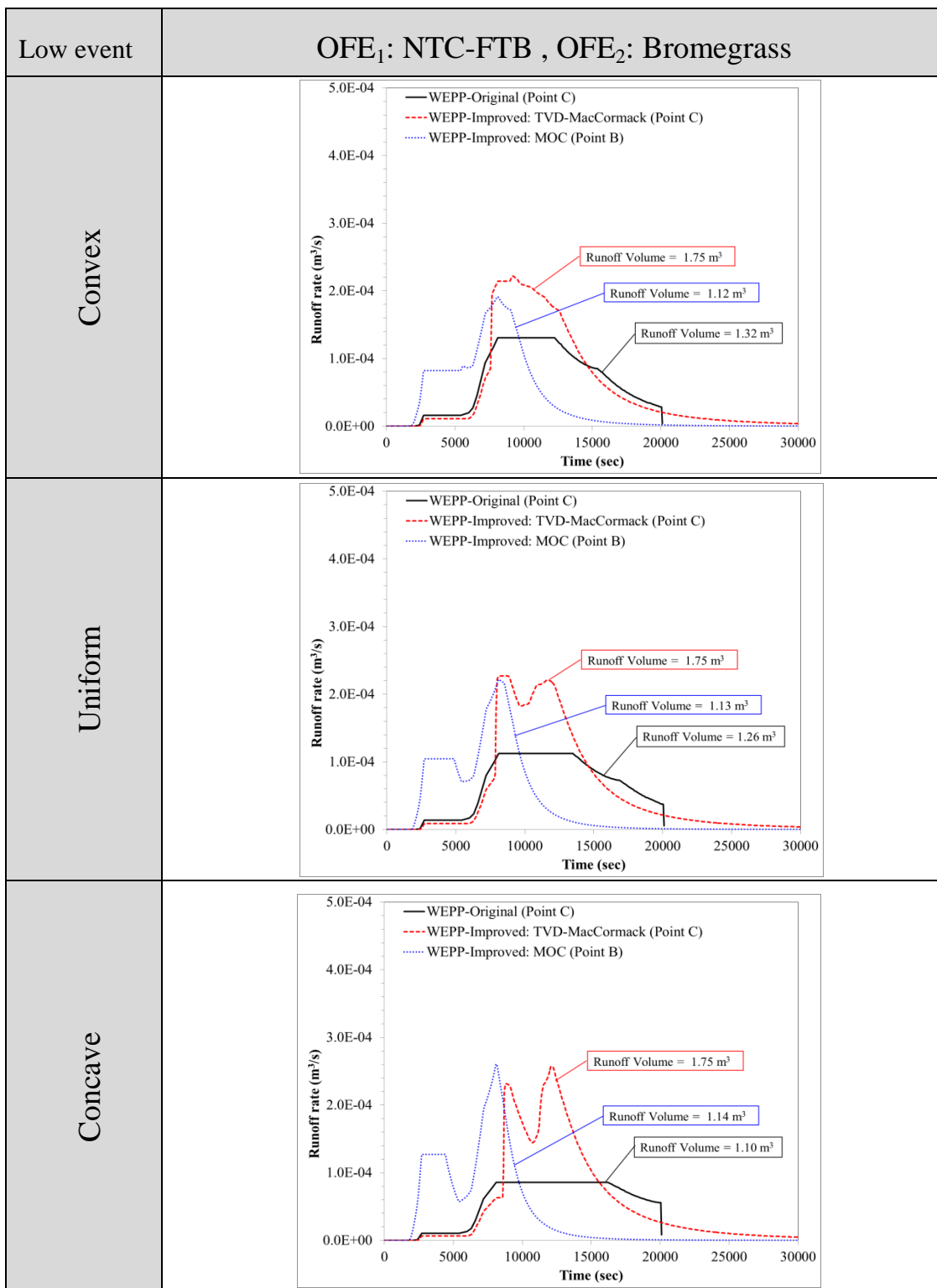


Figure 6.5 Runoff hydrographs for Sc-3 (OFE<sub>1</sub>: NTC-FTB, OFE<sub>2</sub>: Bromegrass) for the low rainfall event and for the convex, uniform, and concave hillslopes.

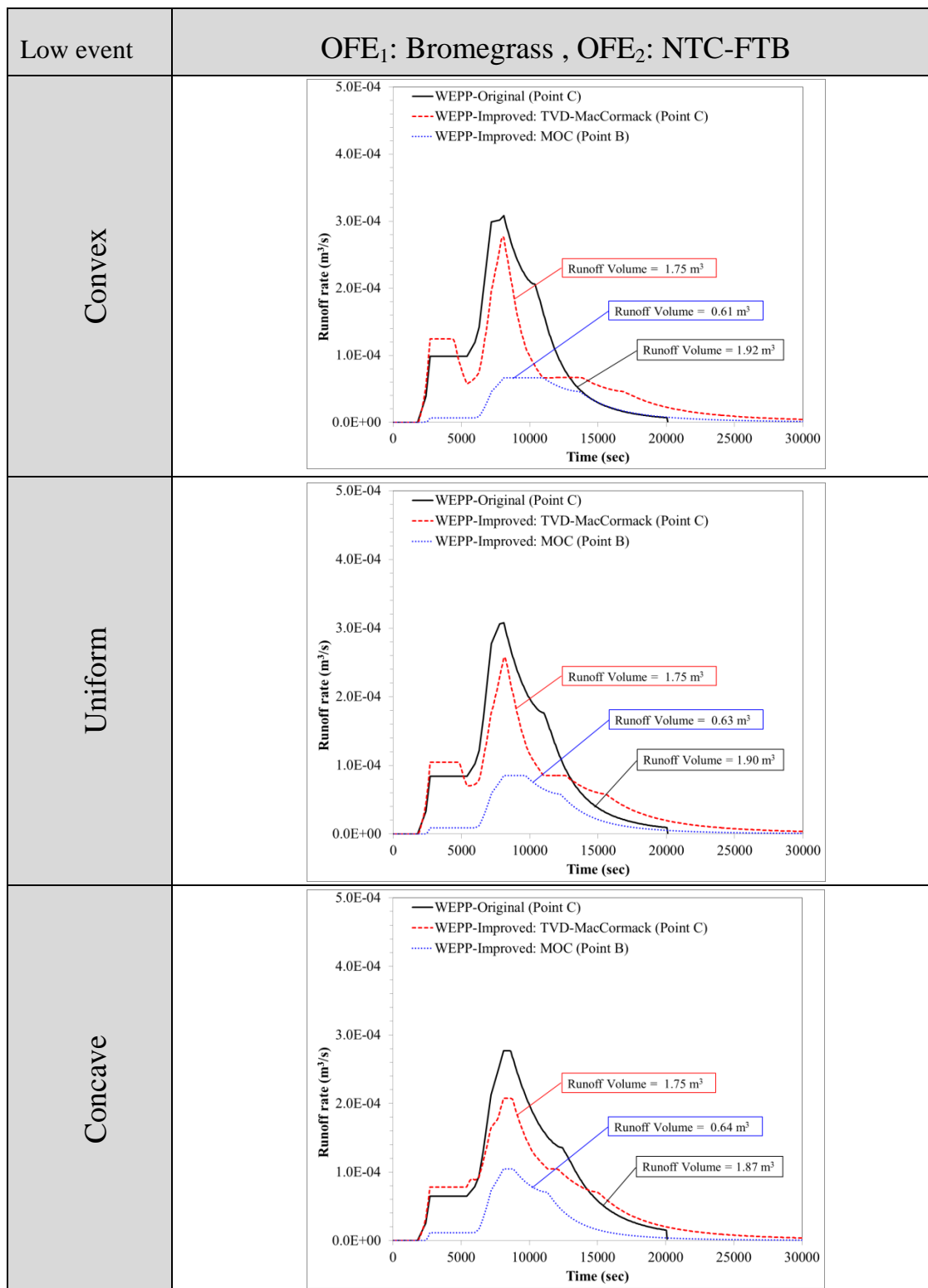


Figure 6.6 Runoff hydrographs for Sc-4 (OFE<sub>1</sub>: Bromegrass, OFE<sub>2</sub>: NTC-FTB) for the low rainfall event and for the convex, uniform, and oncave hillslopes.

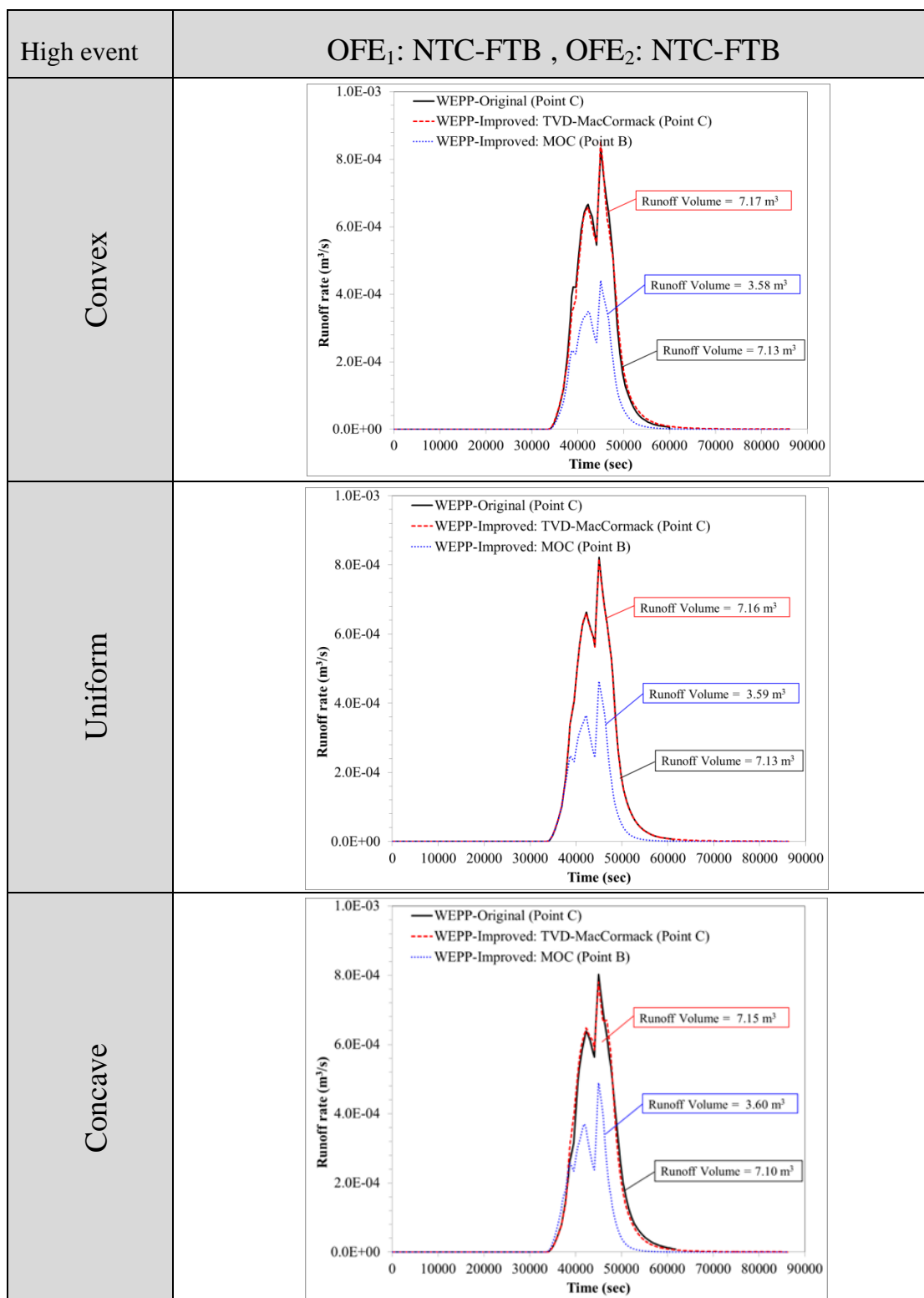


Figure 6.7 Runoff hydrographs for Sc-1 (OFE<sub>1</sub>: NTC-FTB, OFE<sub>2</sub>: NTC-FTB) for the high rainfall event and for the convex, uniform, and concave hillslopes.

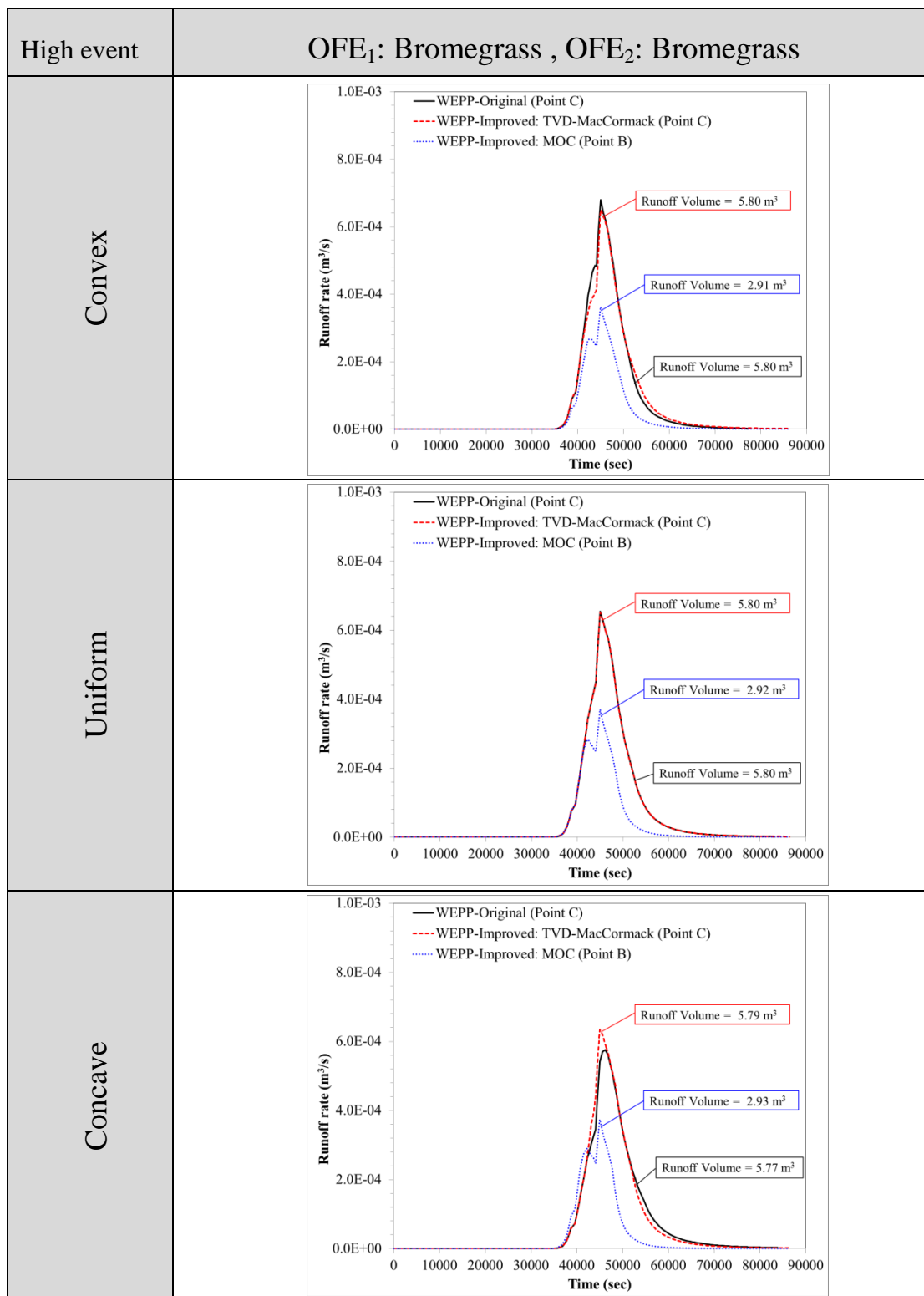


Figure 6.8 Runoff hydrographs for Sc-2 (OFE<sub>1</sub>: Bromegrass, OFE<sub>2</sub>: Bromegrass) for the high rainfall event and for the convex, uniform, and concave hillslopes.

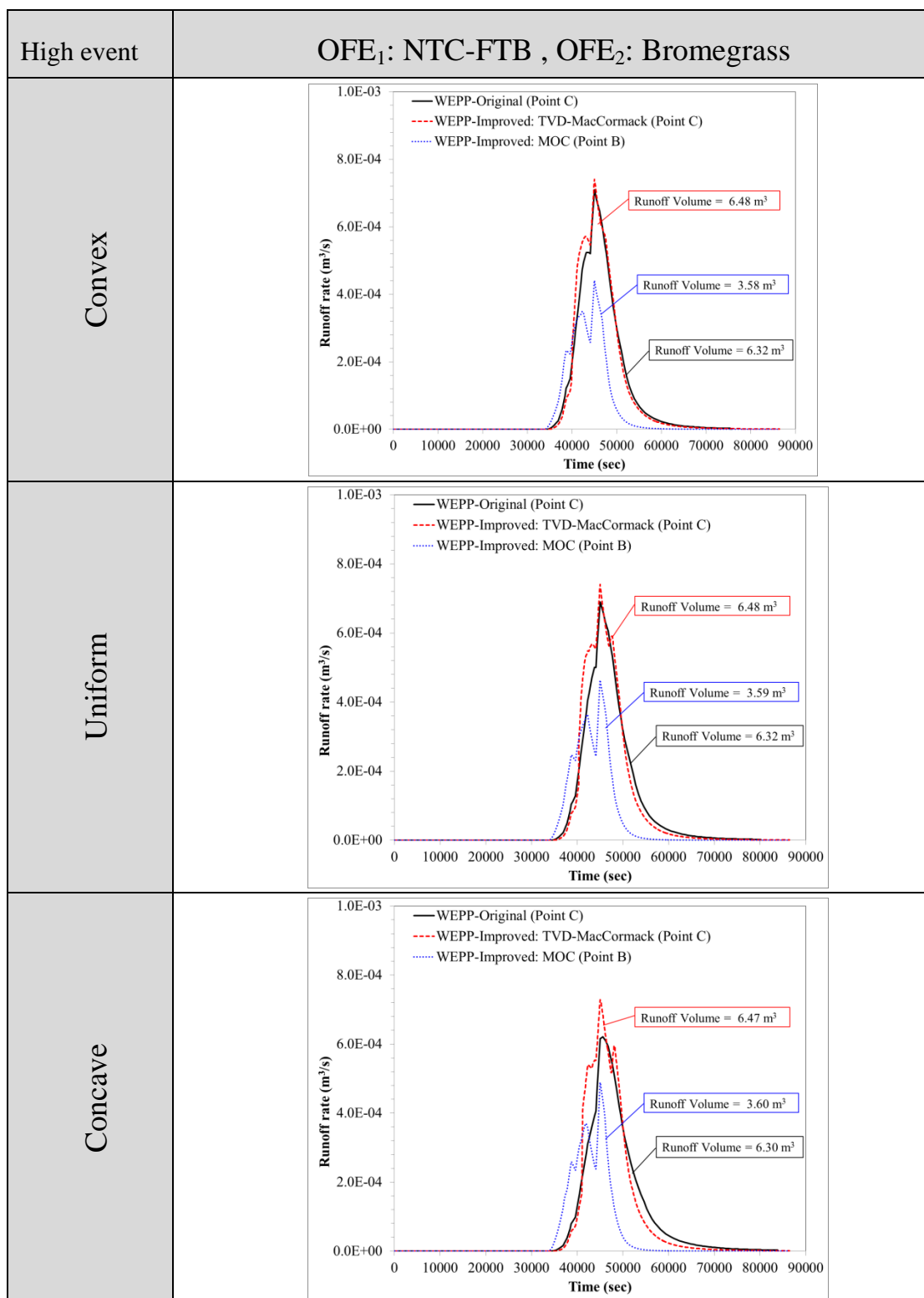


Figure 6.9 Runoff hydrographs for Sc-3 (OFE<sub>1</sub>: NTC-FTB, OFE<sub>2</sub>: Bromegrass) for the high rainfall event and for the convex, uniform, and concave hillslopes.

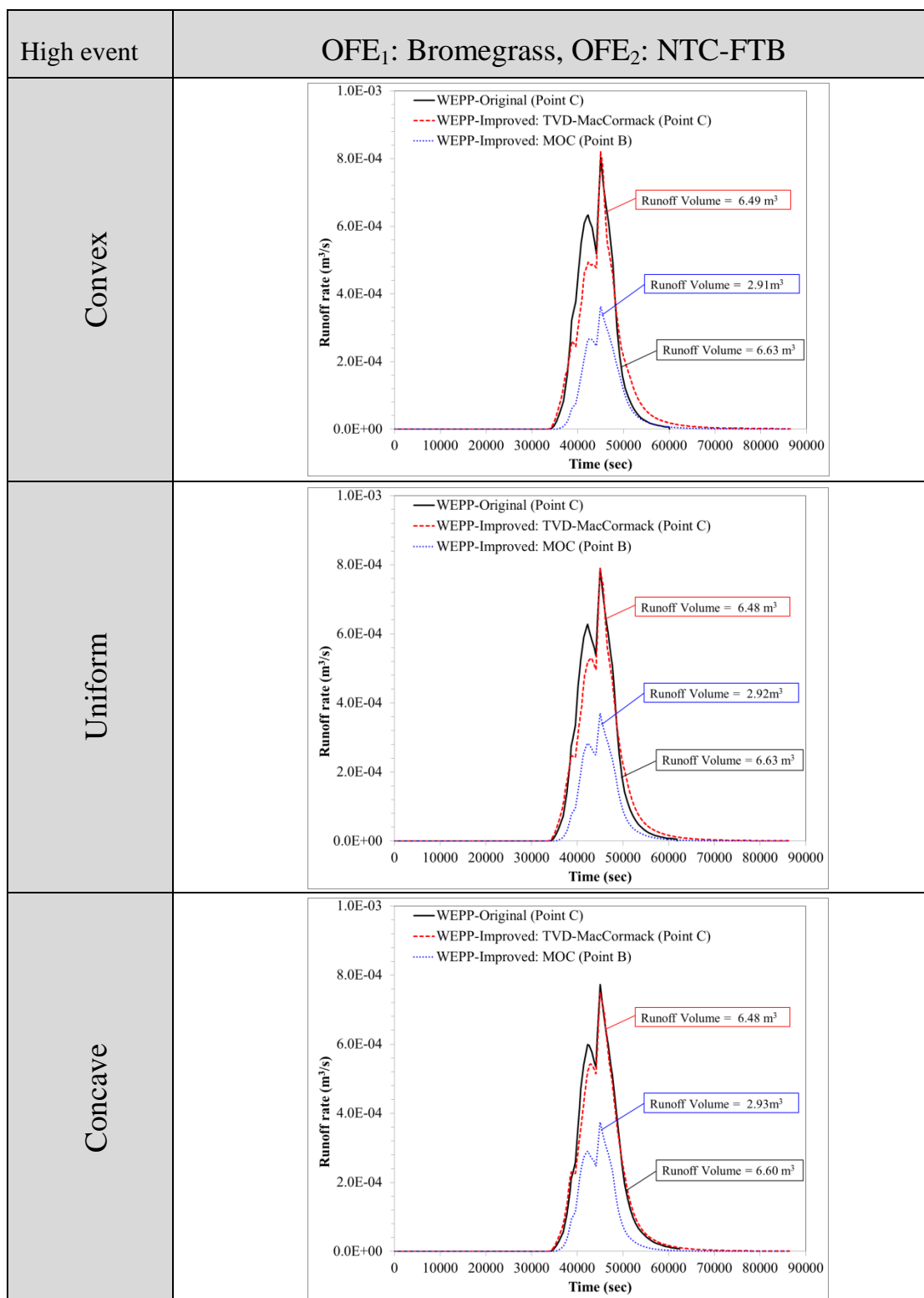


Figure 6.10 Runoff hydrographs for Sc-4 (OFE<sub>1</sub>: Bromegrass, OFE<sub>2</sub>: NTC-FTB) for the high rainfall event and for the convex, uniform, and concave hillslopes.

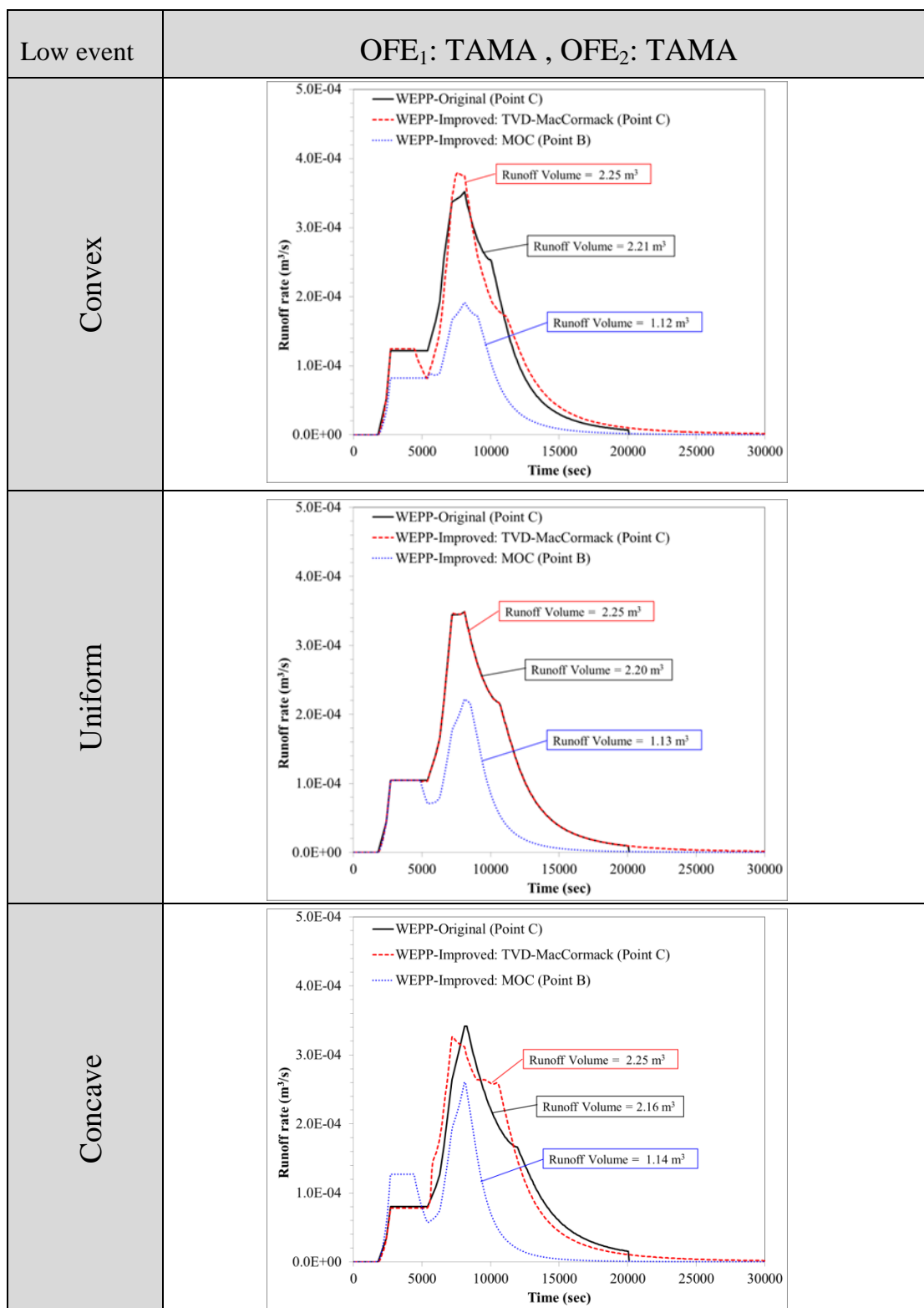


Figure 6.11 Runoff hydrographs for Sc-5 (OFE<sub>1</sub>: TAMA, OFE<sub>2</sub>: TAMA) and for the convex, uniform, concave hillslopes. LU/LC is NTC-FTB in both OFEs.

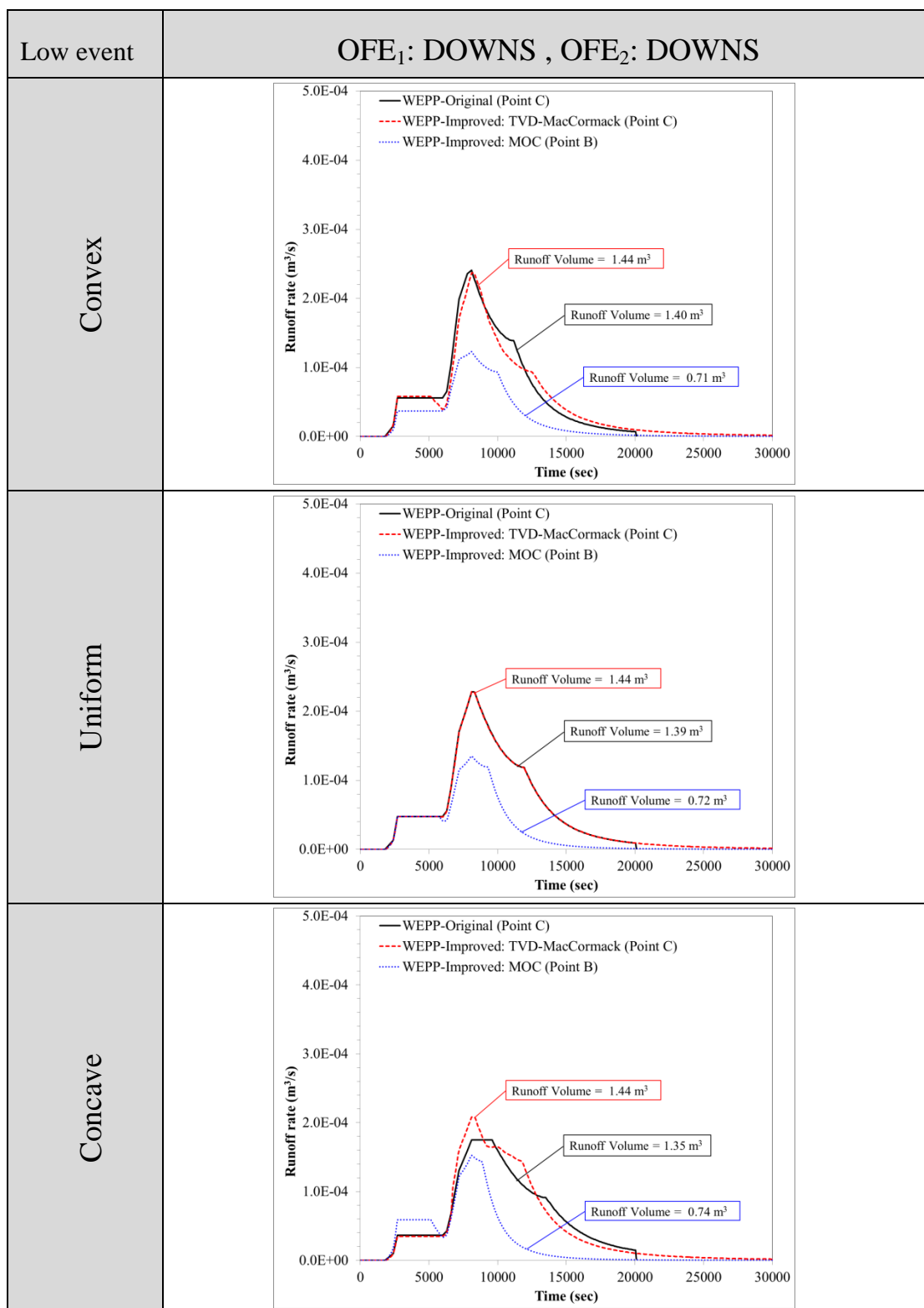


Figure 6.12 Runoff hydrographs for Sc-6 (OFE<sub>1</sub>: DOWNS, OFE<sub>2</sub>: DOWNS) and for the convex, uniform, concave hillslopes. LU/LC is NTC-FTB in both OFEs.



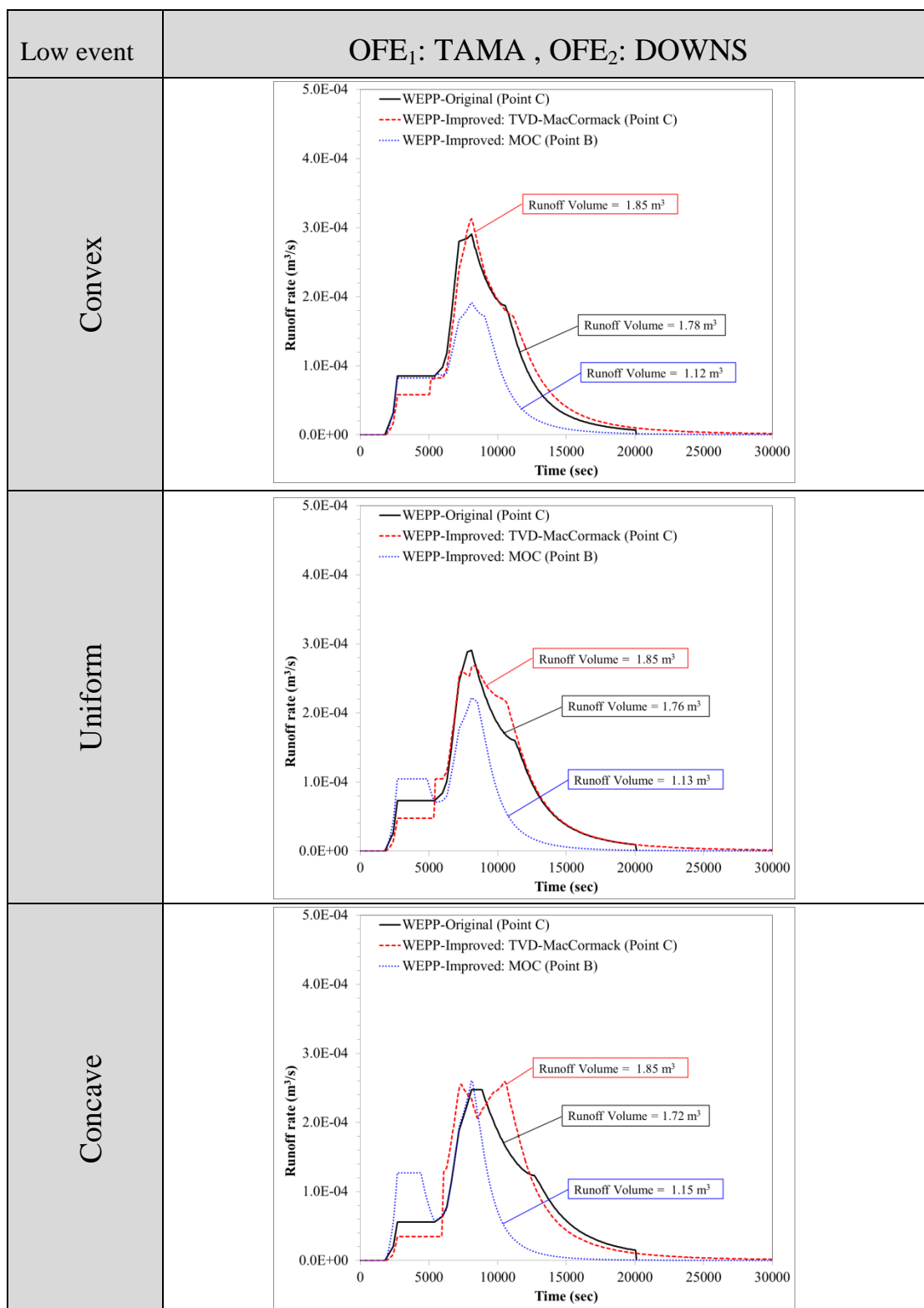


Figure 6.13 Runoff hydrographs for Sc-7 (OFE<sub>1</sub>: TAMA, OFE<sub>2</sub>: DOWNS) and for the convex, uniform, concave hillslopes. LU/LC is NTC-FTB in both OFEs.

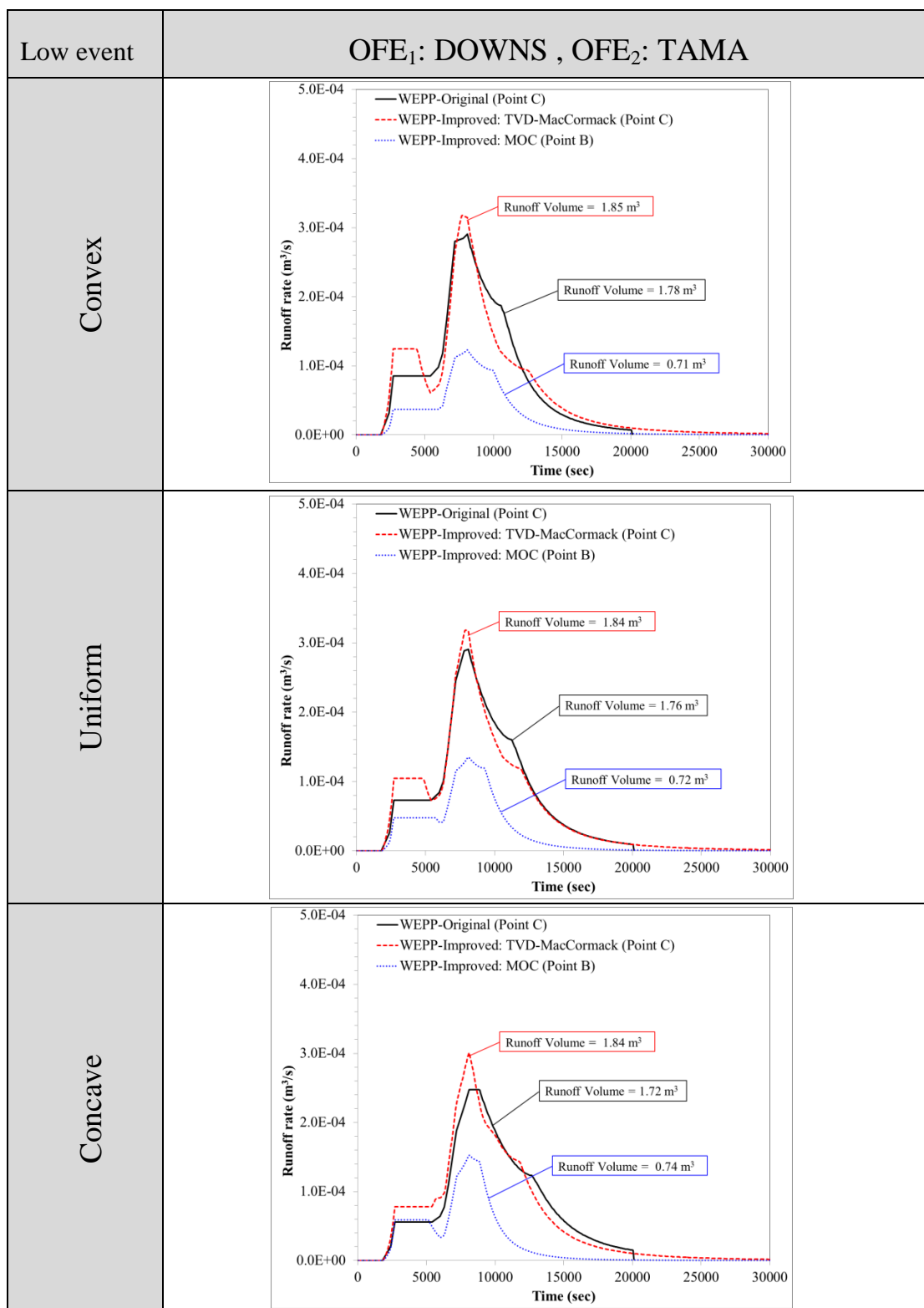


Figure 6.14 Runoff hydrographs for Sc-8 (OFE<sub>1</sub>: DOWNS, OFE<sub>2</sub>: TAMA) and for the convex, uniform, concave hillslopes. LU/LC is NTC-FTB in both OFEs.

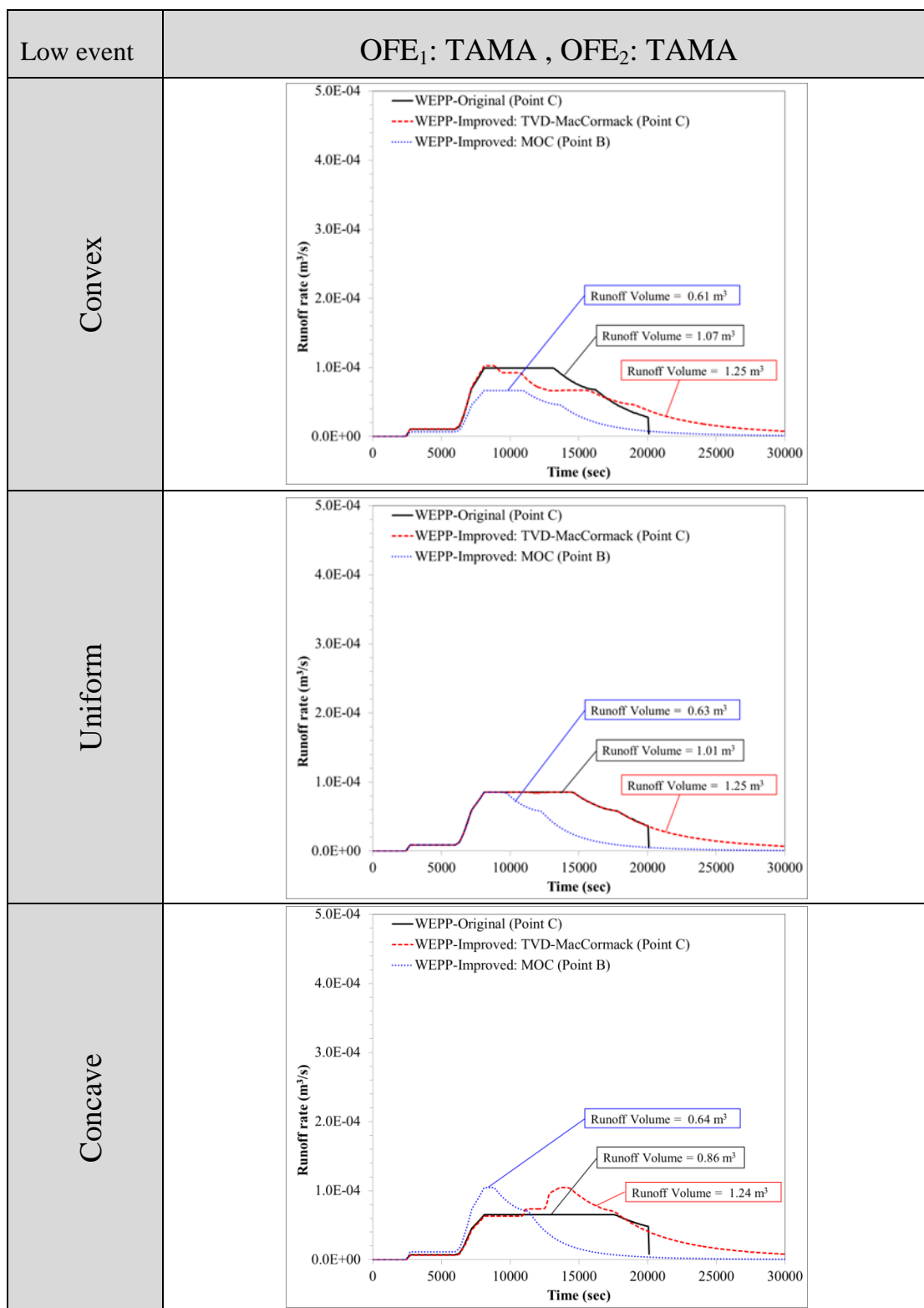


Figure 6.15 Runoff hydrographs for Sc-5 (OFE<sub>1</sub>: TAMA, OFE<sub>2</sub>: TAMA) and for the convex, uniform, concave hillslopes. LU/LC is Bromegrass in both OFEs.

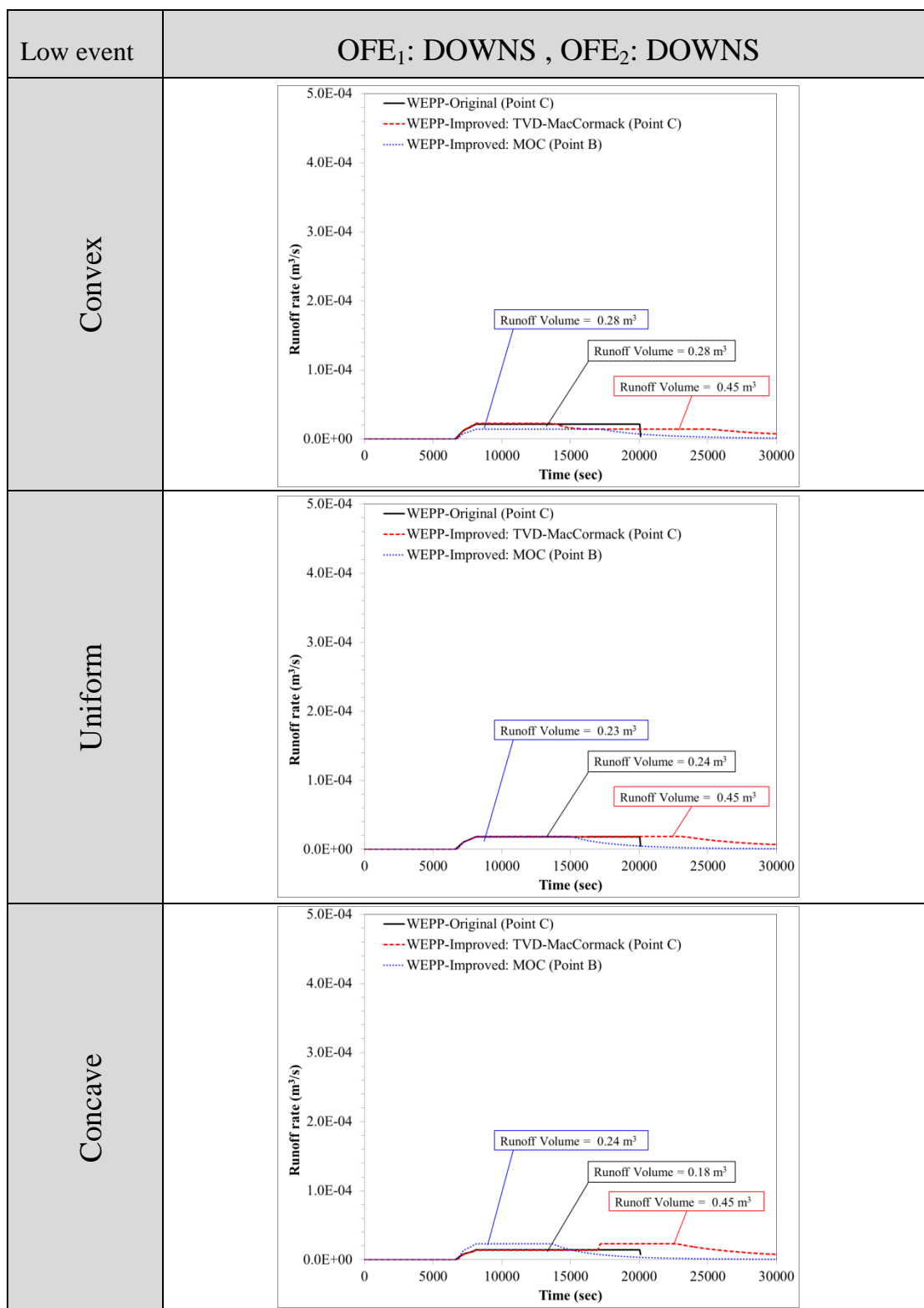


Figure 6.16 Runoff hydrographs for Sc-6 (OFE<sub>1</sub>: DOWNS, OFE<sub>2</sub>: DOWNS) and for the convex, uniform, concave hillslopes. LU/LC is Bromegrass in both OFEs.

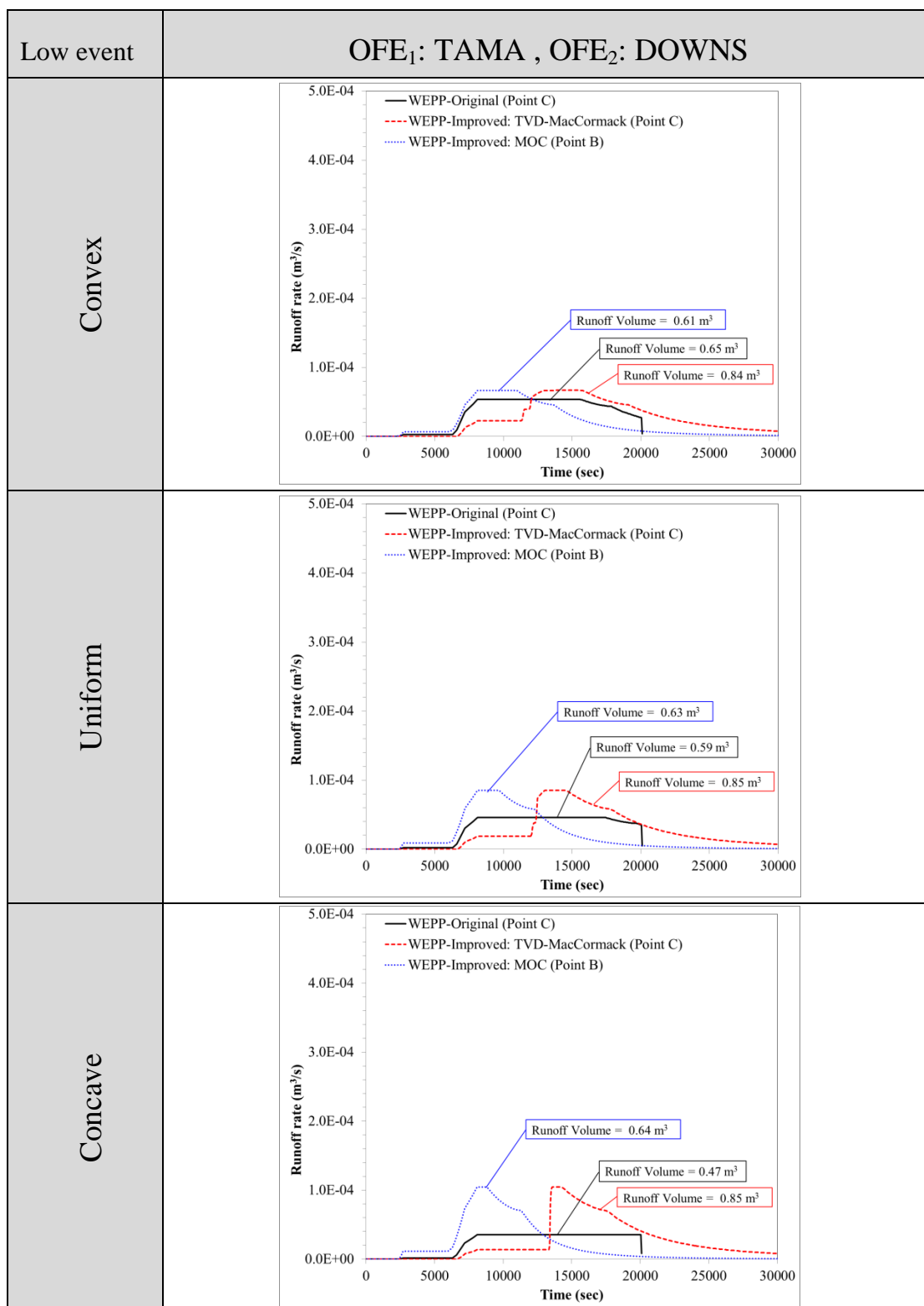


Figure 6.17 Runoff hydrographs for Sc-7 (OFE<sub>1</sub>: TAMA, OFE<sub>2</sub>: DOWNS) and for the convex, uniform, concave hillslopes. LU/LC is Bromegrass in both OFEs.

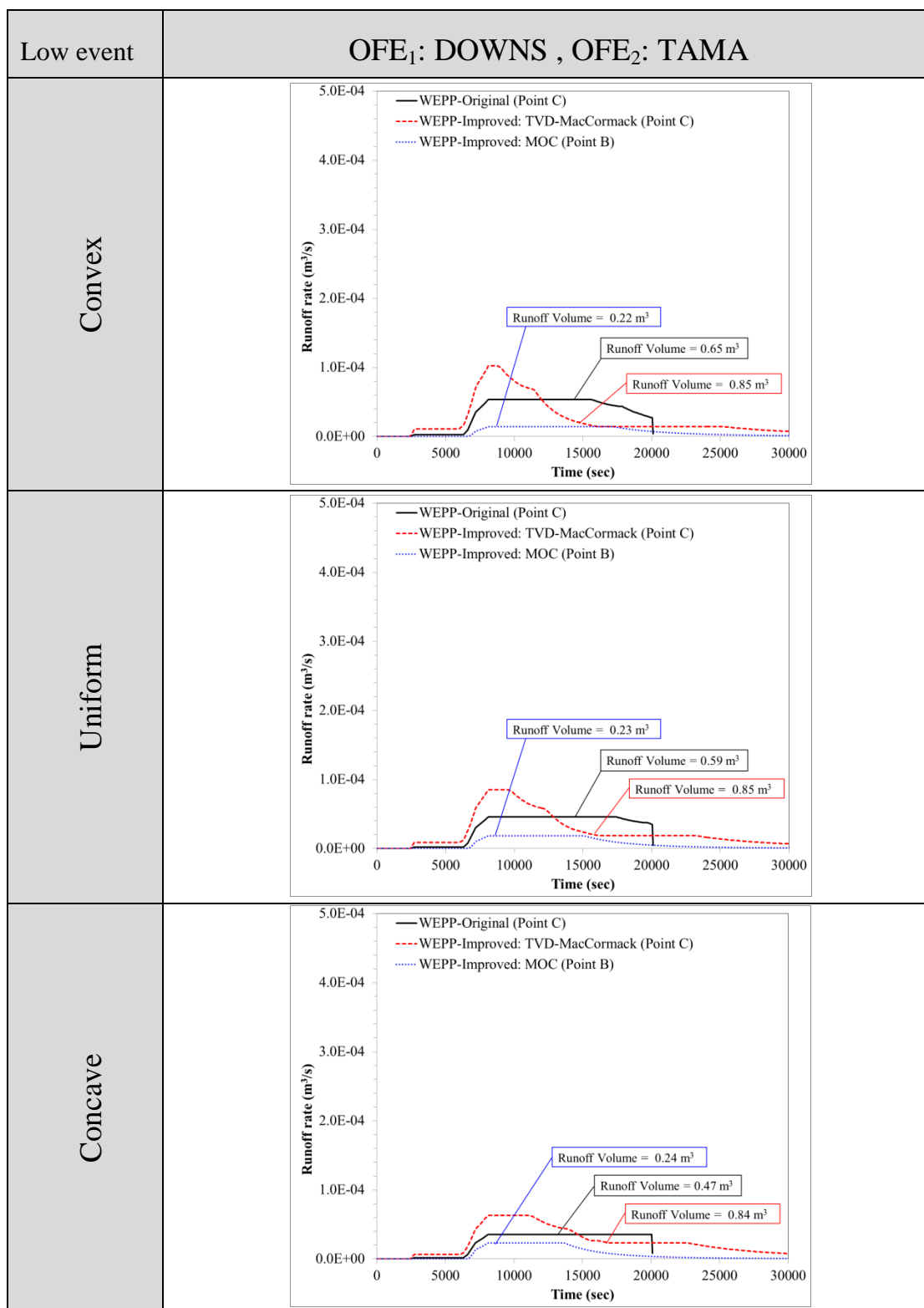


Figure 6.18 Runoff hydrographs for Sc-8 (OFE<sub>1</sub>: DOWNS, OFE<sub>2</sub>: TAMA) and for the convex, uniform, concave hillslopes. LU/LC is Bromegrass in both OFEs.

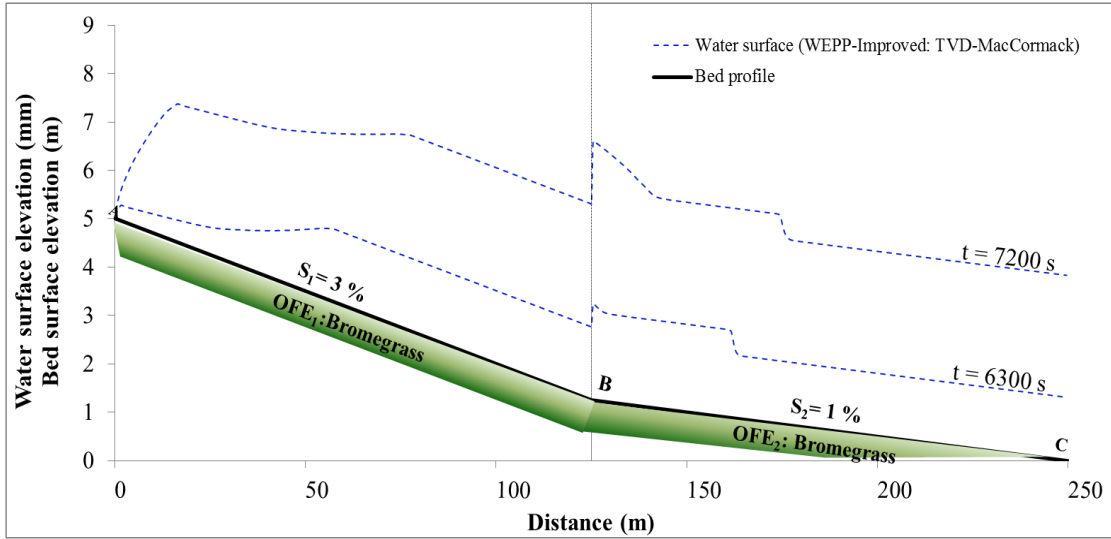


Figure 6.19 Water surface profile for Sc-2 (low magnitude event, concave profile, Bromegrass and TAMA soil for both OFEs).

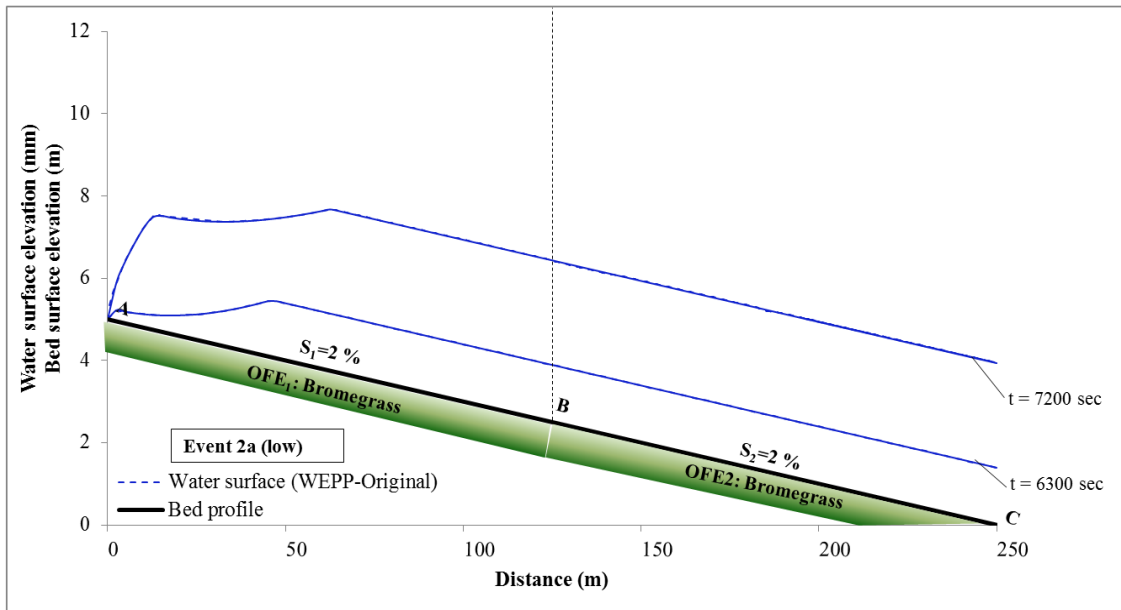


Figure 6.20 Water surface profile for the equivalent, uniform slope profile (low magnitude event, Bromegrass and TAMA soil for both OFEs).

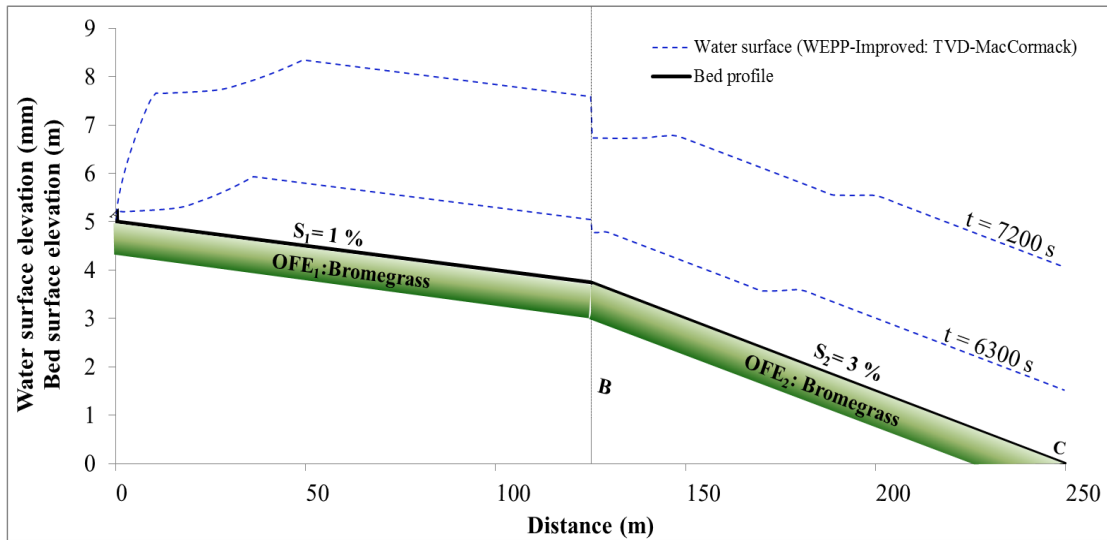


Figure 6.21 Water surface profile for Sc-2 (low magnitude event, convex profile, Bromegrass and TAMA soil for both OFEs).

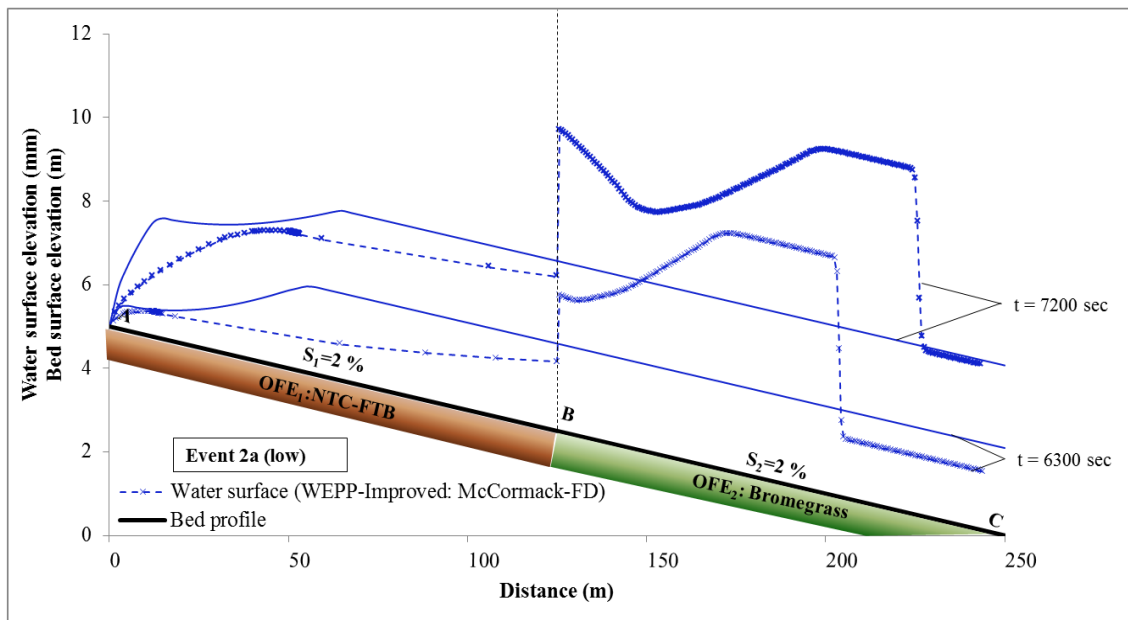


Figure 6.22 Water surface profile for Sc-3 (low magnitude event, uniform profile, NTC-FTB/Bromegrass and TAMA soil for both OFEs).



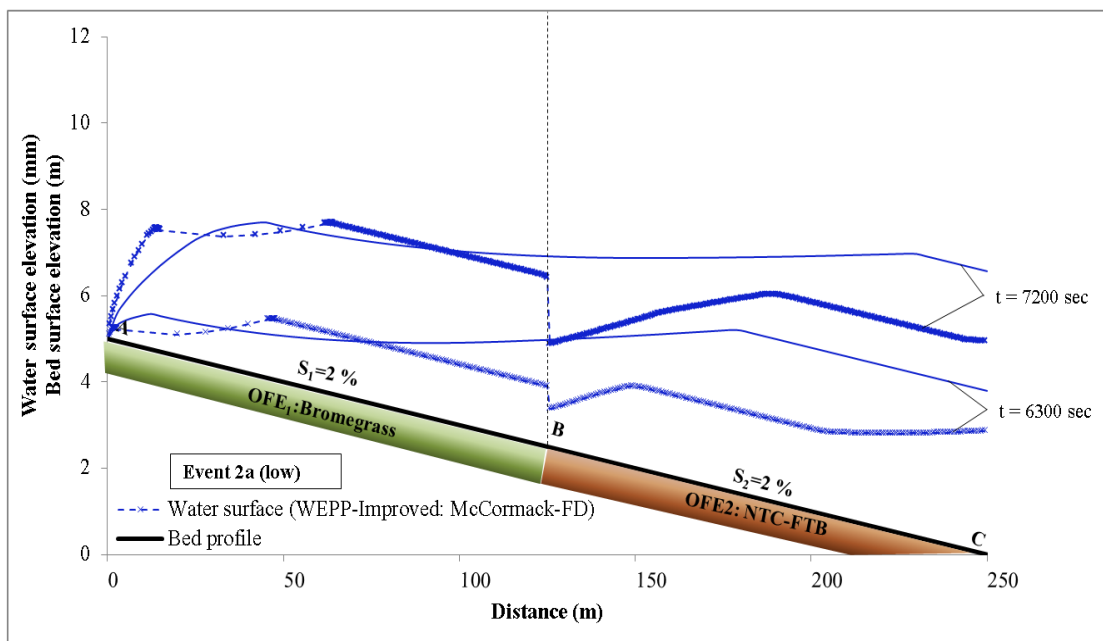


Figure 6.23 Water surface profile for Sc-4 (low magnitude event, uniform profile, Bromegrass/NTC-FTB and TAMA soil for both OFEs).

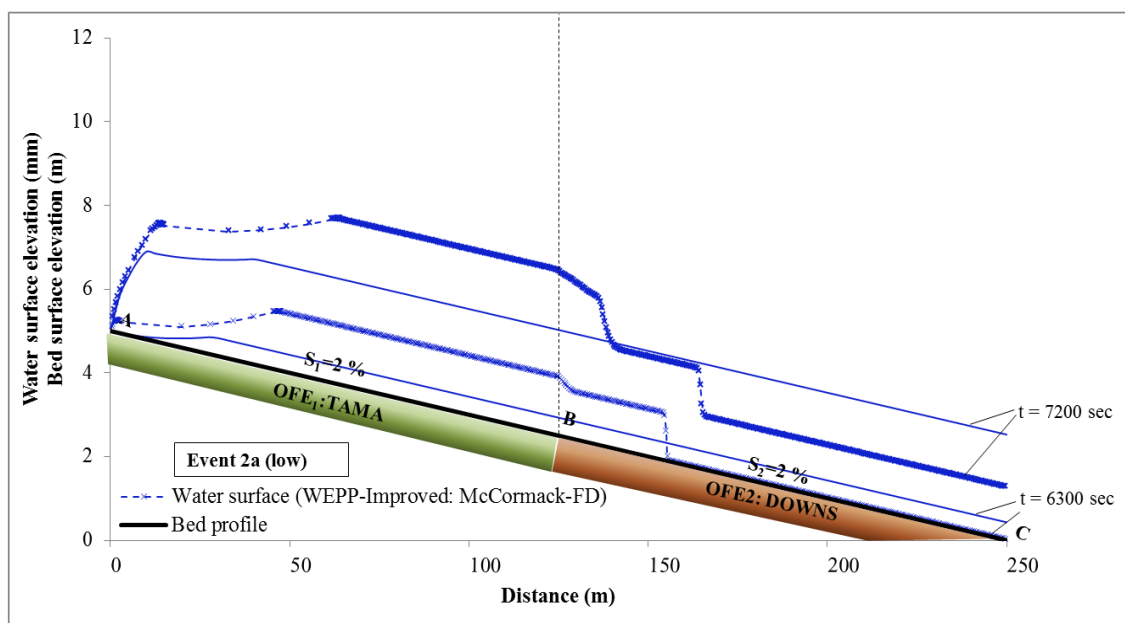


Figure 6.24 Water surface profile for Sc-7 (low magnitude event, uniform profile, TAMA/DOWNS and Bromegrass soil for both OFEs).

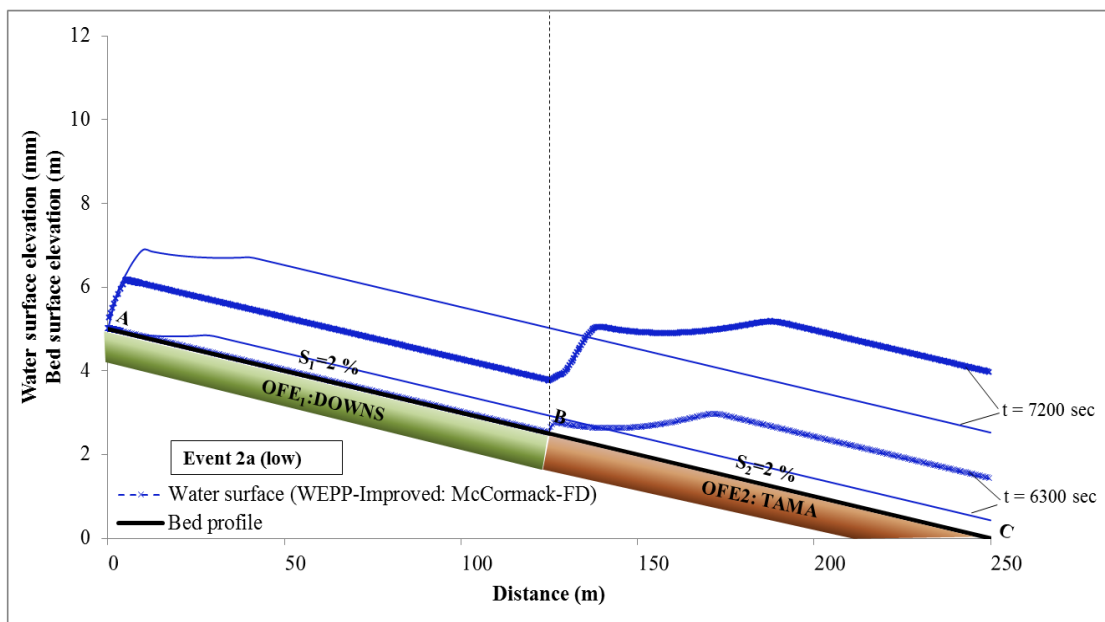


Figure 6.25 Water surface profile for Sc-8 (low magnitude event, uniform profile, DOWNS/TAMA and Bromegrass soil for both OFEs).

## CHAPTER 7

### CONCLUSIONS

The major motivation of this work was based on the recognition that although current distributed parameter erosion models use as inputs spatially variable physical and biogeochemical properties along the hillslope through the form of different GIS layers, these models lack the physics in their formulation to account for the collective effects and interplay of key physical and biogeochemical properties that vary in space and time within the hillslope continuum. In lieu of this limitation, this research aimed here towards the development, validation, and testing of an improved modeling framework that accounts for the effects of spatial heterogeneity on overland flow and erosion processes and it is computationally sound for shallow, overland flows with shock waves.

It was sought here that an upland erosion model, which overall provides a more accurate representation of the spatial heterogeneity within an agricultural setting, such as WEPP, could aid in addressing this need. As explained in chapter 3 of this thesis, WEPP, being a distributed parameter model, allowed adequate representation of heterogeneity for the governing soil, land use and topography parameters and was deemed to be a suitable model for meeting the goals of this study.

A hindrance in performing erosion simulations within areas exhibiting heterogeneous physical and biogeochemical properties has been the lack of a model (including WEPP) designed to handle kinematic shock waves introduced by the spatial heterogeneity along the hillslope in terms of topography, LU/LC and soil type. To the best of our knowledge, there are few shock-capturing numerical schemes available to simulate shallow, overland flows. This important issue was addressed herein by (1) improving the original version of the WEPP model to account for shock formation in the overland flow routing using a well-established shock-capturing numerical scheme; (2) validating the improved model via detailed field experiments within an experimental plot

in the study area of SASW; and (iii) testing the ability of the improved WEPP model via generic simulations at the hillslope scale to account for the effects of spatial heterogeneity (in terms of topography, governing soil parameters and LU/LC at different OFEs) in both the spatial and temporal distribution of overland flow.

In continuance, this study described in great detail the diligent and laborious steps required for preparing the field experiments at the plot scale to validate the WEPP-Improved model. Validation of the WEPP-Improved model was conducted by comparing the measured runoff hydrograph and sediment transport rates at the outlet of the experimental plot as well as the flow depths within the plot with the simulated data.

Once the WEPP model was modified to account for the formation and propagation of shock waves and validated based on the experimental datasets, it was employed to test our hypothesis that spatial heterogeneity of the landscape, in terms of the key physical and biogeochemical properties, affects the propagation rate of overland flow over erodible surfaces as well as soil erosion through a cascade of different phase processes and interactions. To test the hypothesis, “thought” numerical simulations were performed for two management practices, i.e., No Till Corn-Fall Till Bean (NTC-FTB) and Bromegrass (CRP), two soil types, i.e., TAMA and DOWNS, three topographies, i.e., convex, uniform and concave, and two single storm events, low vs. high rainfall intensity.

The key results of this study can be summarized as follows:

1. The WEPP-Improved model could simulate the “degree of readiness” of the plot system expressed via the time lag, corresponding to the time required for the flow rate to reach equilibrium condition.
2. The WEPP-Improved model provided only a steady-state sediment transport rate (i.e., constant over time) and could not capture the increase on the sediment transport rate recorded during the experiments. Nonetheless, for the low rainfall intensity experiment, the simulated steady-state sediment transport rate agreed well with the measured, steady-state sediment transport rate. However, for the

high rainfall intensity experiment, the WEPP-Improved model under-estimated the value of the steady state sediment flux.

3. The WEPP-Improved model provided a range of values for the flow depth within the experimental plot. The simulated flow depths along the longitudinal direction of the plot were lower in magnitude than the measured flow depths and the WEPP-Improved model under-predicted the values of the flow depth. One of the reasons for this difference is the fact that the WEPP-Improved model does not partition the flow into interrill and rill areas and calculates only an averaged flow depth along the plane using the equivalent friction factor (see section 3.1).
4. The generic simulations verified the hypothesis that spatial heterogeneity of the landscape plays an important role on overland flow hydraulics (in terms of the peak flow rate and the shape of the hydrograph) and the underlying assumption that there is a threshold storm event, beyond which the role of heterogeneity minimizes. Landscape variability resulted in differences in the predicted peak runoff rate,  $Q_{\text{peak}}$ , between the WEPP-Improved vs. WEPP-Original models ranging  $\sim 3 - 62\%$  (avg.  $19\%$ ) due to curvature effects,  $\sim 17 - 170\%$  (avg.  $\sim 66\%$ ) due to added effects of LU/LC variability and  $\sim 5\% - 200\%$  (avg.  $\sim 52\%$ ) due to added effects of soil type variability. The highest reported differences on the predicted  $Q_{\text{peak}}$  between the two models were attributed to the formation of the shock waves, presented as sharp, water fronts propagating downhill, thus, affecting the water depth and water surface profile along the longitudinal direction of the hill. Differences in the  $Q_{\text{peak}}$  between the two models attenuated for the high storm event.

In short, spatial heterogeneity of the landscape plays an important role on overland flow hydraulics due to the formation and propagation of shock waves, which affect the magnitude of the flow depth downhill and the outlet runoff hydrograph.

Further, it is believed that differences in the flow frictional characteristics between the interrill and rill areas may affect the partitioning of flow and the flow depth distribution in the rill and interrill areas, which are not currently modeled in the WEPP-Improved model. Consequently, there is a need to improve in the future the flow component of WEPP to account for flow decomposition between the rills and interrills, which will also affect the soil erosion calculations.

If the physical processes for runoff are represented accurately at the hillslope scale using the suggested modeling approach described in this thesis, then by using an appropriate routing scheme of the flow and sediment within the stream network, it will be possible to scale-up the flow/sediment routing from the hillslope (small) to the watershed (large) scale without losing the degree of heterogeneity encapsulated from different hillslopes within the drainage network.

## REFERENCES

- Abaci, O., & Papanicolaou, A. N. (2009). Long-term effects of management practices on water-driven soil erosion in an intense agricultural sub-watershed: monitoring and modelling. *Hydrological Processes*, 23(19), 2818-2837.
- Adams, R., & Elliott, S. (2006). Physically based modelling of sediment generation and transport under a large rainfall simulator. *Hydrological processes*, 20(11), 2253-2270.
- Aksoy, H., & Kavvas, M. L. (2005). A review of hillslope and watershed scale erosion and sediment transport models. *Catena*, 64(2), 247-271.
- An, Y., & Liu, Q. Q. (2009). Two-Dimensional Hillslope Scale Soil Erosion Model. *Journal of Hydrologic Engineering*, 14(7), 690-697.
- Arnold, J. G., Williams, J. R., Nicks, A. D., & Sammons, N. B. (1990). *SWRRB; a basin scale simulation model for soil and water resources management*. Texas A & M University Press.
- Baird, A. J., Thornes, J. B., & Watts, G. P. (1992). Extending overland flow models to problems of slope evolution and the representation of complex slope-surface topographies. *Overland Flow*. New York: Chapman and Hall, 1991223.
- Beare, M. H., Hendrix, P. F., Cabrera, M. L., & Coleman, D. C. (1994). Aggregate-protected and unprotected organic matter pools in conventional-and no-tillage soils. *Soil Science Society of America Journal*, 58(3), 787-795.
- Bell, N. C., Wheater, H. S., & Johnston, P. M. (1989). Evaluation of overland flow models using laboratory catchment data II. Parameter identification of physically based (kinematic wave) models. *Hydrological sciences journal*, 34(3), 289-317.
- Bonilla, C. A., Norman, J. M., & Molling, C. C. (2007). Water erosion estimation in topographically complex landscapes: Model description and first verifications. *Soil Science Society of America Journal*, 71(5), 1524-1537.
- Borah, D. K., Prasad, S. N., & Alonso, C. V. (1980). Kinematic wave routing incorporating shock fitting. *Water Resources Research*, 16(3), 529-541.
- Brater, E. F., King, H. W., & James E. Lindell. (1996). *Handbook of hydraulics*. McGraw Hill.
- Brown, L. C., Foster, G. R., & Beasley, D. B. (1989). Rill erosion as affected by incorporated crop residue and seasonal consolidation. *Transactions of the ASAE*, 32(6), 1967-1978.
- Chenu, C., Le Bissonnais, Y., & Arrouays, D. (2000). Organic matter influence on clay wettability and soil aggregate stability. *Soil Science Society of America Journal*, 64(4), 1479-1486.
- Chu, X., Nelis, J., & Rediske, R. (2012). A Preliminary Study on the Effects of Surface Microtopography on Tracer Transport in a Coupled Overland and Unsaturated Flow System. *Journal of Hydrologic Engineering*.

- Cochrane, T. A., & Flanagan, D. C. (1999). Assessing water erosion in small watersheds using WEPP with GIS and digital elevation models. *Journal of Soil and Water conservation*, 54(4), 678-685.
- Coulthard, T. J., Hicks, D. M., & Van De Wiel, M. J. (2007). Cellular modelling of river catchments and reaches: Advantages, limitations and prospects. *Geomorphology*, 90(3), 192-207.
- Cox, C., Hug, A., & Bruzelius, N. (2011). *Losing ground*. Environmental Working Group, Washington, DC. Available online at: <http://www.ewg.org/losingground>.
- Darboux, F., & Huang, C. H. (2003). An instantaneous-profile laser scanner to measure soil surface microtopography. *Soil Science Society of America Journal*, 67(1), 92-99.
- Davis, S. F. (1984). *TVD finite difference schemes and artificial viscosity*, ICASE Report, No. 84-20, NASA, Langley Research Center, Hampton, VA.
- de Vente, J., Poesen, J., Verstraeten, G., Van Rompaey, A., & Govers, G. (2008). Spatially distributed modelling of soil erosion and sediment yield at regional scales in Spain. *Global and planetary change*, 60(3), 393-415.
- Deng, Z. Q., de Lima, J. L., & Jung, H. S. (2008). Sediment transport rate-based model for rainfall-induced soil erosion. *Catena*, 76(1), 54-62.
- Dermisis, D., Abaci, O., & Wilson, C. G. (2010). Evaluating grassed waterway efficiency in southeastern Iowa using WEPP. *Soil Use and Management*, 26(2), 183-192.
- Di Stefano, C., Ferro, V., Porto, P., & Tusa, G. (2000). Slope curvature influence on soil erosion and deposition processes. *Water resources research*, 36(2), 607-617.
- Elhakeem, M., & Papanicolaou, A. N. (2009). Estimation of the runoff curve number via direct rainfall simulator measurements in the State of Iowa, USA. *Water resources management*, 23(12), 2455-2473.
- Favis-Mortlock, D. (1998). A self-organizing dynamic systems approach to the simulation of rill initiation and development on hillslopes. *Computers & Geosciences*, 24(4), 353-372.
- Fiener, P., & Auerswald, K. (2006). Seasonal variation of grassed waterway effectiveness in reducing runoff and sediment delivery from agricultural watersheds in temperate Europe. *Soil and Tillage Research*, 87(1), 48-58.
- Finkner, S. C. (1988). *Hydraulic roughness coefficients as affected by random roughness*. M.S. Thesis, Univ. of Nebraska, 89 pp.
- Flanagan, D. C., & Nearing, M. A. (1995). *Water Erosion Prediction Project: Hillslope Profile and Watershed Model Documentation-NSERL Report No.10*. USDA-ARS National Soil Erosion Research Laboratory, West Lafayette, IN.
- Flanagan, D. C., Gilley, J. E., & Franti, T. G. (2007). Water Erosion Prediction Project (WEPP): Development history, model capabilities, and future enhancements. *Transactions of the American Society of Agricultural Engineers*, 50, 1603-1612.



- Foster, G. R., & Meyer, L. D. (1975). Mathematical simulation of upland erosion by fundamental erosion mechanics. *Present and prospective technology for predicting sediment yields and sources*, 190-207.
- Gabet, E. J., & Dunne, T. (2003). Sediment detachment by rain power. *Water Resources Research*, 39(1), 1002.
- Garcia-Navarro, P., Alcrudo, F., & Saviron, J.M. (1992). 1-D open channel flow simulation using TVD-MacCormack scheme. *Journal of Hydraulic Engineering*, 118(10), 1359-1372.
- Gilley, J. E., & Finkner, S. C. (1991). Hydraulic roughness coefficients as affected by random roughness. *Transactions of the American Society of Agricultural Engineers*, 32(3), 897-903.
- Gilley, J. E., Risse, L. M., & Eghball, B. (2002). Managing runoff following manure application. *Journal of soil and water conservation*, 57(6), 530-533.
- Gilley, J. E., Woolheiser, D. A., & McWhorter, D. (1985). Interrill Soil Erosion, Part I. Development of Model Equations. *Biological Systems Engineering: Papers and Publications*, 133.
- Gimenez, R., & Govers, G. (2008). Effects of freshly incorporated straw residue on rill erosion and hydraulics. *Catena*, 72(2), 214-223.
- Gomez, J. A., & Nearing, M. A. (2005). Runoff and sediment losses from rough and smooth soil surfaces in a laboratory experiment. *Catena*, 59(3), 253-266.
- Gomez, J. A., Darboux, F., & Nearing, M. A. (2003). Development and evolution of rill networks under simulated rainfall. *Water resources research*, 39(6), 1148.
- Hairsine, P. B., & Rose, C. W. (1992a). Modeling water erosion due to overland flow using physical principles: 1. Sheet flow. *Water resources research*, 28(1), 237-243.
- Hairsine, P. B., & Rose, C. W. (1992b). Modeling water erosion due to overland flow using physical principles: 1. Sheet flow. *Water resources research*, 28(1), 237-243.
- Hancock, G. R., Nuake, J., & Fityus, S. G. (2006). Modelling of sediment dynamics in a laboratory-scale experimental catchment. *Hydrological processes*, 20(1), 67-84.
- Helming, K., Römken, M. J. M., & Prasad, S. (1998). Surface roughness related processes of runoff and soil loss: a flume study. *Soil Science Society of America Journal*, 62(1), 243-250.
- Huang, C., Gascuel-Oudou, C., & Cros-Cayot, S. (2002). Hillslope topographic and hydrologic effects on overland flow and erosion. *Catena*, 46(2), 177-188.
- Jain, S. C. (1992). Note on lag in bedload discharge. *Journal of Hydraulic Engineering*, 118(6), 904-917.
- Jetten, V., de Roo, A., & Favis-Mortlock, D. (1999). Evaluation of field-scale and catchment-scale soil erosion models. *Catena*, 37(3), 521-541.

- Jirka, G. H., & Uijtewaal, W. (2004). *Shallow Flows*. A. A. Balkema Publishers, Rotterdam.
- Jomaa, S., Barry, D. A., Brovelli, A., Sander, G. C., Parlange, J. Y., Heng, B. C. P., & Tromp-van Meerveld, H. J. (2010). Effect of raindrop splash and transversal width on soil erosion: Laboratory flume experiments and analysis with the Hairsine–Rose model. *Journal of Hydrology*, 395(1), 117-132.
- Jomaa, S., Barry, D. A., Heng, B. C. P., Brovelli, A., Sander, G. C., & Parlange, J. Y. (2012). Influence of rock fragment coverage on soil erosion and hydrological response: Laboratory flume experiments and modeling. *Water Resources Research*, 48(5), W05535.
- Katopodes, N. D., & Bradford, S. (1999). Mechanics of Overland Flow. In *International Workshop on Numerical Modeling of Hydrodynamic Systems*. Zaragoza, Spain (pp. 1-23).
- Kavvas, M. L., Yoon, J., Chen, Z. Q., Liang, L., Dogrul, E. C., Ohara, N., Aksoy, H., Anderson, M. L., Reuter, J., & Hackley, S. (2006). Watershed environmental hydrology model: Environmental module and its application to a California watershed. *Journal of Hydrologic Engineering*, 11(3), 261-272.
- Kibler, D. F., & Woolhiser, D. A. (1972). Mathematical properties of the kinematic cascade. *Journal of Hydrology*, 15(2), 131-147.
- Lal, R. (2005). Soil erosion and carbon dynamics. *Soil and Tillage Research*, 81(2), 137-142.
- Lal, R., & Stewart, B. A. (1994). *Soil processes and water quality*. CRC/ Lewis Publishers, Boca Raton, FL, 398 pp.
- Lawrence, D. S. L. (1997). Macroscale surface roughness and frictional resistance in overland flow. *Earth Surface Processes and Landforms*, 22(4), 365-382.
- Lawrence, D. S. L. (2000). Hydraulic resistance in overland flow during partial and marginal surface inundation: Experimental observations and modeling. *Water Resources Research*, 36(8), 2381-2393.
- Le Bissonnais, Y., Renaux, B., & Delouche, H. (1995). Interactions between soil properties and moisture content in crust formation, runoff and interrill erosion from tilled loess soils. *Catena*, 25(1), 33-46.
- Lewis, S. M., Barfield, B. J., Storm, D. E., & Ormsbee, L. E. (1994). PRORIL-An erosion model using probability distributions for rill flow and density I. Model development. *Transactions of the ASAE*, 37(1), 115-124.
- Liu, Q. Q., Xiang, H., & Singh, V. P. (2006). A simulation model for unified interrill erosion and rill erosion on hillslopes. *Hydrological processes*, 20(3), 469-486.
- Loperfido, J. V., Just, C. L., Papanicolaou, A. N., & Schnoor, J. L. (2010). In situ sensing to understand diel turbidity cycles, suspended solids, and nutrient transport in Clear Creek, Iowa. *Water Resources Research*, 46(6), W06525.

- Lu, J. Y., Chen, J. Y., Hong, J. H., Lu, T. F., & Liu, C. S. (2001). Turbulence intensities of shallow rain-impacted flow over rough bed. *Journal of Hydraulic Engineering*, 127(10), 881-886.
- MacCormack, R. W. (1969). The effect of viscosity in hypervelocity impact cratering. *Frontiers of Computational Fluid Dynamics*, 27-44.
- Mancilla, G. A. (2004). Critical shear stress and rill sediment transport capacity of Palouse soil. *Unpublished PhD diss. Pullman, Wash.: Washington State University, Department of Agricultural Engineering*.
- Marshall, J. S., & Palmer, W. M. K. (1948). The distribution of raindrops with size. *Journal of meteorology*, 5(4), 165-166.
- Merz, B., & Bardossy, A. (1998). Effects of spatial variability on the rainfall runoff process in a small loess catchment. *Journal of Hydrology*, 212, 304-317.
- Mingham, C. G., Causon, D. M., & Ingram, D. M. (2001). A TVD MacCormack scheme for transcritical flow. *Proceedings of the Institution of Civil Engineers. Water, maritime and energy*, 148(3), 167-175.
- Moore, I. D., & Burch, G. J. (1986). Modelling erosion and deposition: topographic effects. *Transactions of the ASAE*, 101.
- Moorman, T. B., Cambardella, C. A., James, D. E., Karlen, D. L., & Kramer, L. A. (2004). Quantification of tillage and landscape effects on soil carbon in small Iowa watersheds. *Soil and Tillage Research*, 78(2), 225-236.
- Morgan, R. P. C., Quinton, J. N., Smith, R. E., Govers, G., Poesen, J. W. A., Auerswald, K., Chisci, G., Torri, D., & Styczen, M. E. (1998). The European Soil Erosion Model (EUROSEM): a dynamic approach for predicting sediment transport from fields and small catchments. *Earth Surface Processes and Landforms*, 23(6), 527-544.
- Nearing, M. A., Lane, L. J., Alberts, E. E., & Laflen, J. M. (1990). Prediction technology for soil erosion by water: status and research needs. *Soil Science Society of America Journal*, 54(6), 1702-1711.
- Nearing, M. A., Liu, B. Y., Risse, L. M., & Zhang, X. (1996). Curve numbers and Green-Ampt effective hydraulic conductivities. *Journal of the American Water Resources Association*, 32(1), 125-136.
- Nikora, V., Nokes, R., Veale, W., Davidson, M., & Jirka, G. H. (2007). Large-scale turbulent structure of uniform shallow free-surface flows. *Environmental Fluid Mechanics*, 7(2), 159-172.
- Nord, G., & Esteves, M. (2007). Evaluation of sediment transport formulae and detachment parameters in eroding rills using PSEM\_2D and the Water Erosion Prediction Project (WEPP) database. *Water Resources Research*, 43(8), W08420.
- Norton, L. D. (2006). A linear variable intensity rainfall simulator for erosion studies. In: *Proc. of 2<sup>nd</sup> biennial stormwater management research symposium*. Wanielista, M., Smoot, J. (Eds.). May 4-5, Univ. of Central Florida, Orlando, 93-103.

- Onstad, C. A. (1984). Depressional storage on tilled soil surfaces. *Transactions of the American Society of Agricultural Engineers*, 27(3).
- Papanicolaou, A. N., & Dermisis, D. C. (2011). Investigating the effects of land management practices on upland erosion using a state-of-the-art laser scanner technique. *EGU General Assembly*, Vienna, Austria, April 3-8.
- Papanicolaou, A. N., Bdour, A., & Wicklein, E. (2004). One-dimensional hydrodynamic/sediment transport model applicable to steep mountain streams. *Journal of Hydraulic Research*, 42(4), 357-375.
- Papanicolaou, A. N., Elhakeem, M., Wilson, C., Burras, C., & Oneal, B. (2008). Observations of soils at the hillslope scale in the Clear Creek watershed in Iowa, USA. *Soil Survey Horizons*, 49, 83-86.
- Papanicolaou, A. N., Sanford, J. T., Dermisis, D. C., & Mancilla, G. A. (2010). A 1-D morphodynamic model for rill erosion. *Water Resources Research*, 46(9), W09541.
- Paustian, K., Andr n, O., Janzen, H. H., Lal, R., Smith, P., Tian, G., Tiessen, H., Van Noordwijk, M., & Woomer, P. L. (1997). Agricultural soils as a sink to mitigate CO2 emissions. *Soil use and management*, 13, 230-244.
- Paustian, K., Six, J., Elliott, E. T., & Hunt, H. W. (2000). Management options for reducing CO2 emissions from agricultural soils. *Biogeochemistry*, 48(1), 147-163.
- Phillips, B. C., & Sutherland, A. J. (1989). Spatial lag effects in bed load sediment transport. *Journal of Hydraulic Research*, 27(1), 115-133.
- Phillips, B. C., & Sutherland, A. J. (1990). Temporal lag effect in bed load sediment transport. *Journal of Hydraulic Research*, 28(1), 5-23.
- Pimentel, D., Harvey, C., Resosudarmo, P., Sinclair, K., Kurz, D., McNair, M., Crist, S., Shpritz, L., Fitton, L., Saffouri, R., & Blair, R. (1995). Environmental and economic costs of soil erosion and conservation benefits. *Science*, 1117-1117.
- Potter, K. N. (1990). Soil properties effect on random roughness decay by rainfall. *Transactions of the ASAE*, 33(6), 1889-1892.
- Rahuel, J. L., Holly, F. M., Chollet, J. P., Belleudy, P. J., & Yang, G. (1989). Modeling of riverbed evolution for bedload sediment mixtures. *Journal of Hydraulic Engineering*, 115(11), 1521-1542.
- Rieke-Zapp, D. H., & Nearing, M. A. (2005). Slope Shape Effects on Erosion. *Soil Science Society of America Journal*, 69(5), 1463-1471.
- Rodriguez, G. J., Gomez, J. A., & Zarco-Tejada, P. J. (2011). Assessing soil surface roughness using reflectance band indices obtained with an airborne multispectral sensor at very high spatial resolution. *EGU General Assembly*, Vienna, Austria, April 3-8.
- Romkens, M. J. M., & Wang, J. Y. (1986). Effect of tillage on surface roughness. *Transactions of the ASAE-American Society of Agricultural Engineers*, 29.
- Romkens, M. J. M., Helming, K., & Prasad, S. N. (2002). Soil erosion under different rainfall intensities, surface roughness, and soil water regimes. *Catena*, 46(2), 103-123.

- Roth, J. L., & Capel, P. D. (2012). Changes in water budgets and sediment yields from a hypothetical agricultural field as a function of landscape and management characteristics—A unit field modeling approach. *U.S. Geological Survey Scientific Investigations Report 2012-5203*, 42 p.
- Schmidt, J. (1992). Modelling long-term soil loss and landform change. *Overland Flow: Hydraulics and Erosion Mechanics*, 409-433.
- Schoeneberger, P. J., & Wysocki, D. A. (2005). Hydrology of soils and deep regolith: a nexus between soil geography, ecosystems and land management. *Geoderma*, 126(1), 117-128.
- Sivapalan, M., Viney, N. R., Zammit, C., Singh, V. P., & Frevert, D. K. (2002). LASCAM: large scale catchment model. *Mathematical models of large watershed hydrology*, 579-648.
- Skaggs, R. W. (1978). *A Water Management Model for Shallow Water Table Soils*. Water Resources Research Institute of the University of North Carolina, Report No. 134.
- Smith, M. W., Cox, N. J., & Bracken, L. J. (2011). Terrestrial laser scanning soil surfaces: a field methodology to examine soil surface roughness and overland flow hydraulics. *Hydrological Processes*, 25(6), 842-860.
- Smith, R. E., Goodrich, D. C., Woolhiser, D. A., Unkrich, C. L., & Singh, V. P. (1995). KINEROS-A kinematic runoff and erosion model. *Computer models of watershed hydrology.*, 697-732.
- Stone, J. J., Lane, L. J., Shirley, E. D., & Hernandez, M. (1995). Chapter 4. Hillslope surface hydrology. *USDA-Water Erosion Prediction Project hillslope profile and watershed model documentation. NSERL Report*, (10).
- Strom, K. B., & Papanicolaou, A. N. (2008). Morphological characterization of cluster microforms. *Sedimentology*, 55(1), 137-153.
- Taconet, O., Vannier, E., & Le Hégarat-Masclé, S. (2010). A contour-based approach for clods identification and characterization on a soil surface. *Soil and Tillage Research*, 109(2), 123-132.
- Tauro, F., Grimaldi, S., Petroselli, A., Rulli, M. C., & Porfiri, M. (2012). Fluorescent particle tracers in surface hydrology: a proof of concept in a semi-natural hillslope. *Hydrol. Earth Syst. Sci*, 16, 2973-2983.
- Tayfur, G. (2007). Modelling sediment transport from bare rilled hillslopes by areally averaged transport equations. *Catena*, 70(1), 25-38.
- Thompson, S. E., Katul, G. G., & Porporato, A. (2010). Role of microtopography in rainfall-runoff partitioning: An analysis using idealized geometry. *Water Resources Research*, 46(7), W07520.
- Thornes, J. B., Shao, J. X., Diaz, E., Roldan, A., McMahon, M., & Hawkes, J. C. (1996). Testing the MEDALUS hillslope model. *Catena*, 26(3), 137-160.

- Tietje, O., & Richter, O. (1992). Stochastic modeling of the unsaturated water flow using autocorrelation spatially variable hydraulic parameters. *Modeling Geo-Biosphere Processes*, 1(2), 163-183.
- Toy, T. J., Foster, G. R., & Renard, K. G. (2002). *Soil erosion: Processes, prediction, measurement, and control*. Wiley.
- Truman, C. C., & Bradford, J. M. (1990). Effect of antecedent soil moisture on splash detachment under simulated rainfall. *Soil Science*, 150(5), 787.
- Tseng, M. H. (2010). Kinematic wave computation using an efficient implicit method. *Journal of hydroinformatics*, 12(3), 329-338.
- Tucker, G. E., Lancaster, S. T., Gasparini, N. M., & Bras, R. L. (2001). The channel-hillslope integrated landscape development model (CHILD). *Landscape erosion and evolution modeling*, 349, 388.
- U.S. Department of Agriculture. (2009). *Summary Report: 2007 National Resources Inventory*. Natural Resources Conservation Service, Washington, DC, and Center for Survey Statistics and Methodology, Iowa State University, Ames, Iowa, pp. 123.
- Van Oost, K., Cerdan, O., & Quine, T. A. (2009). Accelerated sediment fluxes by water and tillage erosion on European agricultural land. *Earth Surface Processes and Landforms*, 34(12), 1625-1634.
- Vazquez, E., Vivas Miranda, J. G., & Paz González, A. (2005). Characterizing anisotropy and heterogeneity of soil surface microtopography using fractal models. *Ecological Modelling*, 182(3), 337-353.
- Verheijen, F. G., Jones, R. J., Rickson, R. J., & Smith, C. J. (2009). Tolerable versus actual soil erosion rates in Europe. *Earth-Science Reviews*, 94(1), 23-38.
- Vieux, B. E. (2004). *Distributed hydrologic modeling using GIS* (Vol. 48). Springer.
- WATERS Network. (2008). *WATERS Network, Draft Science, Education, and Design Strategy for the WATer and Environmental Research Systems Network*. WATERS Network Project Office, Available online at: <http://www.watersnet.org/docs/SEDS-20080227-draft.pdf>.
- West, L. T., Abreu, M. A., & Bishop, J. P. (2008). Saturated hydraulic conductivity of soils in the Southern Piedmont of Georgia, USA: field evaluation and relation to horizon and landscape properties. *Catena*, 73(2), 174-179.
- Wicks, J. M., & Bathurst, J. C. (1996). SHESED: a physically based, distributed erosion and sediment yield component for the SHE hydrological modelling system. *Journal of Hydrology*, 175(1), 213-238.
- Wischmeier, W. H., & Smith, D. D. (1978). Predicting rainfall erosion losses-A guide to conservation planning. *Predicting rainfall erosion losses-A guide to conservation planning*.
- Wood, E. F., Sivapalan, M., Beven, K., & Band, L. (1988). Effects of spatial variability and scale with implications to hydrologic modeling. *Journal of Hydrology*, 102(1), 29-47.

- Woods, R., Sivapalan, M., & Duncan, M. (1995). Investigating the representative elementary area concept: an approach based on field data. *Hydrological Processes*, 9(3-4), 291-312.
- Wu, W. (2007). *Computational river dynamics*. CRC.
- Wu, Y. H., Yevjevich, V., & Woolhiser, D. A. (1978). *Effects of surface roughness and its spatial distribution on runoff hydrographs*. Colorado State University.
- Young, R. A., & Mutchler, C. K. (1969). Effect of slope shape on erosion and runoff. *Trans. Am. Soc. Agric. Engrs*, 12, 231-239.
- Young, R. A., Onstad, C. A., Bosch, D. D., & Anderson, W. P. (1989). AGNPS: A nonpoint-source pollution model for evaluating agricultural watersheds. *Journal of soil and water conservation*, 44(2), 168-173.
- Zielinski, J. (2002). Watershed vulnerability analysis. *Center for Watershed protection*, 8391, Available online at: [www.cwp.org/vulnerability analysis.pdf](http://www.cwp.org/vulnerability%20analysis.pdf).